UNIVERSITÀ DEGLI STUDI DI PADOVA

UNIVERSITA' DEGLI STUDI DI PADOVA

Dipartimento di Ingegneria Industriale DII

Corso di Laurea Magistrale in Ingegneria dell'Energia Elettrica

Investigation of stability aspects in a Pan-European interconnected grid with different wind power penetration

RELATORE: Prof. Roberto Turri

Dipartimento di Ingegneria Industriale

CORRELATORE: Ph.D. Mattia Marinelli

Department of Electrical Engineering – Technical University of Denmark

CORRELATORE: Ph.D. Student Michael Pertl

Department of Electrical Engineering – Technical University of Denmark

Caterina Toigo mat: 1084116

Anno Accademico 2015/2016

I would like to thank my DTU supervisors
Mattia Marinelli and Michael Pertl and professor
Roberto Turri of the University of Padua
for their help and support

Abstract

The remarkable growth of Renewable Energy Resources (RES) in recent years has led them to take up a significant share of the power generation system worldwide. RES units, notably inverter connected wind turbines and photovoltaics, are effectively displacing conventional generators and their rotating machinery. This has implications for frequency dynamics and power system stability. In fact, frequency dynamics are faster in power systems with low rotational inertia, making it more difficult to control the frequency and maintain system stability after disturbances.

This thesis presents studies on power system stability in a Pan-European interconnected grid with particular focus on voltage, frequency and rotor angle stability after disturbances: i.e. 3-phase fault on a tie-line and a load step in one area.
The analyzed system consists of a HV transmission grid and a meshed 725 kV HVDC grid. It was developed within the framework of the EU project, called ELECTRA, where it serves as a benchmark grid for RES integration studies. A set of scenarios has been defined with different levels of renewable wind generation and gradual turning off of traditional rotating generation units.

Root-mean-square (RMS) simulation studies have been carried out in the DIgSILENT PowerFactory software environment using a simulation time between 1 to 50 s following the disturbance. Simulation results have been analyzed referring to the new EU network code "Final draft Network Code on Requirements for grid connection of Generators" (2015) together with CENELEC technical specification CLC/TS EN50549 (2014) and technical standard EN 50160 (2011). At first, a set of simulations was performed with a severe fault, i.e. 3-phase fault on a tie line. The second analysis evaluated the behavior of the grid after an imbalance between load and generation, i.e. a load step. The conducted simulations show that the increasing wind power generation, replacing conventional generation, does not necessarily lead to worse stability behavior, but can positively contribute to achieve a steady state equilibrium after a disturbance and reduce oscillations.

Introduzione

Negli ultimi anni, le fonti di energia rinnovabile (FER) hanno visto una crescita rilevante che le ha portate ad occupare una quota significativa della generazione nel sistema elettrico mondiale. La generazione fotovoltaica ed eolica, connessa alla rete tramite inverter, sta prendendo il posto dei generatori rotanti convenzionali e sta portando serie implicazioni per le dinamiche di variazione della frequenza e per la stabilità del sistema elettrico. Di fatto, nei sistemi elettrici con bassa inerzia, le variazioni di frequenza a seguito di perturbazioni sono più veloci: ci sono perciò maggiori difficoltà nel controllo e nel mantenimento della stabilità del sistema.

Questa tesi presenta uno studio effettuato sulla stabilità della rete elettrica d'interconnessione Pan-Europea. Viene posta particolare attenzione alla stabilità della tensione, della frequenza e dell'angolo rotorico, a seguito di due tipologie di disturbi in rete: un guasto trifase su una linea d'interconnessione e un gradino di carico in un'area.

Il sistema analizzato è composto principalmente da una rete di trasmissione in AT e da una rete magliata in corrente continua a 725 kV. Questo sistema elettrico è stato realizzato all'interno di un progetto dell'Unione Europea chiamato ELECTRA e serve come riferimento per gli studi sull'integrazione delle fonti di energia rinnovabile. Per lo studio, sono stati definiti una serie di scenari con differenti livelli di penetrazione eolica e graduale disattivazione delle forme di generazione rotante convenzionale. Gli studi sono stati possibili grazie a simulazioni ai valori efficaci eseguite con il software DIgSILENT PowerFactory con tempi di osservazione, seguenti al disturbo, tra 1 e 50 s. I risultati delle simulazioni sono stati analizzati riferendosi al nuovo codice di rete europeo, relativo alle regole di connessione alla rete dei generatori, denominato "Final draft Network Code on Requirements for grid connection of Generators"(2015), insieme alla specifica CENELEC CLC/TS EN50549 (2014) e alla norma europea EN 50160 (2011). In una prima fase, è stato valutato il comportamento della rete dopo un guasto trifase in una linea di interconnessione. Successivamente, ne è stato analizzato il comportamento dopo uno sbilanciamento tra generazione e assorbimento, quale un gradino di carico in un'area.

Alla luce dei risultati ottenuti, si può concludere che la crescente penetrazione eolica e la conseguente diminuzione della generazione convenzionale, non porta necessariamente ad una peggiore stabilità, ma può contribuire positivamente al raggiungimento di un valore di regime stabile, dopo un disturbo, riducendo le oscillazioni.

Contents

Chapter 1

Introduction

This chapter contains an introduction to the thesis goals as well as a description of new topology of power system in the future vision of an interconnected Pan-European grid. The project ELECTRA, which goes in this direction, is described.

The problem of system stability is figured out with a detailed description of voltage, frequency and rotor angle stability. Furthermore the main indexes defined in literature to analyze the transient stability behaviour of a network have been described.

The commercially available power system simulation tool DIgSILENT PowerFactory, used to perform the simulation, is briefly described in this section.

In the end of the chapter a description of the new EU code "Final draft Network Code on Requirements for grid connection of Generators" (2015) has been reported together with CENELEC technical specification CLC/TS EN50549 (2014) and technical standard EN 50160 (2011), principally focusing on regulations for voltage characteristic of electricity supplied by public distribution system.

1.1. Project Goals

The aim of this thesis is the study of the stability issue after severe events, i.e. fault and power imbalance, in a future transmission grid with different penetrations of wind generation. In the interest of the thesis is the analysis of a new type of grid in the future vision of smart

grids. For that reason the Pan-European network of the EU project Electra Task 5.4 has been taken as the test grid. This grid derives from the European HV Benchmark network proposed by the Cigré with the integration of a high Voltage Direct Current HVDC part.

In order to develop the study, a set of scenarios has been defined with increasing levels of wind generation and gradual disconnection of conventional generators, i.e. synchronous generators.

The stability behavior of the grid has been tested by carrying out simulations with the power simulation tool DIgSILENT PowerFactory. A first set of simulations is carried out with a three-phase fault in a tie line to test the stability behavior of the grid after the most severe disturbance. Finally a second set of simulations is developed by defining a load step in a part of the grid to simulate a power imbalance between generation and consumption.

1.2. Problem Statement

In new power systems, generation will shift from classical dispatchable units to more intermittent renewables. When it comes to penetration of renewable energy resources a significant part of the generation units will shift from big centralized power plants to many smaller units, such as photovoltaic and small wind generation. The generation will move from central transmission system connected generation to decentralized distribution system connected generation. However, there will also be some big and centralized power plants, mainly composed by RES (Renewable energy resources) generation and placed in onshore and offshore locations.

To support and foster research in the European Research area in this vision, the European Union/European commission has created the funding program for Research and Technological Development, also called the Framework Programs or abbreviated FP1 through FP7 with “FP8” being named “Horizon 2020”. The targets of the Horizon 2020 are to reduce greenhouse gas emission by 20%, increase energy efficiency by 20% and to have, by 2020, 20% more of renewable energy resources in the EU energy mix compared to 1990. The key EU technology challenges to meet the 2020 targets also included [1] :

- Doubling the power generation capacity of the largest wind turbines, with off-shore wind as the lead application;
- Demonstrating commercial readiness of large-scale photovoltaic and concentrated solar power;

- Enabling a single, smart European electricity grid able to accommodate the massive integration of renewable and decentralized energy resources;

In fact the EU energy strategy sets ambitious goals for the energy systems of the future that foresees a substantial increase in the share of renewable electricity production. The whole-sale deployment of Renewable Energy Resources connected to the network at all voltage levels will require a radically new approach to real time control, one that can accommodate the coordinated operation of millions of devices, of various technologies, at many different scales and voltage levels, dispersed across the EU grid. To address this challenge, an European Liaison named ELECTRA (European Liaison on Electricity Committed Towards long-term Research Activity) has been constituted.

The ELECTRA Integrated Research Program on Smart Grid (IRP) brings together the partners of the EERA (European Energy Research Alliance) Joint Program on Smart Grid (JP SG) to reinforce and accelerate Europe's medium to long term research cooperation in the field of smart grids. The goal is studying new power systems in the view of smart grids, with high penetration of renewable resources and observability of the grid.

In the proposal of project Electra the EU grid is divided into a web of cell structures. Each cell is a group of interconnected loads, concentrated plants and/or distributed energy resources and storage units. Each cell is managed by a single system operator, called cell system operator, that is responsible for establishing and maintaining automatic control mechanism as well as procuring sufficient reserves within is cell. To maintain the balance, the system operator can procure reserves from within its area but also "cross cell border" reserves from neighboring cells. In this way no global system state information is required and a "divide and conquer" way of tackling voltage and balancing issues is implemented. Thus, local problems are resolved in the cell in a fast and secure manner, limiting complexity and communication overheads. However, inter-cell coordination is possible to support global optimization if needed. In order to regain reliable control over the power grid, distributed generators and loads should also be controlled in a way that increases the predictability of the maximum power imbalance as perceived system-wide by the TSO's.

A new control concept [2] in the future power system is shown in Figure 1-1.

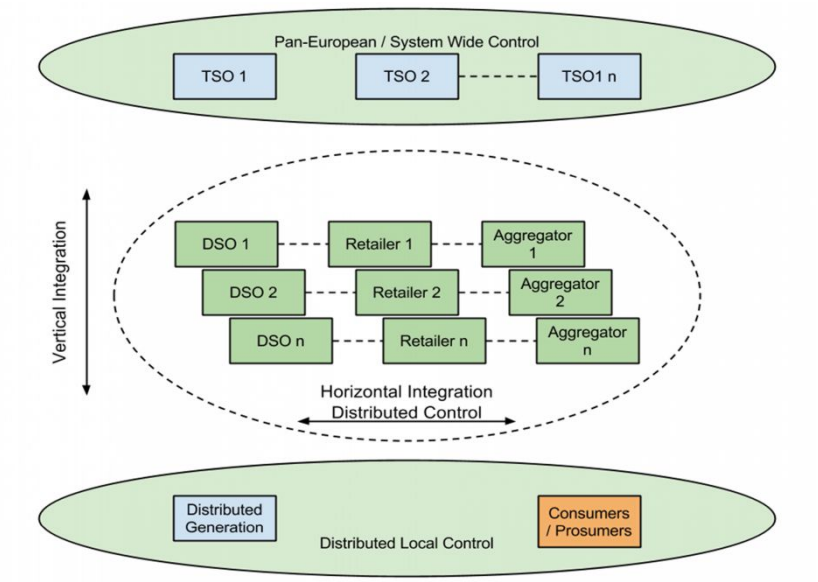

Figure 1-1: Vertical and horizontal integration of distributed control schemes

A vertical integration control scheme reinforced by a horizontally-distributed control scheme is expected to provide for a dynamic power balance that is closer to its equilibrium value than a conventional center control scheme. This enables grid operators to regain control in a future power system with a high share of decentralized generators.

1.3. Background to power system stability

Power system stability is the ability of an electrical power system, for a given initial operating condition, to regain a state of operating equilibrium after being subjected to a physical disturbance, with most system variables bounded so that practically the entire system remains intact [3] .

This definition applies to an interconnected power system, however the stability of a particular generator or a particular load or load areas is also of interest. It could be that a generator may lose stability without causing cascading instability in the main system.

When subjected to a disturbance, the stability of the system depends on the initial operating conditions as well as the nature of the disturbance.

Power systems are subjected to a wide range of disturbances, small and large. Small disturbances in the form of load changes occur continually and the system must be able to adjust to the changing condition and operate satisfactorily. It must also be able to survive numerous large disturbances, such as short circuit on a transmission line or loss of a large generator.

Power system stability could be defined by considering the following:

- The physical nature of the resulting mode of instability as indicated by the main system variable in which instability can be observed;
- The size of the disturbance considered, which influences the method of calculation and prediction of stability;
- The devices, processes, and the time span that must be taken into consideration in order to assess stability.

Based on the considerations explained above, power system stability could be divided into the categories and subcategories reported in Figure 1-2. In any given situation, however, any one form of instability may not occur in its pure form; as a system fails one form of instability may ultimately lead to another form.

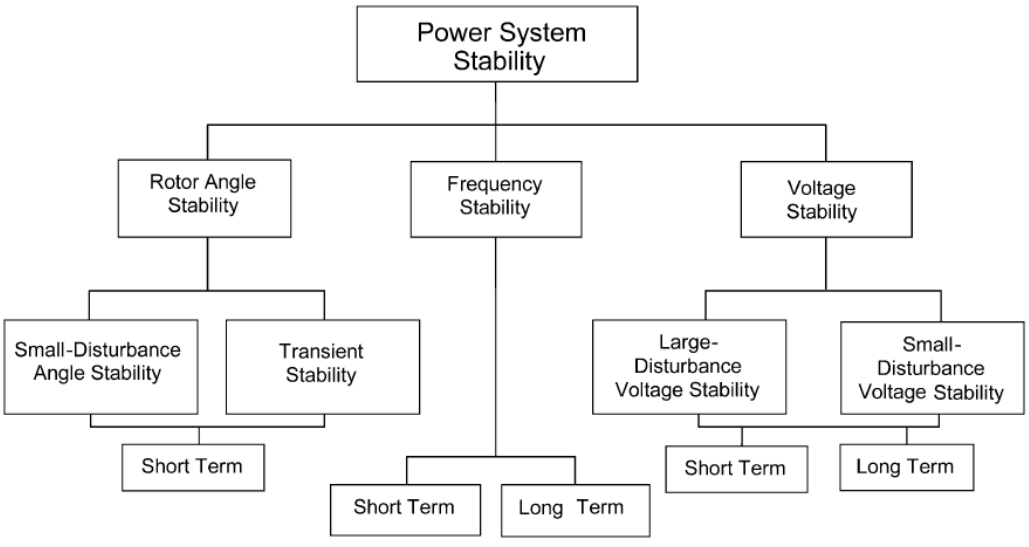

Figure 1-2: Classification of power system stability [3]

1.3.1 Rotor angle stability

Rotor angle stability refers to the ability of synchronous machines of an interconnected power system to remain in synchronism after being subjected to a disturbance. It depends on the ability to maintain/restore equilibrium between the electromagnetic torque and the mechanical torque of each synchronous machine in the system. The instability that may result occurs in the form of increasing angular swings of some generators, leading to their loss of synchronism with other generators. In fact, if the system is perturbed, the equilibrium between the input mechanical torque and the output electromagnetic torque is upset, resulting in acceleration or deceleration of the rotors of the machines according to the laws of motion of a rotating body.

It is useful to characterize rotor angle stability in terms of the following two subcategories:

- Small-disturbance rotor angle stability concerns the ability of the power system to maintain synchronism under smaller disturbances. The small-disturbance rotor angle stability problem is usually associated with insufficient damping of oscillations. The time frame of interest in this case is in the order of 10 to 20 seconds following the disturbance.
- Large-disturbance rotor angle stability or transient stability, as it is commonly referred to, concerns the ability of power system to maintain synchronism when subjected to a severe disturbance, such as short circuit on a transmission line. The time frame of interest in transient stability studies is usually 3 to 5 seconds following the disturbance; it may be extended to 10-20 seconds for very large systems with dominant inter-area swing.

As identified in Figure 1-2, small-disturbance rotor angle stability as well as transient stability are categorized as short term phenomena.

1.3.2 Voltage stability

Voltage stability refers to the ability of a power system to maintain steady voltages at all buses in the system after being subjected to a disturbance from a given initial operating condition. It depends on the ability to maintain/restore equilibrium between load demand and load supply from the power system. The driving force of voltage instability is usually the loads. In response to a disturbance, power consumed by the loads tends to be restored by the

action of motor slips adjustment, distribution voltage regulators and tap-changing transformer. Restored loads increase the stress on the high voltage network by increasing the reactive power consumption and cause further voltage reduction. If the restored power consumption is beyond the capability of the transmission network and the connected generation, a run-down situation occurs causing voltage instability.

Problems of voltage stability could lead to loss of load in an area or tripping of transmission lines and other elements by their protective system, leading to cascading outages. Loss of synchronism of some generators may result from these outages, and on the other hand pole slips between groups of machines could lead to a rapid drop in bus voltages.

While the most common form of voltage instability is the progressive drop of bus voltages, the risk of overvoltage instability also exists. It is caused by a capacitive behavior of the grid and the inability of the combined generation and transmission system to operate below some load level.

Voltage instability problems may also be experienced at the terminals of HVDC links associated by the unfavorable reactive power load characteristic of the converters. The HVDC link control strategies have a very significant influence on such problems, since the active and reactive power at the ac/dc junction node are determined by the controls.

Another form of voltage stability problems that result in uncontrolled over voltages is the self-excitation of synchronous machines. This can arise if the capacity load of the machines is too large, for example in the case of open ended high voltage lines and shunt capacitors and filter banks from HVDC stations.

As in the case of rotor angle stability, it is useful to classify voltage stability into the following subcategories:

- Large-disturbance voltage stability refers to the system's ability to maintain steady voltages following large disturbance such as system fault, loss of generation or circuit contingencies.
- Small-disturbance voltage stability refers to the system's ability to maintain steady voltages when subjected to small perturbation such as incremental changes in system load.

As the time frame of interest may extend from a few seconds to tens of minutes, voltage stability may be either a short-term or a long-term phenomenon as identified in Figure 1-2.

The short-term voltage stability study involves the dynamics of fast acting load components such as induction motors, electronically controlled loads and HVDC converters. The study period in this case is in the order of several seconds.

Long-term voltage stability involves slower acting equipment such as tap-changing transformers, thermostatically controlled loads and generators current limiters. The study period of interest may extend to a few to several minutes.

1.3.3 Frequency stability

Frequency stability refers to the ability of a power system to maintain steady frequency following a severe system upset resulting in a significant imbalance between generation and load. The instability that may result occurs in the form of sustained frequency swings leading to tripping of generating units and/or loads. Generally frequency stability problems are associated with inadequacies in equipment response, poor coordination of control and protection equipment or insufficient generation reserve.

Frequency stability, as identified in Figure 1-2, may be a long-term or a short-term phenomenon. In fact, during frequency excursion, the study period of interest will range from a fraction of a second, corresponding to the response time of devices such as under frequency load shedding and generator controls and protections, to several minutes, corresponding to the response time of devices such as prime mover energy supply systems and load voltage regulators.

During frequency excursion, voltage magnitude may change significantly. Voltage magnitude changes affect the load generation imbalance and may cause undesirable generator tripping.

1.3.4 Index for transient stability evaluations

In the literature there are two main defined indexes for evaluating transient stability behavior of power systems: TRASI, transient rotor angle severity index and CCT, critical clearing time. A brief description of these indexes is reported below.

As said in 1.3.1 transient stability is defined as the ability of synchronous generator angles to regain their operating equilibrium following a transient fault in a network. When the maximum rotor angle difference between two generators or a group of generators exceeds 180° there will be a high probability of losing stability. Therefore this measure can be used as an indicator of transient stability following a transient grid disturbance. In fact an index could be defined, named TRASI, using the maximum rotor angle difference to analyze the severity of the angular separation between synchronous generators.

The transient rotor angle severity index (TRASI) is defined as follow:

$$TRASI = \left(\frac{360° - max(\delta^{pst}_{\max\ \_d})}{360° - \delta^{pre}_{\max\ \_d}} \right) \tag{1-1}$$

The coefficients $\delta^{pst}_{\max\ \_d}$ and $\delta^{pre}_{\max\ \_d}$ represent the post-disturbance and pre-disturbance maximum rotor angle difference in the network respectively [4]. The maximum rotor angle difference can be specified in equation (1-2) based on the rotor angles measured with reference to the reference machines angle.

$$\begin{aligned} \delta_{\max\ \_d}(t) = max\left[\delta_{ref\_m1}(t), \delta_{ref\_m2}(t), \delta_{ref\_m3}(t), \dots, \delta_{ref\_mn}(t)\right] \\ - min\left[\delta_{ref\_m1}(t), \delta_{ref\_m2}(t), \delta_{ref\_m3}(t), \dots, \delta_{ref\_mn}(t)\right] \end{aligned} \tag{1-2}$$

The relative rotor angle δ_{ref_m} could be specified based on the rotor angle w.r.t. the local bus voltage δ_{local}, the generator bus voltage angle w.r.t. the reference machine voltage angle α and the reference machines rotor angle δ_{ref} as: $\delta_{ref\_m} = \delta_{local} + \alpha - \delta_{ref}$. The graphical representation of the defined angles is reported in Figure 1-3.

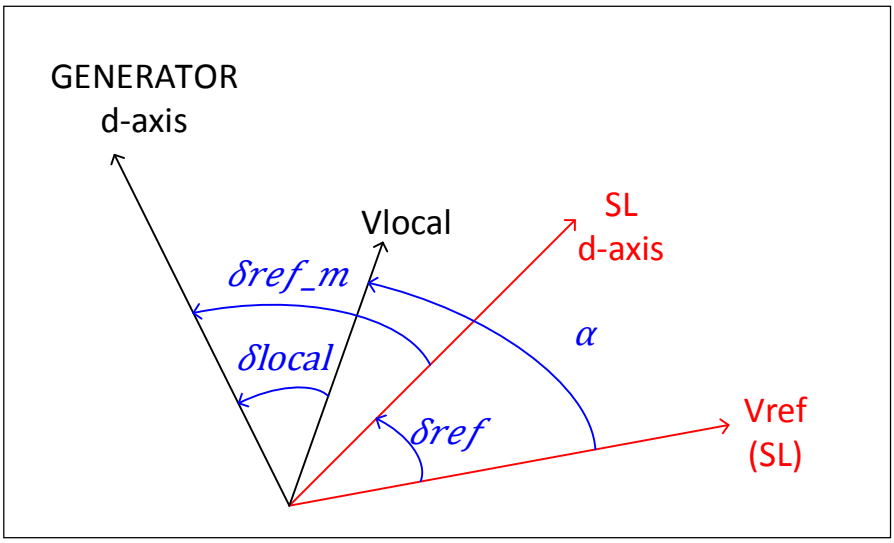

Figure 1-3: Relative rotor angle measurement

The TRASI index varies from 0 to 1, with values closer to 1 considered to be more stable, since the angular separation between the synchronous machines in the system are less compared to the pre-fault values.[4]

Critical clearing time (CCT) is widely used as an important transient stability index which is defined as the maximum duration of a disturbance that the power system can sustain without losing its capability to recover to a normal operating condition [5]. CCT is usually calculated by iterative time domain simulation, more specifically by adjusting the fault duration time in the time-domain simulation to find out the maximum duration of a short circuit that can be withstood without losing the synchronization of central power plants in the whole power grid. For synchronous generator units this means the maximum duration of a short circuit without any synchronous generator going out of step.

The indexes defined above are significant to the transient stability study but the definition implies the presence of a synchronous generator. However, in a power grid with many RES generation units the conventional synchronous generation is replaced more and more by inverter connected generation. There is therefore a lack of parameters for studying and comparing the transient stability of a grid. One possible approach in a grid with inverter connected generation is to define the limit, over which the system stability is lost, as the fault-ride-through capability of the connected generation.

1.3.5 System rotational inertia

In this chapter, a synthetic definition of system inertia is reported. In fact, the inertia of the system plays a key role in determining the initial frequency behavior after a disturbance has occurred in the system. Inertia of a power system is a measure of the energy stored within the rotating masses connected to that system. Due to electro-mechanical coupling, a generator´s rotating mass (as synchronous generator) provides kinetic energy to the grid, or absorbs it from the grid, in case of a frequency deviation Δf.

Following a frequency deviation, kinetic energy stored in the rotating masses of the generator system is released, rendering power system frequency dynamics slower and therefore easier to regulate. The rotational energy is given as

$$E_{kin} = \frac{1}{2} J(2\pi f_m)^2 \tag{1-3}$$

with J as the moment of inertia of the synchronous machine and f_m the rotating frequency of the machine. The inertia constant H for a synchronous machine is defined by

$$H = \frac{E_{kin}}{S_B} = \frac{J(2\pi f_m)^2}{2\, S_B} \tag{1-4}$$

With S_B as the rated power of the generator. H denotes the time during which the machine can supply its rated power solely with its stored kinetic energy. Typical value of H are in the range of 2-10 s [6].

The classical swing equation describes the inertial response of the synchronous generator as the change in rotational frequency f_m (or rotational speed $\omega_m = 2\,\pi\, f_m$) of the synchronous generator following a power imbalance as

$$\dot{E}_{kin} = J(2\pi)^2 f_m\, \dot{f}_m = \frac{2H\, S_B}{f_m}\, \dot{f}_m = (P_m - P_e) \tag{1-5}$$

with P_m as the mechanical power supplied by the generator and P_e as the electric power demand.

Noting that the frequency excursions are usually small deviations around the reference value, f_m could be replaced by the reference frequency f_0. It is often desirable to also include a component of load-damping constant D_{load} that takes into account the self-stabilizing

property of power system. Considering the system change (Δ) before and after a disturbance the relative swing equation is

$$\Delta \dot{f} = -\frac{f_0}{2\,H\,S_B D_{load}}\,\Delta f + \frac{f_0}{2\,H\,S_B}\,(\Delta P_m - \Delta P_e) \tag{1-6}$$

The equation (1-6) describes the change that will occur in the frequency in response to an unbalance between P_m and P_e. As seen in the equation the kinetic energy provided is proportional to the rate of change of frequency $\Delta\dot{f}$: the higher the inertia constant H, the slower and more benign are frequency dynamics.

1.4. Power system simulation tool

The routine used to perform the simulations is implemented in the commercially available power system simulation tool DIgSILENT PowerFactory [7].

The calculation program PowerFactory, as written by DIgSILENT, is a computer aided engineering tool for the analysis of transmission, distribution, and industrial electrical power systems. It has been designed as an advanced integrated and interactive software package dedicated to electrical power system and control analysis in order to achieve the main objectives of planning and operation optimization.

"DIgSILENT" is an acronym for "**DIg**ital **SI**mu**L**ation of **E**lectrical **N**e**T**works". This power system analysis software presents an integrated graphical command-line interface that includes drawing functions, editing capabilities and all relevant static and dynamic calculation features.

PowerFactory uses a hierarchical, object-oriented database. All the data, which represents power system Elements, Single Line Diagrams, Study Cases, system Operation Scenarios, calculation commands, program Settings etc., are stored as objects inside a hierarchical set of folders. The folders are arranged in order to facilitate the definition of the studies and optimize the use of the tools provided by the program.

The objects are grouped according to the kind of element that they represent. These groups are known as 'Classes' within the PowerFactory environment.

All data which defines a power system model is stored in "Project" folders within the database. Inside a "Project" folder, "Study Cases" are used to define different studies of the

system considering the complete network, parts of the network, or variations on its current state. This 'project and study case' approach is used to define and manage power system studies in a unique application of the object-oriented software principle.

1.5. Background to European network code on voltage and frequency variation range

The European Commission, together with many stakeholders, have established that greater effort is needed to create a secure, competitive and low carbon European energy sector and a pan-European Internal Energy Market. To reach this objective ENTSO-E, with guidance from the Agency for the Cooperation of Energy Regulators (ACER), has drafted the Network codes. They are a set of rules to facilitate the harmonization, integration and efficiency of the European electricity market. At present, ENTSO-E is working on 10 network codes. Each code is submitted to the European Commission for approval through the Comitology process, to then be voted into EU law and implemented across Member States. These new network codes will work together with the European Standard EN norms and technical CENELEC specification.

It is remarkable, for the scope of this thesis, to evaluate the network code for grid connection of generators and the main requirements for voltage characteristics of electricity supplied by public distribution systems. In this view a description of these regulations has been reported in the following chapters.

1.5.1 Requirements for grid connection of generators

The Network Code on Requirements for Generators [8] lays down the requirements for grid connection of power generating facilities, synchronous power generating modules, power park modules and offshore power park modules, to the interconnected system.

On 26 June 2015, the network code on Requirements for Generators was adopted by European Union Member States in Comitology. The network code will now be reviewed by the European Parliament and Council who will check its compliance with the main principles of the European Union and the 3rd Energy Package (scrutiny). It is expected to become a binding regulation in Europe in early 2016, which will mark the start of a 3 years implementation period across Europe.

It is in the interest of the analysis to report the permitted variation ranges of the network code related to the synchronous area of continental Europe.

The requirements for grid connection of generation state the limit of disconnection of the power generating modules after voltage and frequency variation. To ensure system security in the grid it should be possible for the generators to remain connected to the system for the specified frequency and voltage ranges. In the regulations the definition of power generating module includes either a synchronous power generating module or a power park module. A park module is a unit or ensemble of units which is either non-synchronously connected to the network or connected through power electronics.

In view of the different voltage levels at which generators are connected and their maximum generating capacity, the regulation makes a distinction between different types of generators by establishing different levels of requirements. Power generating modules are divided into four categories in the basis of the voltage level of their connection point and their maximum capacity:

- **Type A**: connection point below 110 kV and maximum capacity of 0.8 kW or more;
- **Type B**: connection point below 110 kV and maximum capacity at or above 1 MW;
- **Type C**: connection point below 110 kV and maximum capacity at or above 50 MW;
- **Type D**: connection point at or above 110 kV and maximum capacity above 75 MW, a power generation module is also of type D if its connection point is below 110 kV and its maximum capacity is at or above 75 MW.

A power generating module, regardless of the type, should be capable of remaining connected to the network and operate within the frequency ranges and time periods specified in Table 1-1.

Synchronous area	Frequency range	Time period for operation
Continental Europe	**47.5 Hz**-48.5 Hz	To be specified by each TSO, but not less than 30minutes
	48.5 Hz-49.0 Hz	To be specified by each TSO, but not less than the period for 47.5 Hz - 48.5 Hz
	49.0 Hz-51.0 Hz	Unlimited
	51.0 Hz-**51.5 Hz**	30 minutes

Table 1-1: Minimum time periods for which a power generating module has to be capable of operating on different frequencies without disconnecting from the network.

In fact if the frequency range goes outside the values of 47.5 Hz – 51.5 Hz, corresponding to 0.95 – 1.03 in p.u. (with a base of 50 Hz), the interface protection trips and this could led to a loss of generation and consequently to system failure.

Regarding the fault-ride-through capability there are different requirements according to the different power generating module's types. The fault-ride-through curve is a voltage-against-time profile which describes the conditions in which the power generating module is capable of staying connected to the network and continuing to operate stably after the power system has been disturbed by faults on the transmission system.

Regarding power generating units belonging to type A there is no specific requirement with respect to the fault-ride-through profile.

With regards to fault-ride-through capability of type B and C power generating units each TSO specifies a voltage-against-time profile in line with Figure 1-4. The profile expresses a lower limit of the actual course of the phase-to-phase voltages on the network voltage level at the connection point during a symmetrical fault, as a function of time before, during and after the fault. Regarding the parameters set out in Figure 1-4, U_{ret} is the retained voltage at the connection point during a fault and t_{clear} is the instant when the fault has been cleared. The ranges of variation of the parameters are set out in Table 1-2, for synchronous power generating modules, and in Table 1-3, for power park modules.

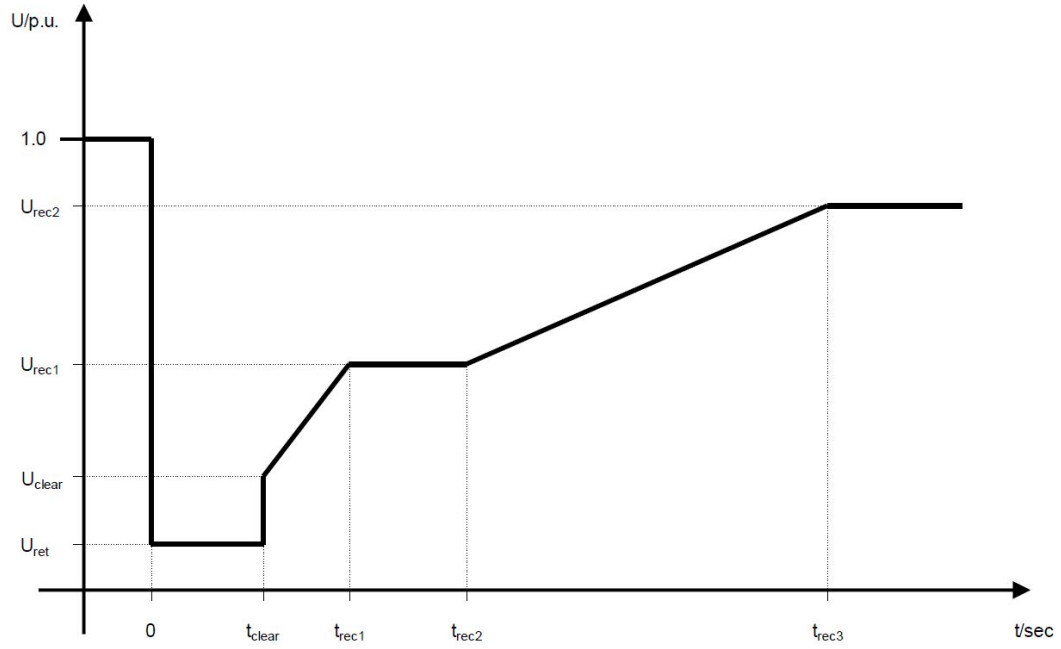

Figure 1-4: Fault-ride-through profile of a power generating module

Voltage parameters [pu]		Time parameters [seconds]	
Uret :	0.05 - 0.3	tclear :	0.14 - 0.15 (or 0.14 - 0.25 if system protection and secure operation so require)
Uclear :	0.7 - 0.9	trec1 :	tclear
Urec1 :	Uclear	trec2 :	trec1 - 0.7
Urec2 :	0.85 - 0.9 and ≥ Uclear	trec3 :	trec2 - 1.5

Table 1-2: Parameters for fault-ride-through capability of synchronous power generating modules

Voltage parameters [pu]		Time parameters [seconds]	
Uret :	0.05 - 0.15	tclear :	0.14 - 0.15 (or 0.14 - 0.25 if system protection and secure operation so require)
Uclear :	Uret - 0.15	trec1 :	tclear
Urec1 :	Uclear	trec2 :	trec1
Urec2 :	0.85	trec3 :	1.5 - 3.0

Table 1-3: Parameters for fault-ride-through capability of power park modules

With regards to voltage stability, type C power generating modules shall be capable of automatic disconnection when voltage at the connection point reaches levels specified by the relevant system operator in coordination with the relevant TSO. In addition, with regards to loss of angular stability or loss of control, a power generating module shall be capable of disconnecting automatically from the network in order to help preserve system security or to prevent damage to the power generating module.

With regards to type D power generating modules, specific voltage ranges and a fault-ride-through capability are defined. The power generating modules shall be capable of staying connected to the network and operating within the ranges of the network voltage at the connection point, expressed by the voltage at the connection point related to the reference 1 p.u. voltage, and for the time periods specified in Table 1-4 and Table 1-5 for different voltage base values.

Synchronous area	Voltage range	Time period for operation
Continental Europe	**0.85 pu** - 0.90 pu	60 minutes
	0.90 pu - 1.118 pu	Unlimited
	1.118 - **1.15 pu**	To be specified by each TSO, but not less than 20 minutes and not more than 60 minutes

Table 1-4: The table shows the minimum time periods during which a power generating module must be capable of operating for voltage deviation from the reference 1 p.u. at the connection point without disconnecting from the network. The voltage base for p.u. values is from 110 kV to 300 kV

Synchronous area	Voltage range	Time period for operation
Continental Europe	**0.85 pu** - 0.90 pu	60 minutes
	0.90 pu - 1.05 pu	Unlimited
	1.05 - **1.10 pu**	To be specified by each TSO, but not less than 20 minutes and not more than 60 minutes

Table 1-5: The table shows the minimum time periods during which a power generating module must be capable of operating for voltage deviation from the reference 1 p.u. at the connection point without disconnecting from the network. The voltage base for p.u. values is from 300 kV to 400 kV.

Regarding the fault-ride-through capability, power generating modules of type D shall be capable of staying connected to the grid and continuing to operate stably after the power system has been disturbed by a symmetrical fault. That capability shall be in accordance with a voltage-against-time profile defined by the relevant TSO in line with Figure 1-4.

The ranges for the parameters are set out in Table 1-6 and Table 1-7, for type D power generating modules connected at or above the 110 kV level, and in Table 1-2 and Table 1-3 for type D power generating modules connected below the 110 kV level.

Voltage parameters [pu]		**Time parameters [seconds]**	
U_{ret} :	0	t_{clear} :	0.14 - 0.15 (or 0.14 - 0.25 if system protection and secure operation so require)
U_{clear} :	0.25	t_{rec1} :	t_{clear} - 0.45
U_{rec1} :	0.5 - 0.7	t_{rec2} :	t_{rec1} - 0.7
U_{rec2} :	0.85 - 0.9	t_{rec3} :	t_{rec2} - 1.5

Table 1-6: Parameters for fault-ride-through capability of synchronous power generating modules

Voltage parameters [pu]		**Time parameters [seconds]**	
U_{ret} :	0	t_{clear} :	0.14 - 0.15 (or 0.14 - 0.25 if system protection and secure operation so require)
U_{clear} :	U_{ret}	t_{rec1} :	t_{clear}
U_{rec1} :	U_{clear}	t_{rec2} :	t_{rec1}
U_{rec2} :	0.85	t_{rec3} :	1.5 - 3.0

Table 1-7: Parameters for fault-ride-through capability of power park modules

Offshore power generating modules connected to the interconnected system shall meet the same requirements for onshore power generating modules, unless the connection of power park modules is via a high voltage direct current connection.

To complete the regulation explanation on grid connection of generators, the Technical Specification of CENELEC, CLC/TS 50549 [9] has also been reported. In fact Technical Specification is also intended to serve as a technical reference for the definition of national requirements where European Network Codes requirements allow flexible implementation.

Regarding the high-voltage-ride-through capability of power generating modules the Network code [8] does not define any limits while the technical specification of CENELEC [9] also sets upper limits for the fault-ride-through capability of a power generating modules. Regarding this the regulation defines that a generating plant shall be capable of staying

connected to the grid even if the voltage at the terminals goes beyond the upper limit of the continuous operating voltage range:

- Up to 120% U_c (1.2 p.u.) for a duration of 100 ms and ;
- Up to 115% U_c (1.15 p.u.) for a duration of 1 s.

Where U_c is the declared supply voltage.

1.5.2 Voltage characteristic of public distribution system

The standard EN 50160 [10] defines and describes the main characteristics of the supply voltage: with regards to frequency, magnitude, wave form and symmetry of the three phase voltages. These characteristics are subject to variations during the normal operation of a supply system due to changes of load, disturbances generated by certain equipment and the occurrence of faults which are mainly caused by external events.

Regarding the characteristic of medium-voltage supply, which means a voltage range from 1 kV to 36 kV, the standard gives the ranges briefly described below.

With regards to power frequency range, under normal operating condition the mean value of the fundamental frequency measured over 10 s shall be within a range of:

- 50 Hz ± 1% (i.e. 49.5 - 50.5 Hz) for 99.5% of a year;
- 50 Hz - 6%/+4% (i.e. 47.0 – 52.0 Hz) for 100% of a year.

The first range, valid for 95.5% of the year, has to be viewed as the range for more probable events like loss of load or increased load demand, while the second range also takes into consideration less frequent events like faults.

With regards to supply voltage variation under normal operating conditions, excluding the periods with interruptions, voltage variations should not exceed ± 10% of the declared voltage U_c.

Regarding the characteristics of high-voltage supply, i.e. voltage range from 36 kV to 150 kV, the standard gives the ranges described below.

With regards to power frequency range, under normal operating conditions the mean value of the fundamental frequency measured over 10 s shall be within the same range previously defined for the medium-voltage supply.

As the number of network users supplied directly from HV networks is limited and normally subject to individual contracts, no limits for supply voltage variations are given in this standard.

Chapter 2

Network Layout and Modeling

In this chapter a description of the network Pan-European grid, used for the simulation, is presented. Since the grid comprises RES wind generation, a section has been included to give a brief overview of the different available typology of wind turbines.

The dynamics analysis, RMS simulation, available in DigSILENT Power Factory is presented as well as the basis of modelling approach used in this program, with particular attention to the modelling of synchronous generator, wind turbines, loads and converter.

2.1. Network layout

The European HV Benchmark network proposed in the Cigré report [11] laid the foundations for the derived Pan-European test grid for Electra Task 5.4 [12]. A brief overview of the original Cigré network is reported below before a description of the so called "Pan-European" network.

The original Cigré network is shown in Figure 2-1. The network transmission voltages are 220 kV and 380 kV, which are typical in European transmission systems. Generation bus voltages are 22 kV, and the system frequency is 50 Hz. The system is a balanced three-phase HV transmission network, and assumes ideal line transposition. The network consists of 13 buses and covers three geographical areas, referred to as Areas 1, 2, and 3, denoted by dashed lines. Area 1 is predominantly a generation center. Area 2, situated about 500 km from Area 1, is a load center with a small amount of generation available. Area 3 is situated

between the main generation Area 1 and the main load center Area 2. Three voltage levels exist in the network: generation bus voltage of 22 kV, primary transmission high voltage of 220 kV, and a long line connecting Area 1 and 2 at the extra high voltage (EHV) level of 380 kV. Bus 6a in Area 3 is a suitable location for studying the incorporation of large-scale renewable energy sources such as wind energy conversion systems.

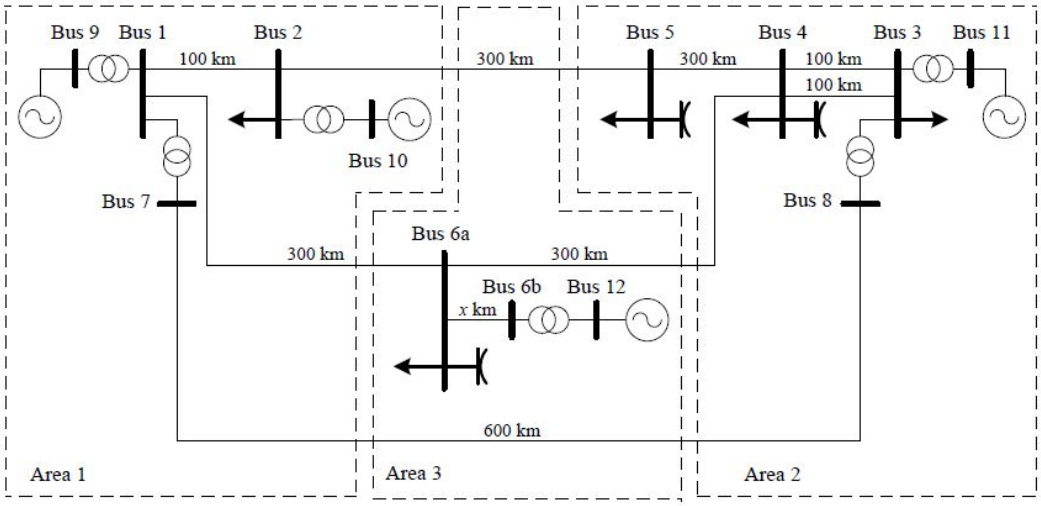

Figure 2-1: Topology of European HV transmission network benchmark [11]

Since the Cigré grid only represents a pure AC grid and ELECTRA focuses on the future power grid, the grid has been extended with a DC part. In fact High Voltage Direct Current (HVDC) technology will play an important role in the European energy grid system as it could be viable when used to connect offshore wind farms to the grid and as interconnectors between countries. Moreover the Cigré grid has been subjected to a revision of the AC side in order to improve load flow convergence. Furthermore, the grid topology has been modified in order to create a more diverse and flexible model while trying to keep it as simple as possible. The network includes a 220 and 400 kV AC grid together with a meshed DC 725 kV grid. In fact the 380 kV AC level has been updated to 400 kV. The DC voltage level has been chosen so that it allows direct connection of HVDC VSC (voltage source converters) without need of internal transformers for stepping down the AC side. The generation units are connected to the 20 kV AC buses (it has been chosen to change the 22 kV level with the more common 20 kV level).

Most of the buses have both conventional and renewable units. The conventional units are either gas turbine or hydraulic power plants. Renewable units are mainly wind turbines type 3 and 4. A more detailed description of the types of wind turbines is reported in the following chapter.

In this grid no PV is included, however from a stability point of view, the transient behavior of a PV system can be compared to the one of a type 4 wind turbine, being both units connected with PWM converter.

In the extended ELECTRA grid, shown in Figure 2-2, four cells are identified and the main information for each cell are reported in the Table 2-1 below.

It has to be noted that the loads have been chosen so that it is not possible for the generation units to produce full power at the same time. In this way it is possible to investigate several renewable penetration scenarios, having conventional plant progressively displaced (i.e. physically disconnecting synchronous machines from the network) in order to make room for renewable resources.

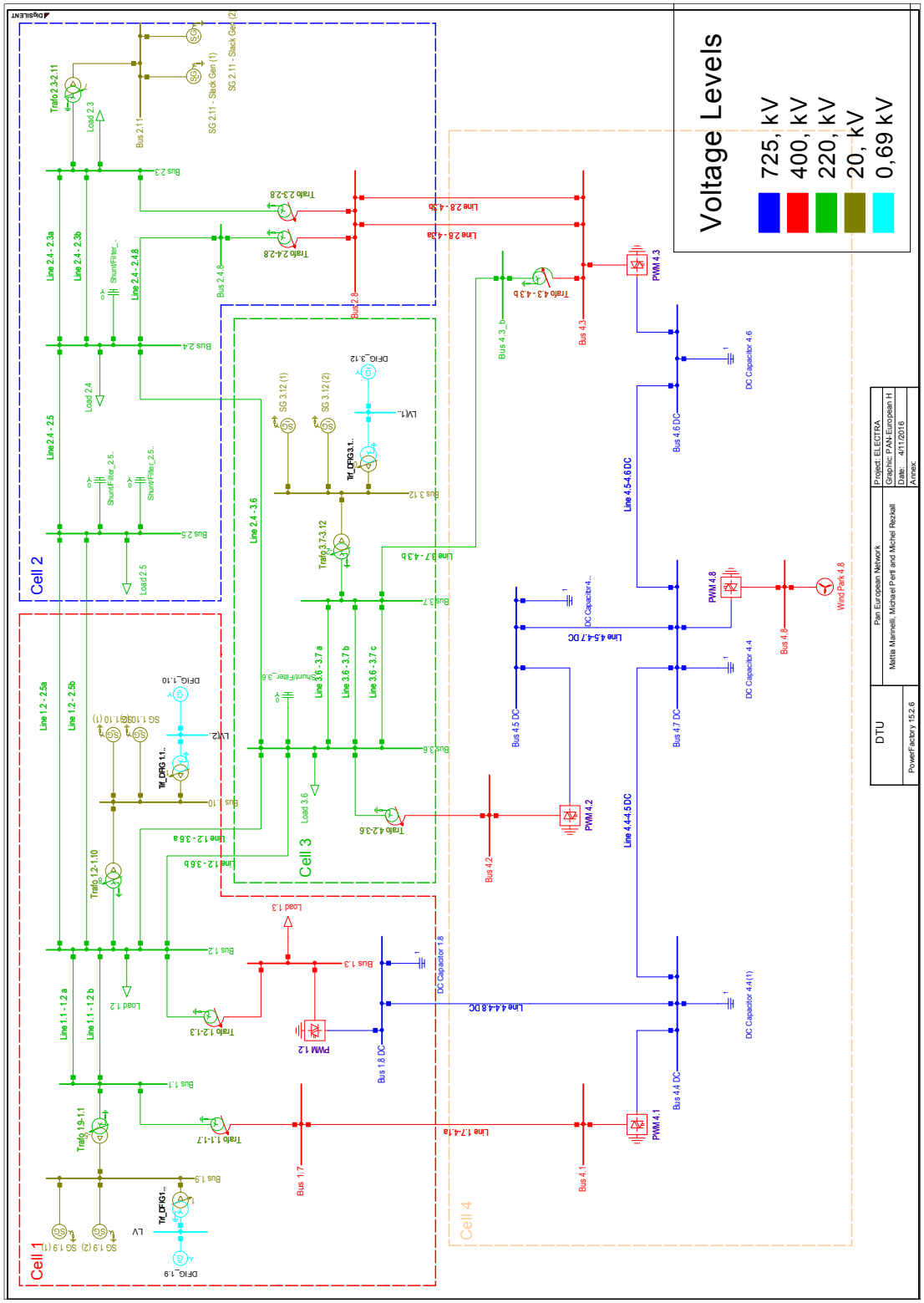

Figure 2-2: Pan-European grid [13]

	Cell 1	**Cell 2**	**Cell 3**	**Cell 4**
Voltage levels [kV]	20; 220; 400; 725	20; 220; 400	20; 220	220; 400; 725
AC/DC	AC and DC	AC	AC	AC and DC
Nominal generation power	2x500 MVA 2x500 MVA Synchronous machines (gas turbine governor) 65x6 MW 65x6 MW (type 3 wind turbines)	2x500 MVA Synchronous machines (gas turbine governor) Note: this machines is used as slack for LF calculations	2x500 MVA Synchronous machines (hydraulic governor) 65x6MW (type 3 wind turbines)	1x1500 MVA equivalent wind generation (type 4)
Nominal consumption power	2x500 MW+ j 2x165 MVar loads	3x400 MW+ j 3x130 MVar loads	1x400 MW+ j 1x130 MVar loads	no load
Number of tie-lines	Cell 1-2 : 2 AC 220 kV tie lines Cell 1-3 : 2 AC 220kV tie lines Cell 1-4 : 1 AC 400 kV tie line Cell 1-4 : 1 DC 725 kV tie line	Cell 2-1 : 2 AC 220 kV tie lines Cell 2-4: 2 AC 400 kV tie lines Cell 2-3: 1 AC 220 kV tie line	Cell 3-1 : 2 AC 220 kV tie lines Cell 3-2 : 1 AC 220 kV tie line Cell 3-4 : 1 220/400 kV transformer Cell 3-4 : 1 AC 220 kV tie line	Cell 4-1 : 1 AC 400 kV tie line Cell 4-1: 1 DC 725kV tie line Cell 4-2: 2 AC 400 kV tie lines Cell 4-3: 1 220/400 kV transformer Cell 4-3: 1 AC 220 kV tie line
Number of internal lines	2 x 220 kV lines	4 x 220 kV lines	3 x 220 kV lines	3 x 725 kV lines
Nominal HVDC capacity	2 x 500 MVA PWM converters	no PWM converters	no PWM converters	3 x 500 MVA PWM converters

Table 2-1: Overview of cell generation and consumption level

2.2. Wind turbine

Beyond mechanical power regulation, turbines are further divided into fixed speed (Type 1), limited variable speed (Type 2), or variable speed with either partial (Type 3) or full (Type 4) power electronic conversion [14].

Type 1 wind turbine generator (WTG) is implemented with a squirrel-cage induction generator and is connected to a step-up transformer directly .The turbine speed is fixed to the electrical grid's frequency, and generates real power when the turbine shaft rotates faster than the electrical grid frequency.

In Type 2 turbines, wound rotor induction generators are connected directly to the WTG step-up transformer in a fashion similar to Type 1, but also include a variable resistor in the rotor circuit. Adding resistance to the rotor circuit allows some ability to control the speed to achieve the best energy capture.

The Type 3 turbine, known commonly as the Doubly Fed Induction Generator (DFIG), consists of a wound rotor induction generators with the stator windings directly connected to the three-phase grid by a step-up transformer and with the rotor windings connected to a back-to-back partial scale power converter. The back-to-back converter is a bi-directional partial scale power converter. It consists of two independent controlled voltage source converters connected to a common DC-bus. These converters are illustrated in Figure 2-3 [15], as rotor-side converter and grid-side converter. The behavior of the generator is governed by these converters and their controllers both in normal and fault conditions. The converters control the rotor voltage in magnitude and phase angle and are therefore used for active and reactive power control.

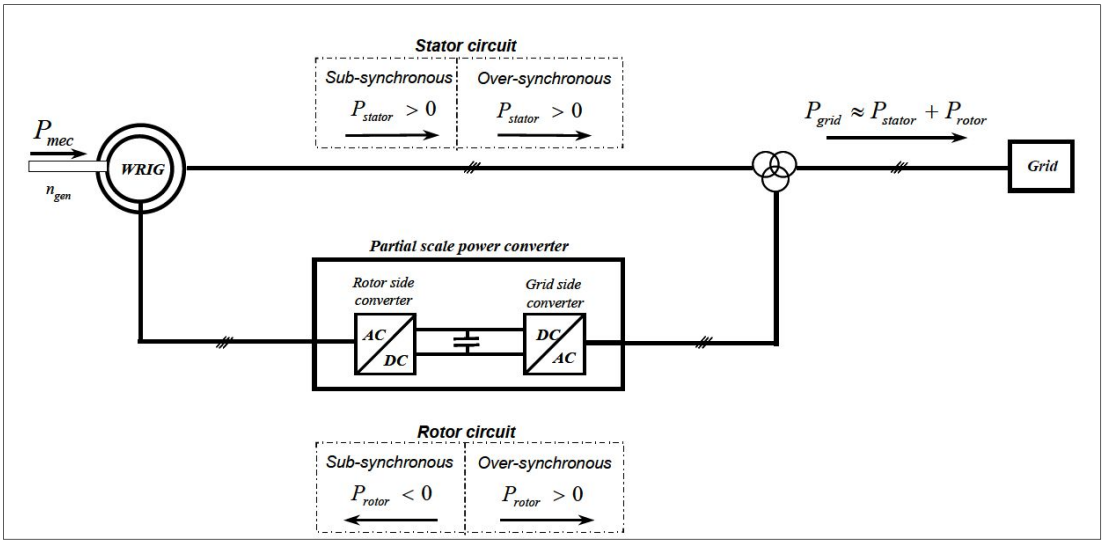

Figure 2-3: DFIG structure and power flow

A small amount of power injected into the rotor circuit can affect a large control of power in the stator circuit. This is a major advantage of the DFIG, a great deal of control of the output is available with the presence of a set of converters that typically are only 30% of the rating of the machine. In addition to the real power that is delivered to the grid from the generator's stator circuit, power is delivered to the grid through the grid-connected inverter when the generator is moving faster than synchronous speed (over-synchronous operating area, $s<0$) as could be seen in Figure 2-3. When the generator is moving slower than synchronous speed (sub-synchronous operating area, $s>0$), real power flows from the grid, through both converters, and from rotor to stator. This is the reason why a back-to-back PWM (bi-directional) converter configuration is used.

The greatest advantage of the DFIG, is that it offers the benefits of separate active and reactive power control by independent control of the rotor excitation current, much like a traditional synchronous generator, while being able to run asynchronously. DFIG is therefore capable of producing or absorbing reactive power to or from the grid, for the purpose of voltage control.

The control system of a variable speed wind turbine with DFIG has the aim of controlling the reactive power interchanged between the generator and the grid and the active power drawn from the wind turbine in order to track the wind turbine optimum operation point or to limit the power in the case of high wind speeds.

The overall control system, shown in Figure 2-4 [15], of a variable speed DFIG wind turbine is built up with a hierarchical structure. It consists of two control levels with different bandwidths, strongly connected to each other. A slow dynamic control level named wind turbine control and a faster control, DFIG control.

The fast dynamic control level, i.e. DFIG control, encompasses the electrical control of the power converters and of the doubly-fed induction generator. Since this controller is an electric one, it works very fast. The DFIG control level has as its goal the control of the active and reactive power of the wind turbine independently. The DFIG control contains two controllers:

- Rotor-side converter controller, which controls independently the active and reactive power on the grid point M. The active power set-point $P_{grid}^{conv,ref}$ for the RSC is defined, in normal operating condition, by the maximum power tracking point (MPT) as a function of the optimal generator speed: for each wind speed there is only one generator speed resulting in maximum aerodynamics coefficient C_p. The reactive power set-point Q_{grid}^{ref} for the RSC can be set to a certain value or to zero according to whether or not the DFIG is required to contribute with reactive power.
- Grid-side converter controller, which controls the DC link voltage U_{DC} and guarantees unity power factor in the rotor branch. The transmission of the reactive power from DFIG to the grid is thus only through the stator.

On the other hand, the wind turbine control is a control with slow dynamic response. It contains two cross-coupled controllers: a speed controller and a power limitation controller. It supervises both the pitch angle actuator system of the wind turbine and the active power set-point of the DFIG control level. It thus provides both a reference pitch angle θ_{ref} directly to the pitch actuator and a converter reference power signal $P_{grid}^{conv,ref}$ to the DFIG control.

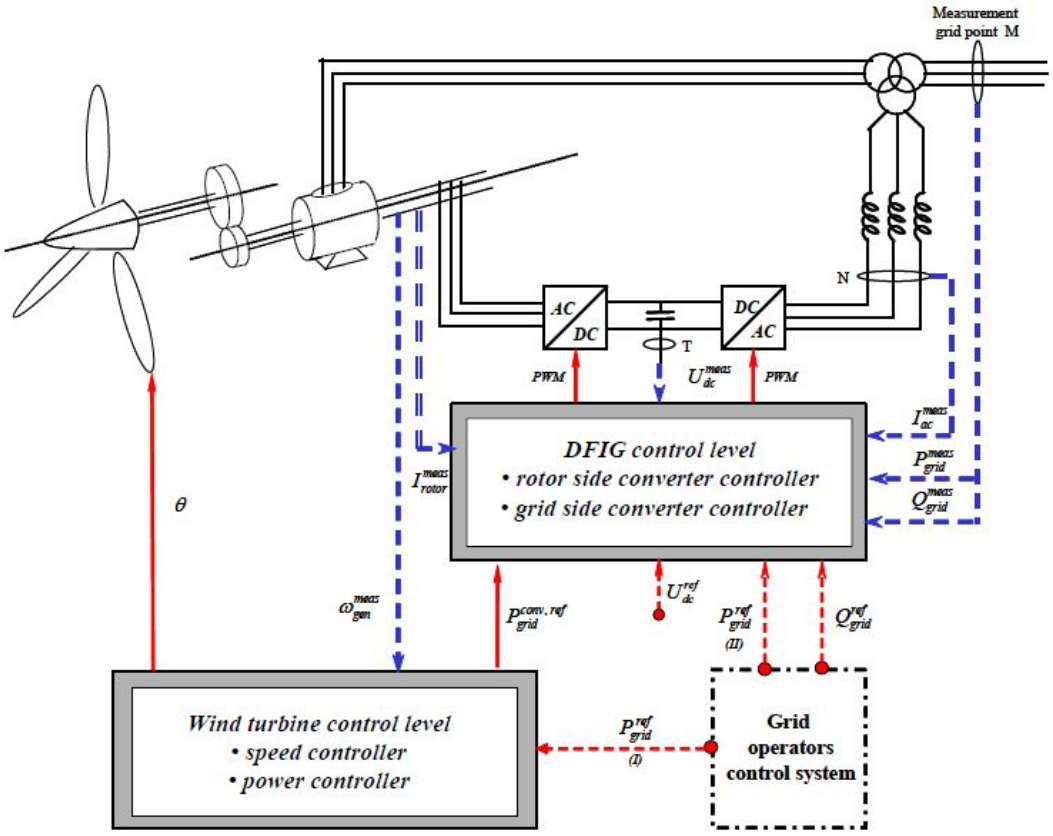

Figure 2-4: Overall control system of variable speed wind turbine with DFIG

In case of grid fault, the generator speed variation is not due to the wind speed change but due to electrical torque reduction. This means that the active power set-point $P_{grid}^{conv,ref}$ for the RSC has to be defined differently in case of grid fault, i.e. as the output of a damping controller. This controller has the task of damping the torsional oscillations that are excited in the drive train owing to the grid fault. When a fault is detected, the definition of the active power set-point is switched between the normal operation definition (i.e. MPT) and the fault operation definition (damping controller) as could be seen in Figure 2-5.

In case of grid fault, the PI damping controller produces the active power reference signal for the RSC control based on the deviation between the actual generator speed and its reference. The speed reference is defined by the optimal speed curve at the incoming wind.

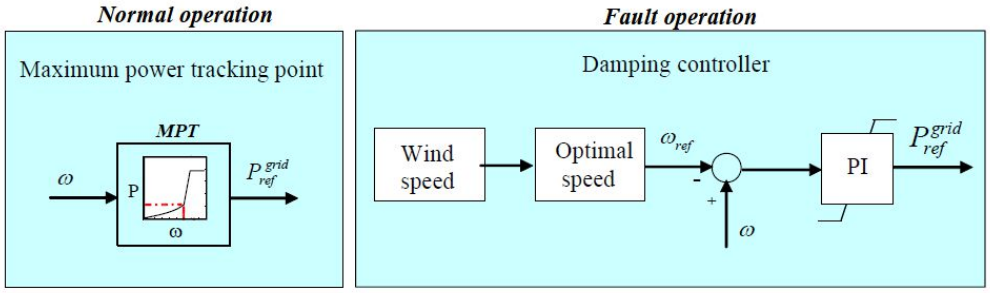

Figure 2-5: Definition of active power set-point for normal and fault operation, using MPT and damping controller respectively.

Type 3 wind turbine has been used in the Pan-European grid for the three wind turbine units connected in the AC grid part, while for the wind turbine unit in Cell 4 a wind turbine of Type 4, which is briefly described below, has been used.

The Type 4 turbine offers a great deal of flexibility in design and operation as the output of the rotating machine is sent to the grid through a full-scale back-to-back frequency converter. The turbine is allowed to rotate at its optimal aerodynamic speed, resulting in a "wild" AC output from the machine. In addition, the gearbox may be eliminated, so that the machine spins at the slow turbine speed and generates an electrical frequency well below that of the grid. This is no problem for a Type 4 turbine, as the inverters convert the power, and offer the possibility of reactive power supply to the grid, much like a STATCOM. The rotating machines of this type have been constructed as wound rotor synchronous machines, similar to conventional generators found in hydroelectric plants with control of the field current and high pole numbers, as permanent magnet synchronous machines, or as squirrel cage induction machines. However, based upon the ability of the machine side inverter to control real and reactive power flow, any type of machine could be used. Advances in power electronic devices and controls in the last decade have made the converters both responsive and efficient. It is worth mentioning, however, that the power electronic converters have to be sized to pass the full rating of the rotating machine, plus any capacity to be used for reactive compensation.

2.3. Dynamics analysis – RMS Simulation in DIgSILENT PowerFactory

The dynamics simulation functions available in DIgSILENT PowerFactory are able to analyze the dynamic behavior of small systems and large power systems in the time domain. These functions therefore make it possible to model complex systems such as industrial networks and large transmission grids in detail, taking into account electrical and mechanical parameters [7].

The study of power system stability involves the analysis of the behavior of power systems under conditions before and after sudden changes in load or generation, during faults and outages. The robustness of a system is defined by the ability of the system to maintain stable operation under normal and perturbed conditions. It is therefore necessary to design and operate a power system so that transient events (i.e. probable contingencies), can be withstood without the loss of load or loss of synchronism in the power system. Transients in electrical power systems can be classified according to three possible timeframes:

- Short-term, or electromagnetic transients;
- Mid-term, or electromechanical transients;
- Long-term transients.

The multilevel modeling of power system elements and the use of advanced algorithms means that the functions in PowerFactory can analyze the complete range of transient phenomena in electrical power systems. Consequently, there are three different simulation functions available:

- A basic function which uses a symmetrical steady-state (RMS) network model for mid-term and long-term transients under balanced network conditions;
- A three-phase function which uses a steady-state (RMS) network model for mid-term and long-term transients under balanced and unbalanced network conditions, i.e. for analyzing dynamic behavior after asymmetrical faults;
- An electromagnetic transient (EMT) simulation function using a dynamic network model for electromagnetic and electromechanical transients under balanced and unbalanced network conditions. This function is particularly suited to the analysis of short-term transients.

To carry out transient stability studies in this project the first type of simulation (Balance RMS simulation) has been used because only a symmetrical fault and balance events have to be analyzed. The balanced RMS simulation function considers dynamics in electromechanical, control and thermal devices. It uses a symmetrical, steady-state representation of the passive electrical network. Using this representation, only the fundamental components of voltages and currents are taken into account. Because of the symmetrical network representation, the basic simulation function allows the insertion of symmetrical faults only.

Time-domain simulations in PowerFactory are initialized by a valid load flow, and PowerFactory functions determine the initial conditions for all power system elements including all controller units and mechanical components. These initial conditions represent the steady-state operating point at the beginning of the simulation, fulfilling the requirements for the derivatives of all state variables of loads, machines, controllers, etc. to be zero.

Before the start of the simulation process, it is also determined what type of network representation must be used for further analysis, what step sizes to use, which events to handle and where to store the results.

In the Initial Conditions command (*ComInc*) dialogue, see Figure 2-6, all simulation settings can be defined, such as the simulation type (i.e. RMS or EMT, balanced or unbalanced) and simulation step size settings.

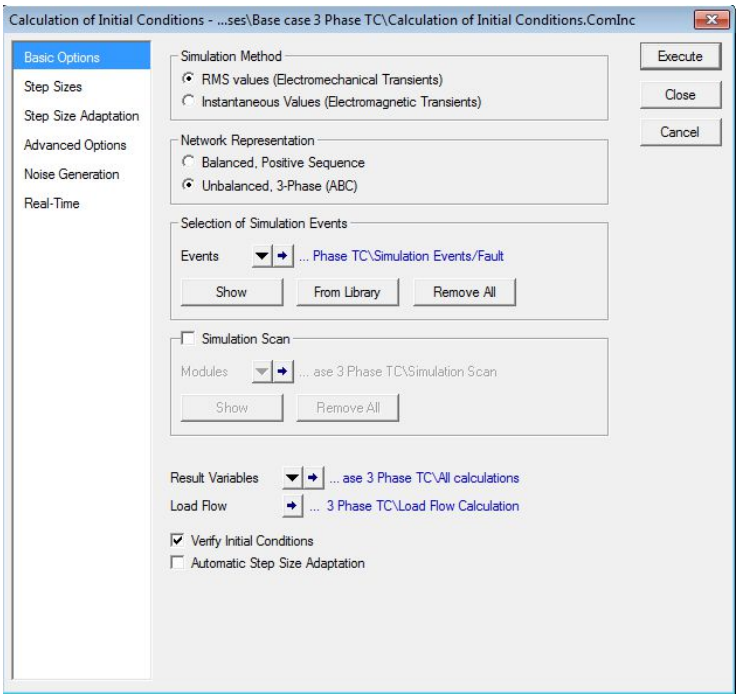

Figure 2-6: Initial conditions command dialogue window

The process of performing a transient simulation typically involves the following steps:

- Calculation of initial values, including a load flow calculation;
- Definition of result variables and/or simulation events;
- Optional definition of result graphs and/or other virtual instruments;
- Execution of simulation;
- Creating additional result graphs or virtual instruments, or editing existing ones;
- Changing settings, repeating calculations;
- Printing results.

During an EMT or RMS simulation, a large number of signal variables are changing over time. To reduce the available data and to narrow down the number of variables to those necessary for the analysis of each particular case, a selection of these signals for later use has to be defined. In this way it is necessary to define for each grid element which variables should be calculated, choosing from different category lists, such as Calculation Parameter, Element Parameter, Type Parameter, Reference Parameter, Bus Results, Signals and Currents, Voltages and Powers. As an example, in Figure 2-7 a variables selection window is shown. Therefore, one or more result objects containing the result variables can be configured. The simulation function needs the reference to a result object to store the results.

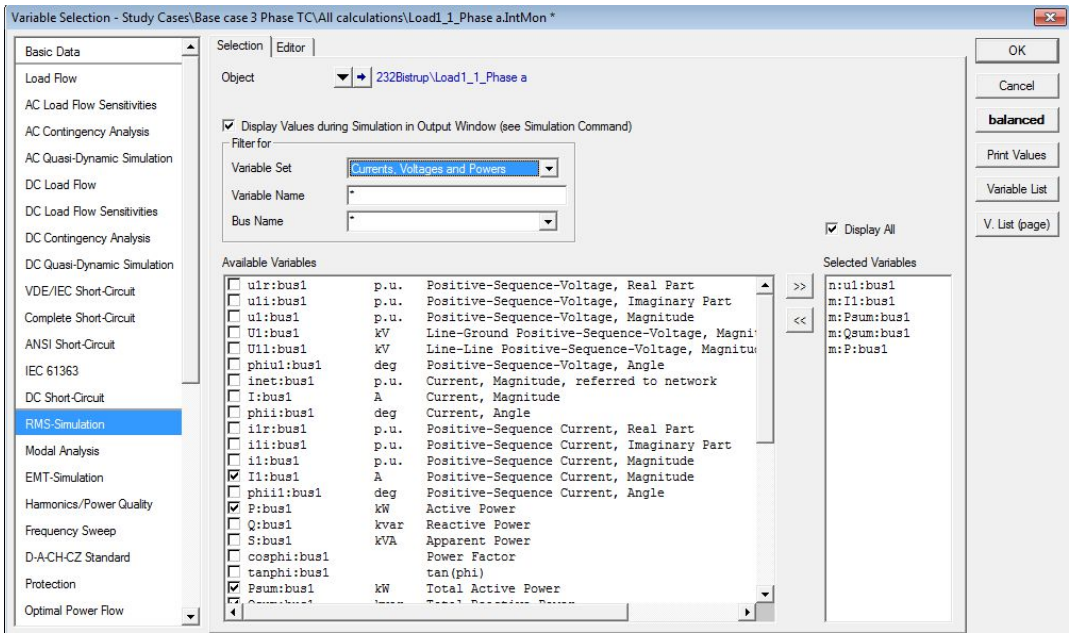

Figure 2-7: Variable selection window

Stability analysis calculations are typically based on predefined system models. In the majority of cases the standard IEEE definitions for controllers, prime movers and other associated devices and functions are used. Anyway it is otherwise possible to improve the system model by not using the IEEE standard models, and instead by building a new block diagram of the individual controller/mechanical system to represent the device. This facilitates highly accurate system modeling. The PowerFactory modeling philosophy is targeted towards a strictly hierarchical system modeling approach, which combines both graphical and script-based modeling methods. All the data, which represents power system Elements, Single Line Diagrams, Study Cases, system Operation Scenarios, calculation commands, program Settings etc., are stored as objects inside a hierarchical set of folders. The folders are arranged in order to facilitate the definition of the studies and optimize the use of the tools provided by the program. The objects are grouped according to the kind of element that they represent. These groups are known as 'Classes' within the PowerFactory environment. The basis for the modeling approach is formed by the basic hierarchical levels of time-domain modeling:

- The **DSL block definitions**, based on the "DIgSILENT Simulation Language" (DSL), form the basic building blocks to represent transfer functions and differential equations for the more complex transient models.

- The **built-in models** and **common models**. The built-in models or elements are the transient PowerFactory models for standard power system equipment, i.e. for generators, motors, static VAR compensators, etc. The common models are based on the DSL block definitions and are the front-end of the user-defined transient models.
- The **composite models** are based on **composite frames** and are used to combine and interconnect several elements (built-in models) and/or common models. The composite frames enable the reuse of the basic structure of the composite model.

The following part explains the relationships between the Composite Model (which is using a Frame as type) and the Common Model (based on a block diagram as type) in detail.

The Composite Model (*ElmComp*) references the definition of a composite frame. This composite frame is basically a schematic diagram containing various empty slots, in which controller or elements can be assigned. These slots are then interconnected according to the diagram. The slots in the composite frame are pre-configured for specific transient models.

The Composite Frame (*BlkDef*) has different slots which are interconnected according to the diagram. The composite model, which uses this composite frame, shows a list of the available slots and the name of the slot, as can be seen in Figure 2-8.

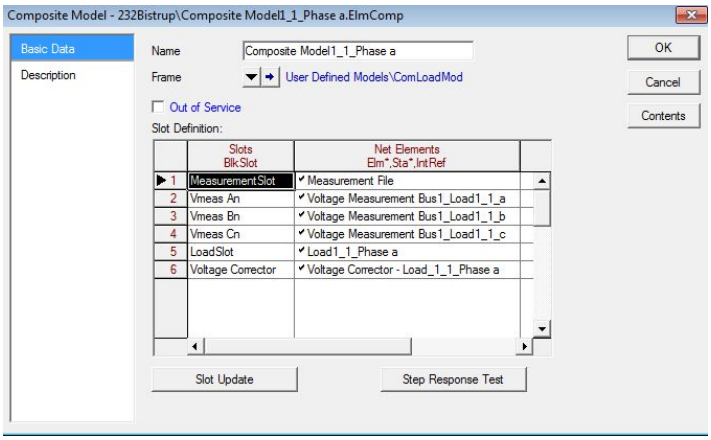

Figure 2-8: Composite model slots list window

The Built-In Models are pre-configured elements which do not need a specific model definition. Any kind of element which is able to provide input or output variables, e.g. converters, busbars, etc, can be inserted into the slots.

The Common Models (*ElmDsl*) combines a model definition with specific parameter settings. There are predefined definitions as well, so that users can create their own model definitions. The common model has a reference to the Model Definition (*BlkDef*), which looks similar to the composite frame. Here different blocks are defined and connected together according to the diagram. The input and output variables have to fit with the slot definition of the slot that the model is defined for. Usually not all slots of the composite model must necessarily be used: there can also be empty slots. In such cases, the input of this slot is unused and the output is assumed to be constant over the entire simulation.

2.4. Grid elements modeling in PowerFactory

2.4.1. Synchronous Generator

As presented in paragraph 2.1 the grid is fed by 8 conventional units, i.e. synchronous generator power plants. It has been decided to equip them with either a gas turbine governor or a hydraulic governor; the excitation system is similar for all of them. Both of them have been represented in PowerFactory with the predefined standard models. A brief description of the used model is reported in the following section.

The governor of gas turbine power plants has been simulated using the standard model GOV_GAST (Gas turbine governor). It represents the principal dynamic characteristics of industrial gas turbines driving generators connected to electric power system [7]. The model consists of a forward path with governor time constant and a combustion chamber time constant, together with a load-limiting feedback path. The load limit is sensitive to turbine exhaust temperature, and the time constant is considered to represent the exhaust gas measuring system. For the excitation system the standard model avr_IEEET1, named 1968 IEEE type 1 excitation system, has been used. This model is widely used to represent systems with shunt dc exciters as well as systems with alternator exciters and uncontrolled shaft-mounted rectifier bridges.

The governor of hydraulic power plants has been represented using the standard model HYGOV (Hydraulic turbine governor). It represents a straightforward hydroelectric plant governor, with a simple hydraulic representation of the penstock with unrestricted head race and tail race, and no surge tank. For the excitation system the same standard model used for the gas turbine power plants, i.e. avr_IEEET1 (1968 IEEE type 1 excitation system), has been used.

2.4.2. Wind turbine (DFIG Generators)

The predefined wind turbine template "DFIG WTG xMW", from the PowerFactory template library, was used for modeling the DFIG wind turbines. This template is a generic model of a wind turbine with a doubly fed induction generator. The model represents one wind turbine but the number of parallel machines can be also changed. The model accounts for the PQ characteristics and short-circuit contribution of the generator (steady-state analysis), the dynamic controllers of the DFIG and converters as well as the mechanical part of the rotor and the aerodynamics. The model from the template is equipped with the 20 kV transformer.

The doubly fed induction generator (DFIG) is represented, in the single line diagram, by an asynchronous machine which is configured as a DFIG. The model of the controller and the dynamic parts are collected in the composite model DFIG Control. The composite model DFIG Control is created from the frame definition Generic DFIG-Turbine_resync. The graphical definition of this frame is shown in Figure 2-9.

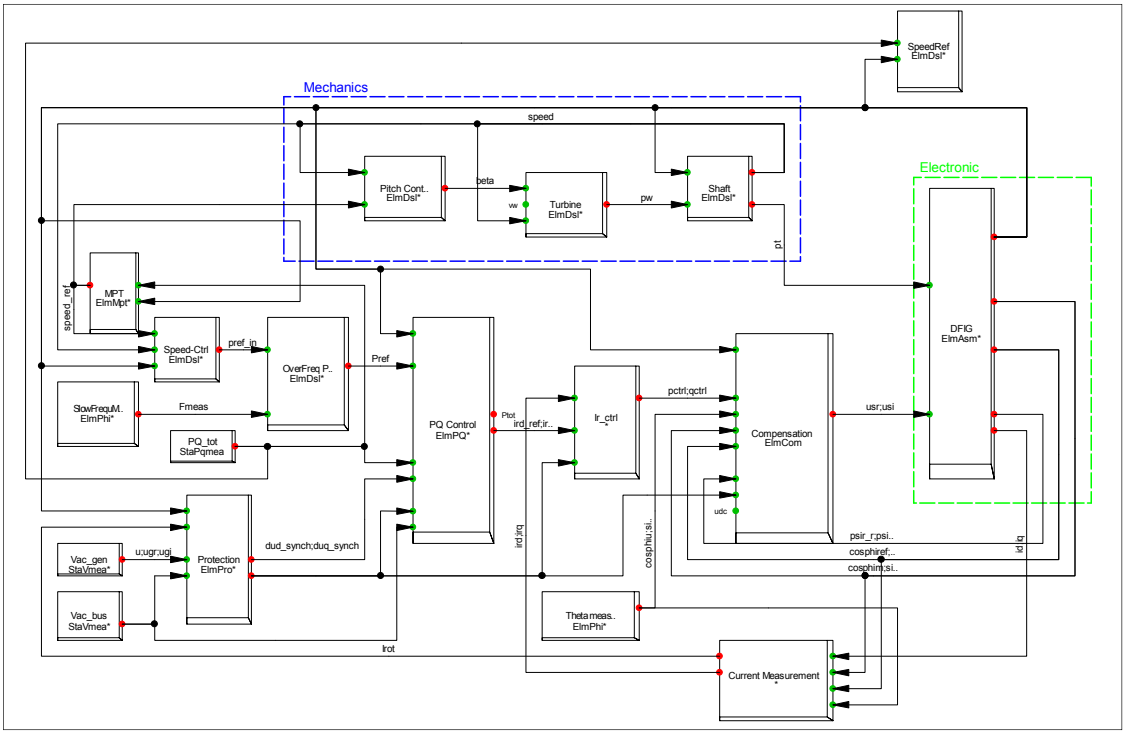

*Figure 2-9: Frame definition generic DFIG-Turbine_resync(.*BlkDef)*

The single slots are briefly described in Table 2-2. Each slot could be filled with either a DSLmodel, a measurement device or a PowerFactory element, such as an asynchronous machine. All measurement devices are connected either to the terminal or to the cubicle, which connects the generator with the terminal.

Slot name	Description	Needed type
Compensation	This models calculates a coordinate transformation of the rotor voltage	DSL-Model
Current Measurement	Calculates the rotor current from angle and id/iq of the DFIG	DSL-Model
DFIG	Asynchronous machine, configurated as DFIG	*.ElmAsm
Ir-ctrl	Calculates a rotor reference voltage for a given rotor current set point	DSL-Model
MPT	Maximum power tracker, calculates optimal speed for max. power	DSL-Model
OverFreq Pwr Reduction	Reduces the power in case of electrical over frequency	DSL-Model
Pitch Control	Controls the pitch angle of the rotor	DSL-Model
PQ Control	Controls active and reactive power through the rotor current	DSL-Model
PQ_tot	Active and reactive power measurement device	*.StaPqmea
Protection	Triggers bypass, in case of high rotor current, high speed or over voltage. Could also disconnect and resynchronize the DFIG	DSL-Model
Shaft	Calculates from wind power and generator speed the mechanical power and the rotor speed	DSL-Model
SlowFrequMeas	Slow frequency measurement device (PLL)	*.ElmPhi
Speed-Ctrl	Calculates a reference power from speed and reference speed	DSL-Model
SpeedRef	Reference speed, needed only for initialisation of the mechanical generator speed	DSL-Model
Theta meas.	Fast frequency and voltage angle measurement device (PLL)	*.ElmPhi
Turbine	Calculates from pitch angle, rotor speed and wind speed the wind power	DSL-Model
Vac_bus	AC-voltage measurement device on bus side	*.StaVmea
Vac_gen	AC-voltage measurement device on generator side	*.StaVmea

Table 2-2: Frame description of DFIG composite frame

It should be noted that the Speed-Ctrl block definition in the composite frame contains the block PI that has the task of damping the torsional oscillation excited at a grid fault in the drive train system, as explained in Chapter 2.2. As shown in Figure 2-10 the controller gives the reference power signal to the next controller through the PI controller from the difference between the speed and the reference speed coming from the MPT controller.

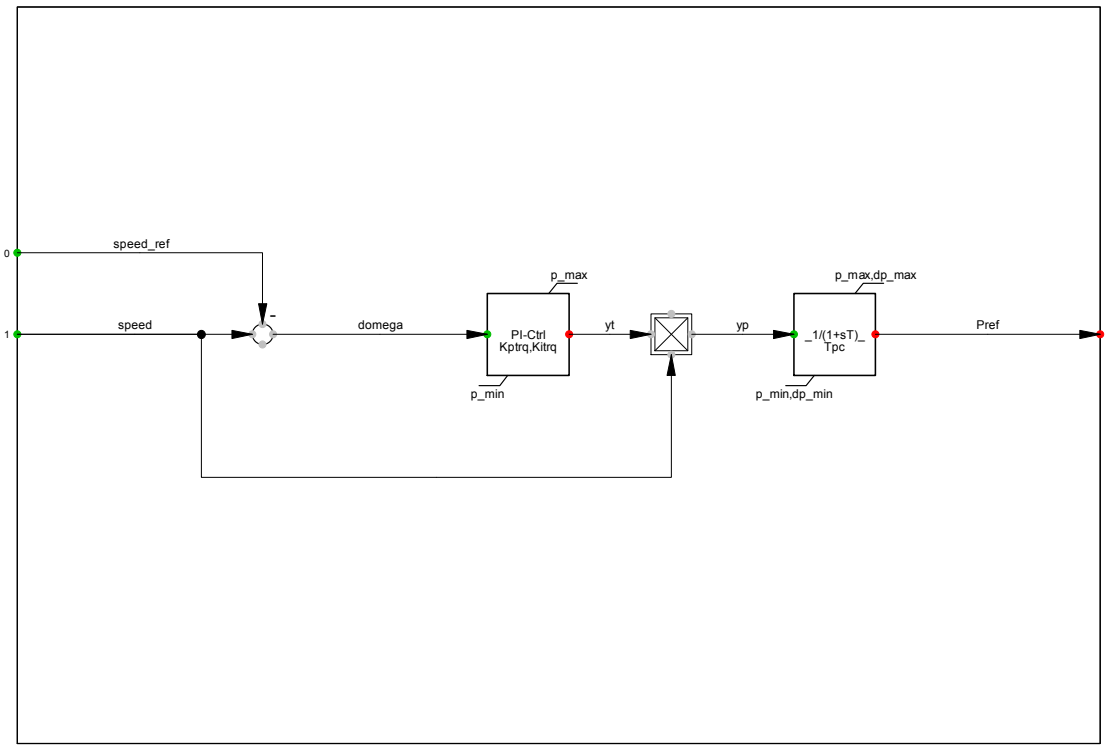

Figure 2-10: Speed Ctrl controller

2.4.3. Load

Loads can be modeled according to the classic ZIP (const impedance Z, const current I and const power P) theory [16]. The polynomial model, commonly referred as ZIP model, has been widely used to present the voltage dependency of loads.

$$P = P_0[p_1 \bar{V}^2 + p_2 \bar{V} + p_3] \quad (2\text{-}1)$$

$$Q = Q_0[q_1 \bar{V}^2 + q_2 \bar{V} + q_3] \quad (2\text{-}2)$$

In the equations (2-1) and (2-2) $\bar{V} = \frac{V}{V_0}$ and V_0, $P_0$and Q_0 are rated values. The proportion of each component is defined by the coefficients p_1 to p_3 with the relation $p_1 + p_2 + p_3 = 1$, and q_1 to q_3 , $q_1 + q_2 + q_3 = 1$. Loads have also been modeled to have frequency dependency.

In PowerFactory the dynamic voltage and frequency dependency of loads is represented by the block diagrams shown in Figure 2-11.

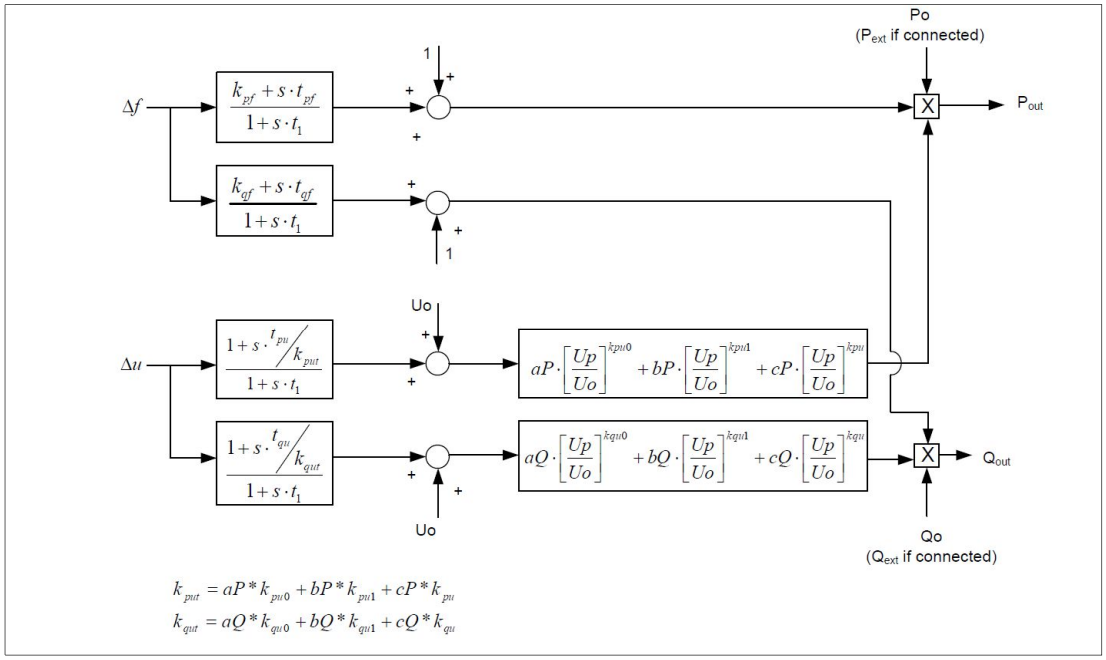

Figure 2-11: Model used to approximate the behavior of the non-linear dynamic load

The values of the parameters, used for the frequency dependency of loads in the block diagrams, are usually $k_{pf} = \frac{\partial P}{\partial f} = 0 \sim 3.0$ and $k_{qf} = \frac{\partial Q}{\partial f} = -2.0 \sim 0$. [16]

As the block diagram, shown in Figure 2-11, represents small signal models, it is only valid over a limited voltage range. This range is defined by the variables u_{min} and u_{max} , set respectively in the model to 0.8 and 1.2. When the voltage is outside of this threshold the load is converted to constant impedance load to avoid computational problems.

For modeling the voltage dependency of load in PowerFactory three polynomial terms are used as shown in (2-3) and (2-4) .

$$P = P_0 \left(aP * \left(\frac{v}{v_0}\right)^{e\_aP} + bP * \left(\frac{v}{v_0}\right)^{e\_bP} + (1 - aP - bP) * \left(\frac{v}{v_0}\right)^{e\_cP} \right) \tag{2-3}$$

$$Q = Q_0 \left(aQ * \left(\frac{v}{v_0}\right)^{e\_aQ} + bQ * \left(\frac{v}{v_0}\right)^{e\_bQ} + (1 - aQ - bQ) * \left(\frac{v}{v_0}\right)^{e\_cQ} \right) \tag{2-4}$$

In equation (2-3) and (2-4) , the subscript "0" indicates the operating point values as defined on the Load Flow page of the load element dialog and $1 - aP - bP$ is equal to cP and $1 - aQ - bQ = cQ$. The exponents e_aP, e_bP, e_cP and e_aQ, e_bQ, e_cQ can be 0,1 and 2 respectively. The load behavior can be modeled by specifying the values of the parameters aP, bP and aQ, bQ, as shown in Table 2-3, on the Load Flow page in the dialog of the general load type.

constant	power	current	impedance
aP, aQ	1	0	0
bP , bQ	0	1	0
cP=1-aP-bP CQ=1-aQ-bQ	0	0	1

Table 2-3: Selection of values for different load model behavior

In the analysis it has been assumed that the loads have a frequency-dependent behavior, in fact in the case of motor loads, such as fans and pumps, the electrical power changes with frequency due to changes in motor speed. Moreover it has been assumed that the active power consumption is linearly dependent on voltage value (constant current behavior $aP = 0, bP = 1$) and linearly dependent on frequency, i.e. $k_{pf} = \frac{\partial P}{\partial f} = 1.5$. The reactive power consumption is quadratically dependent on voltage (constant impedance behavior $aQ = 0, bQ = 0$) and inversely dependent on frequency, i.e. $k_{qf} = \frac{\partial Q}{\partial f} = -1$.

2.4.4. HVDC capacitors

In the HVDC grid five DC capacitors have been inserted in the buses where the converters are connected. The DC capacitors are the energy storage elements for VSC (voltage-source-converter) and they have several primary functions:

- They provide a low-inductance path for switch turnoff current;
- They provide temporary energy storage between the switching instant, stabilizing high frequency dynamics;
- They reduce the DC voltage harmonic ripple;
- They decrease the harmonics coupling between different VSC substations connected to the same DC bus.

To estimate the capacitor size it is possible to use a practical formula [17] :

$$C_{dc} = \frac{2\, S_{VSC}\, E_s}{V_{dc}^2} \tag{2-5}$$

Where S_{VSC} is the converter MVA rating, V_{dc} is the rated DC voltage and E_s [J/VA] is the energy-to-power ratio, in practical converters is 10 (kJ/MVA) < E_s> 50 (kJ/MVA). In the analyzed case E_s has been considered as 20 kJ/MVA and the resulting capacitor size is 38 μF.

2.4.5. Converters

In the analyzed grid there are 5 converters, PWM 1.2, PWM 4.1, PWM 4.2, PWM 4.3 and PWM 4.8. The latter is that of the offshore wind park while the others are part of the onshore grid. The converter PWM 4.3 is configured as a master controller for the DC voltage. Indeed a master-slave control has been used [18]. Only one converter in the DC grid is configured to constant DC mode while all the others are configured to constant power mode, as slave terminals. In the DC grid there is also a wind park so the controller in that terminal, PWM 4.8, must control the frequency, to give it a reference, and the AC voltage.

Basically in this grid three different types of controller have been used: Controller_Vac_Vdc, for the master converter, Controller_P_Vac, for the slave PWM, and Controller_Vac_freq for the converter of the offshore wind park. Consequently three types of frame, Frame_Vac_Vdc, Frame_P_Vac and Frame_Vac_freq have been used. A description of all the types of controllers and frames used in the grid is reported below.

- **Controller_P_Vac**

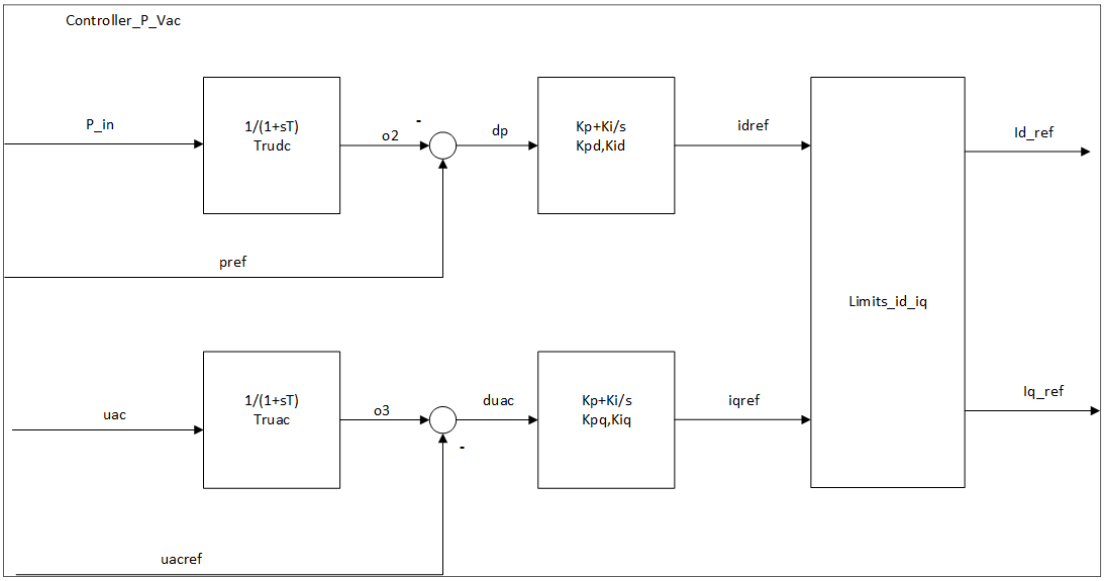

Figure 2-12: Block definition of the Controller_P_Vac

This type of controller is used as model definition for the main controller of the converters PWM 1.2, PWM 4.1 and PWM 4.2 named respectively Common Model_P_Vac_1.2, Common Model_P_Vac_4.1 and Common Model_P_Vac_4.2.

The controller, shown in Figure 2-12, has as input the AC voltage uac and the power P_in, coming from measurements in the related bus. The measurement delay is represented by a first order delay block $\frac{1}{1+s\,T}$ in the scheme. After this first block there is a comparison with the real reference magnitude: $pref$, for the power, and $uacref$, for the voltage. The resulting errors are inserted into a PI block $kp + \frac{ki}{s}$ that gives as output the currents $idref$ and $iqref$. These two currents are used as an input for a limits block which is necessary to link the magnitude of the two currents. In fact the currents id and iq are linked by the relation $I = \sqrt{id^2 + iq^2}$ and the amplitude is fixed at $I = 1.1\,p.u.$ This relation is also explained in Figure 2-13.

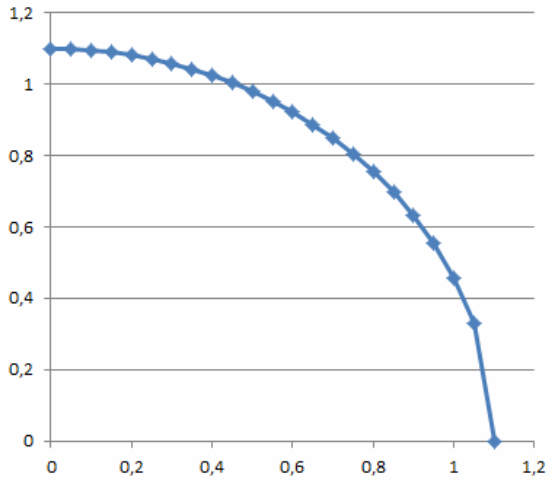

Figure 2-13: Current limit characteristic of onshore controller

The relationship between the two currents has been inserted in the block definition of the Limits_id_iq block as could be seen in Figure 2-14.

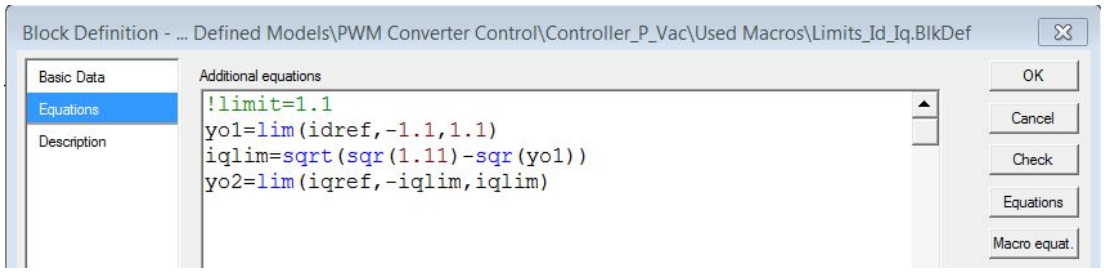

Figure 2-14: Additional equation added in the block definition of the limits block to link the magnitude of the id and iq current

Finally, this controller has as outputs the reference current id_ref and iq_ref.

After modeling the controller it is very important to set the correct initial conditions. The initial conditions are calculated so that the first derivative of the equation is equal to zero (i.e. steady state condition). Initial conditions should be calculated for all the state variables used in the blocks. For example, for the measurement delay block the state variable is x and the block definition equations are: $yo = x$ and $x. = \frac{yi-x}{T}$. For the steady state condition $x. = 0$ so $x = yi = yo$. Consequently the initial condition for the variable x must be equal to the input variable that is P_in. Doing the same for the measurement delay of the voltage (state variables = $x2$), the initial condition obtained is $inc(x2) = uac$.

In the case of the PI blocks for the d axes the state variable is $x1$ and for the q axes the state variable is $x3$ and the block definition equations are: $yo = x$ and $x. = ki * yi$.

For steady state condition $x.=0$ so $x=yi=yo$ and the initial conditions of the state variables of these block are $inc(x1)=idref$ and $inc(x3)=iqref$.

It is also necessary to put in an initial value for the currents id_ref and iq_ref. This value can be a random value. In steady state $id\_ref=idref$ and $iq\_ref=iqref$ so $inc(idref)=id\_ref$ and $inc(iqref)=iq\_ref$.

The reference values of power and voltage $pref$ and $uacref$ are been set as equal to the measured one: $inc(uacref)=uac$ and $inc(pref)=P\_in$.

Figure 2-15 shows the initial condition of all the state variables in the controller.

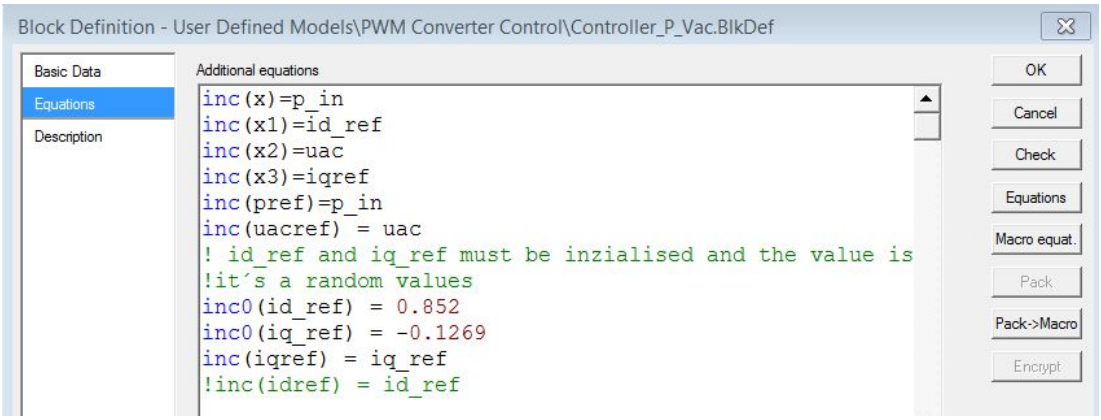

Figure 2-15: Additional equation added in the block definition of the controller to settle the initial condition

For all the three common model associated with this controller (Common Model_P_Vac_1.2, Common Model_P_Vac_4.1, Common Model_P_Vac_4.2) the same values for the parameters $Trudc$, $Truac$, Kpd, Kid, Kpq and Kiq of the blocks have been used. The values assigned are reported in Table 2-4:

Trudc =	0.001
Truac =	0.001
Kpd =	10
Kid =	10
Kpq =	10
Kiq =	10

Table 2-4: Values for the parameters used in the Common Model_P_Vac

- **Frame_P_Vac**

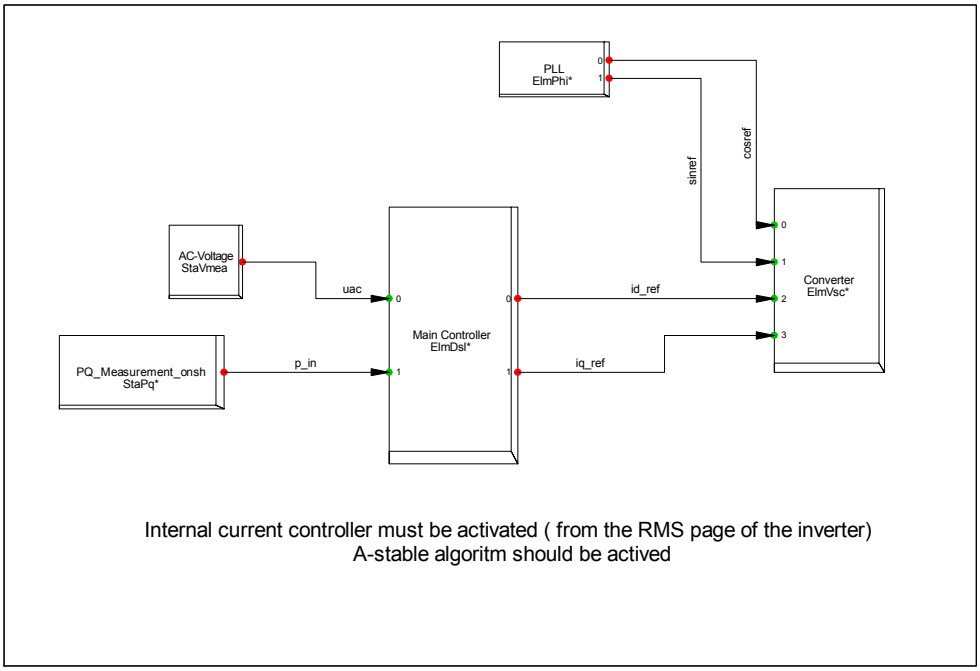

Figure 2-16: Composite Frame of converters 1.2, 4.1 and 4.2

In the frame, shown in Figure 2-16, there are two main slots, Main Controller and Converter, and three measurement slots: AC-Voltage, for the AC voltage measurement, PQ_Measurement_onsh, for the power measurement, and PLL for the Phase measurement device. This device is used for the measurement of cosφ and senφ. The slot Main Controller is related to the Controller_P_Vac described before while the Converter slot has been linked to the relative PWM converter. This frame has been associated with three composite models: Onshore Controller_P_1.2, Onshore Controller_P_4.1 and Onshore Controller_P_4.2.

- **Controller_Vac_Vdc**

This type of controller, shown in Figure 2-17, is used as model definition for the main controller of only the converters PWM 4.3, named Common Model_Vac_Vdc_4.3. In fact, as said before, the converter 4.3 is the master controller for the DC grid and has the task to control the DC voltage.

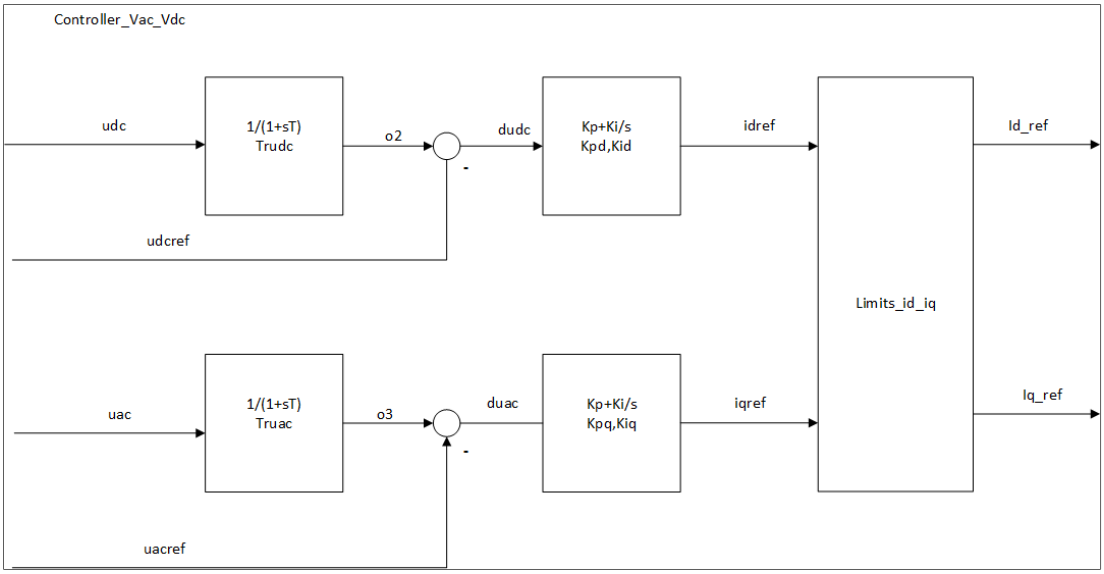

Figure 2-17: Block definition of the controller of the converter 4.3

This type of controller is similar to Controller_P_Vac but it differs in the input; instead of the active power measurement the input is the DC voltage udc coming from a real measurement in the relative bus. The initial condition of all the state variables in the controller has been calculated in the same way as explained for the slave controller. Their values are shown in Figure 2-18.

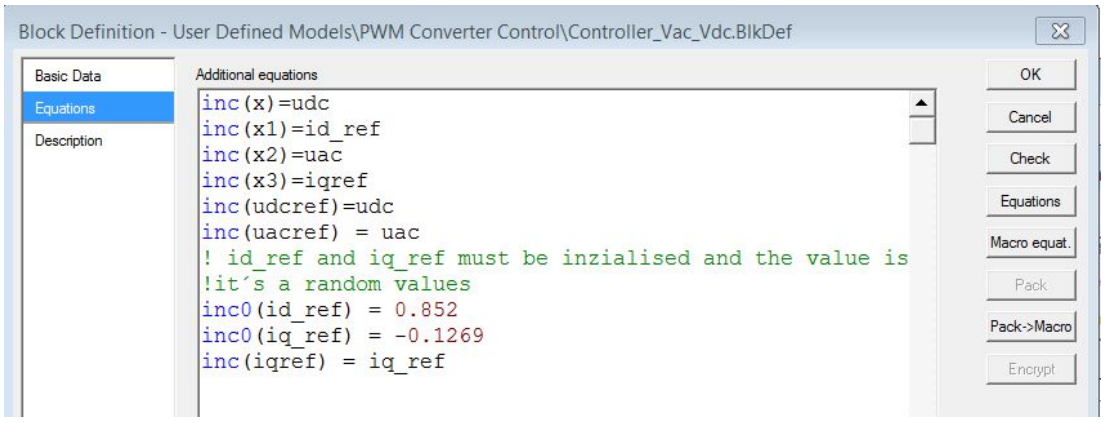

Figure 2-18: Additional equation added in the block definition of the controller to settle the initial condition

For the Common Model_Vac_Vdc_4.3, associated with this controller, the same values used in the previous common model for the parameters $Trudc$, $Truac$, Kpd, Kid, Kpq and Kiq of the blocks have been utilized. The values are reported in Table 2-4.

- **Frame_Vac_Vdc**

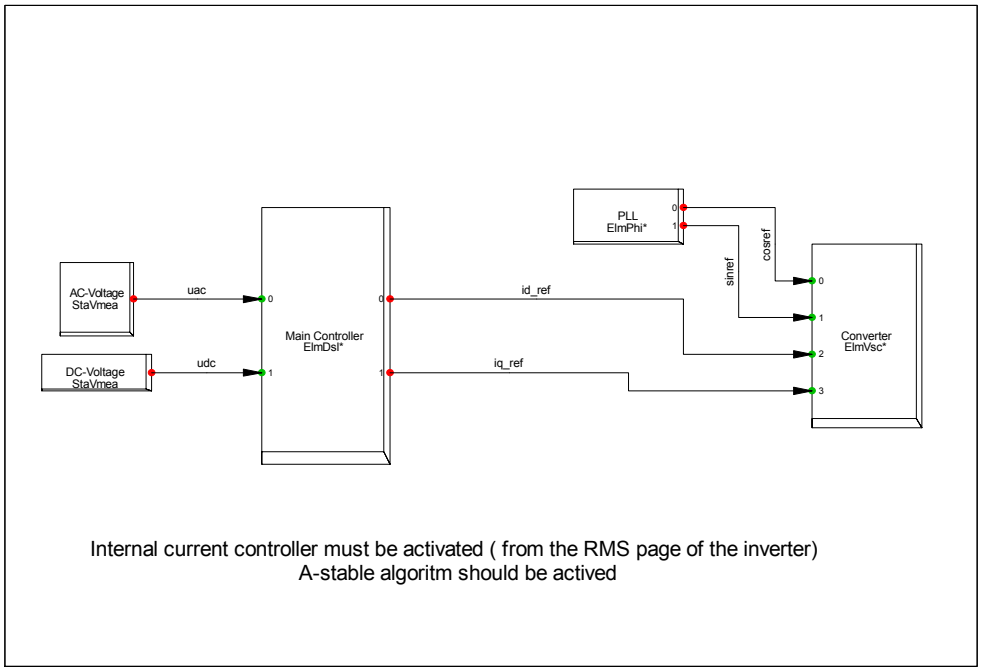

Figure 2-19: Composite Frame of converter 4.3

In the frame shown in Figure 2-19 there are two main slots, Main Controller and Converter, and three measurement slots: AC-Voltage, for the AC voltage measurement, DC-Voltage for the DC voltage measurement, and PLL for the Phase measurement device. This device is used for the measurement of cosφ and senφ.

The slot Main Controller is related to the Controller_Vac_Vdc, described before, while the Converter slot has been linked to the relative PWM converter. This frame has been associated with the composite model Onshore Controller_4.3.

- **Controller_Vac_freq**

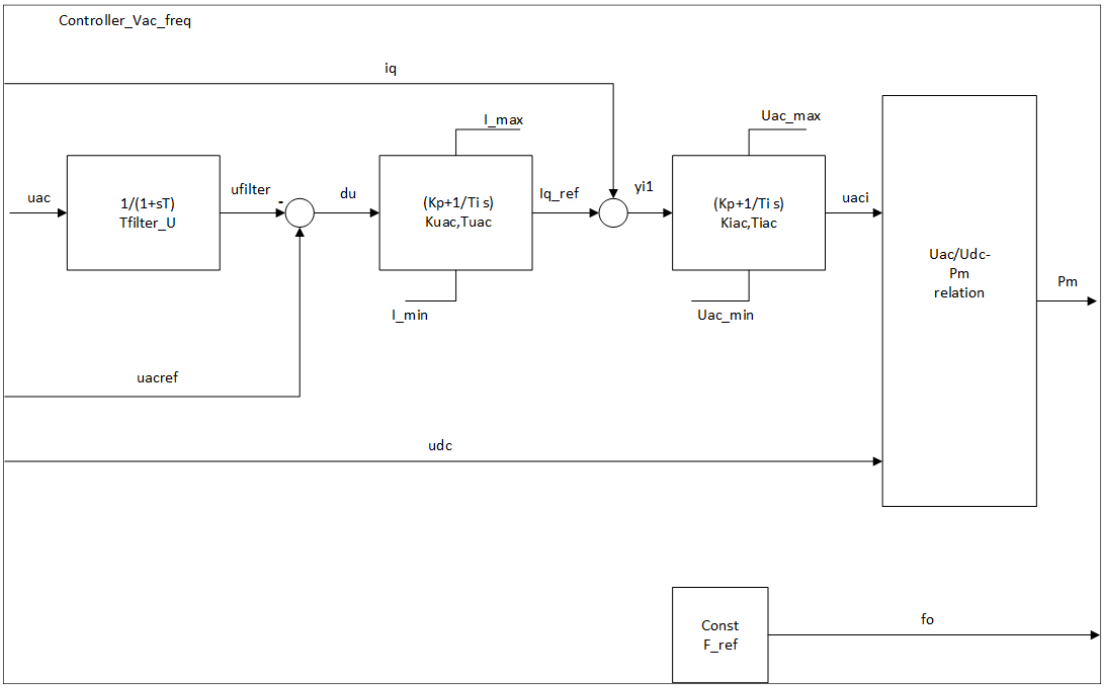

Figure 2-20: Block definition of the controller of the converter 4.8

This type of controller, shown in Figure 2-20, is used as a model definition for the main controller of the offshore wind park PWM 4.8 named CommonModel_Vac_freq.

This controller has as an input the AC voltage, uac, coming from a measurement made in the relative bus. To account for the measurement delay a first order delay block has been inserted. After that a comparison has been made with the real reference magnitude, $uacref$. The resulting error is inserted into a PI block with upper and lower limits. This means that the output value must be 0 if the condition $(Kp * yi + x) \geq y\_max$ or the condition $(Kp * yi + x) \leq y\_min$ are met. Otherwise the value must be $\frac{yi}{Ti}$. The upper and the lower limitation in this case are i_max and i_min. The output of the PI block is the quadrature axis current Iq_ref. This current has then been compared with the real iq current coming from a feedback loops. Like the other controllers the resulting error is inserted into a PI blocks with upper and lower limits, Uac_max and $\_min$. The resulting values, $uaci$, is then inserted with the DC voltage, udc, coming from a measurement in the relative bus, in a block called Uac/Udc-Pm relation. This type of block explains the relation between the AC voltage/DC voltage and the pulse-width amplification factor Pm of the PWM. This relation is shown in Figure 2-21.

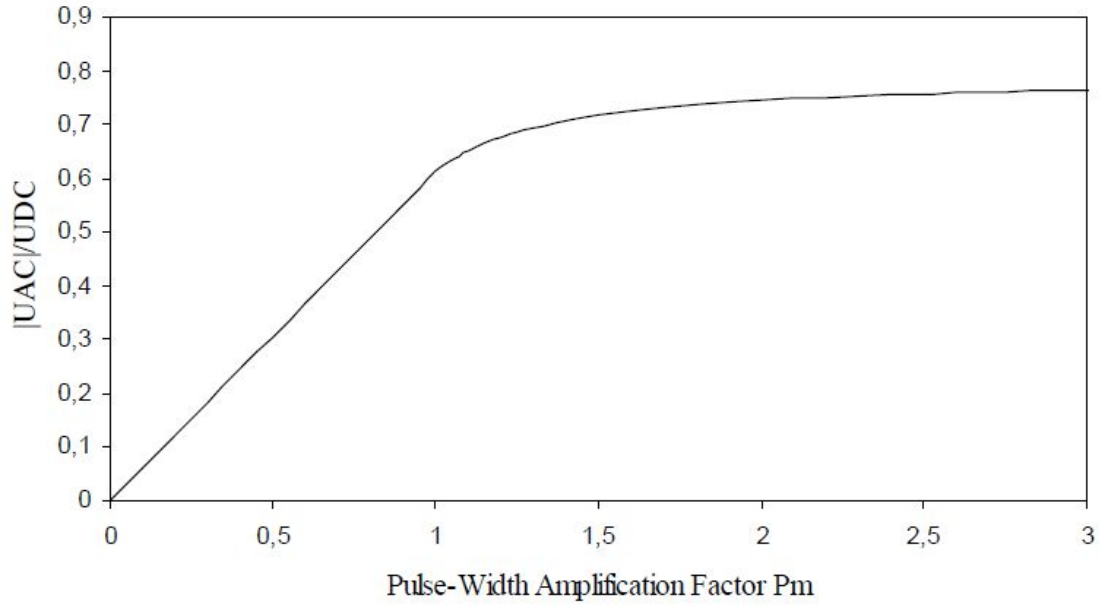

Figure 2-21: PWM converters characteristic

The nonlinear relation between Uac/Udc and Pm could be approximated with five linear relations as shown in Table 2-5.

Pm<1	Uac/Udc<0.6	$pm1 = \frac{uaci/udci}{0.6}$
1 < Pm > 1.25	0.6< Uac/Udc > 0.69	$pm2 = \frac{uaci/udci - 0.24}{0.36}$
1.25 < Pm > 1.5	0.69 < Uac/Udc > 0.72	$pm3 = \frac{uaci/udci - 0.54}{0.12}$
1.5 < Pm > 2	0.72 < Uac/Udc > 0.75	$pm4 = \frac{uaci/udci - 0.63}{0.06}$
2 < Pm > 3	0.75 < Uac/Udc > 0.76	$pm5 = \frac{uaci/udci - 0.73}{0.01}$

Table 2-5: Linear relation for approximate the PWM converter characteristic

The output of the Controller_Vac_freq are the pulse-width amplification factor Pm and the constant reference frequency fo.

Initial conditions of all the state variables in the controller, see Figure 2-22, are calculated in the same way as before. For the measurement delay block, with the state variable xu, the

block definition equations are $yo = x$ and $x. = \frac{yi-x}{T}$ and for steady state should be $x. = 0$. For steady state condition $x = yi = yo$ that implies that $inc(xu) = uac$.

For the first PI controller with limits, state variable $x1$, the initial condition must be $inc(x1) = 0$. In fact:

$$x. = select(\{(Kp * yi + x) >= y\_max\}.or.\{(Kp * yi + x) <= y\_min\},0, yi/Ti)$$

$$yo = lim(Kp * yi + x, y\_min, y\_max)$$

And to have $x. = 0$ the variable yi must be equal to zero and from the second equation $yi = 0$ means $x = yo$. In this case yo must be 0 in steady state. Doing the same for the second PI controller with limits, state variable $x2$, for having $x = yo$ the variable $x2$ must be equal to $uaci$ but from the relation $Pm = {uac}/{udc} * {1}/{0.6}$ and $uac = Pm * udc * 0.6$ so $inc(x2) = Pm * udc * 0.6$.

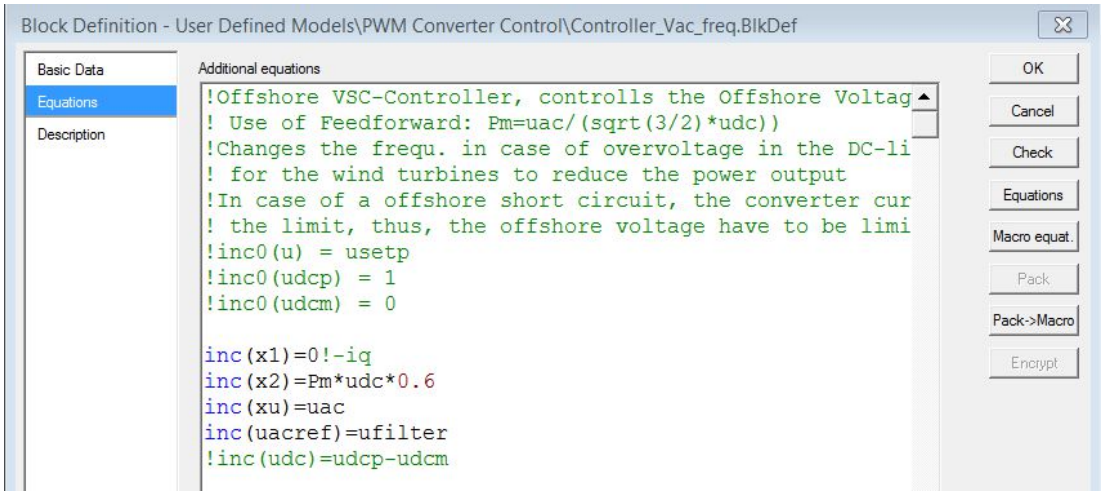

Figure 2-22: Additional equation added in the block definition of the controller to settle the initial condition

This controller has been associated to a Common Model_Vac_freq. The values assigned to the parameters $Kuac$, $Tuac$, $Kiac$, $Tiac$, F_ref, $Tfilter\_U$, i_min, Uac_min, I_max and Uac_max of the blocks are reported in Table 2-6.

Kuac =	2
Tuac =	0.2
Kiac =	2
Tiac =	0.02
F_ref =	1
Tfilter_U =	0.005
i_min =	-0.7
Uac_min =	-0.1
I_max =	0.7
Uac_max =	1.1

Table 2-6: Valuies of the parameters used in Common Model_Vac_freq

- **Frame_Vac_freq**

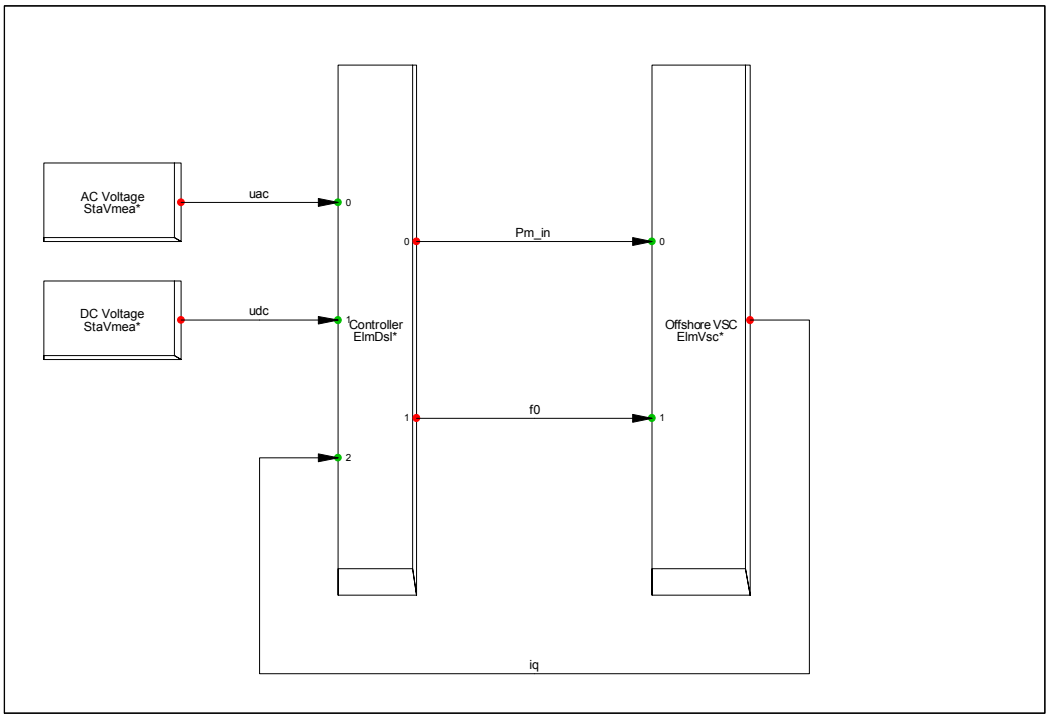

Figure 2-23: Composite Frame of converter 4.8

In the frame shown in Figure 2-23 there are two main slots, Controller and Offshore VSC, and two measurement slots: AC-Voltage, for the ac voltage measurement and DC-Voltage , for the dc voltage measurement. The slot Controller is related to the Controller_Vac_freq described in the previous section, while the Offshore VSC slot is been linked to the relative PWM converter. This Frame has been associated with the Composite Model Offshore Controller_4.8.

Chapter 3

Scenarios Definition

To study the behaviour of the Pan-European grid in the Task 5.4 of the project ELECTRA, it has been decided to define eight scenarios with different cases of penetration of renewable energy sources (RES). In this chapter the description and the configuration of all eight scenarios are reported. Since not all of them have been used for performing the simulation in this thesis a specific subparagraph has been inserted to motivate the choice. The final part of this chapter includes a brief review of regulations' voltage and frequency limits that have to be taken into account in light of the grid characteristics.

3.1. Scenarios definition

The behavior of the Pan-European grid is been analyzed by defining eight different scenarios. These scenarios consider several levels of renewable sources penetration and different numbers of synchronous machines connected. The index $\%\, REN = P_{ren}/P_{load}$ is been used to count the amount of renewable resources penetration in each scenarios. This is defined as the division between the total power generation, P_{ren}, coming from renewable resources and the total amount of power requested by the loads P_{load}.

As said in Chapter 2, the grid can be fed by conventional generation units, as synchronous generators, as well as by renewable wind power generating units. The main characteristics of the conventional generation units are reported in Table 3-1.

Synchronous machines Snom=500MVA		
Snom [MVA]		500
Pnom [MW]		425
Number of units per cell	Cell 1	4
	Cell 2 SL	2
	Cell 3	2
	Cell 4	0
Total conventional generation[MVA]		4000
cos φ		0,85
Total conventional generation [MW]		3400

Table 3-1: Conventional synchronous generation characteristic

The nominal consumption P_{load}, reported in Table 3-2, has been considered constant in all the cases.

Load [MW]	
Cell 1	1000
Cell 2	1200
Cell 3	400
Cell 4	0
Total load[MW]	2600

Table 3-2: Load consumption in each cell

The main characteristics of all the defined scenarios are reported in Table 3-3.

	%REN	Pren (MW)	number of conventional generators enabled	Pgen (MW)	% Pgen	Total inertia 2H (s)
Scenario 1	0%	0	8	325	76	10
Scenario 2	25%	650	8	244	57	10
Scenario 3	25%	650	6	325	76	7.5
Scenario 4	50%	1300	6	217	51	7.5
Scenario 5	50%	1300	4	325	76	5
Scenario 6	75%	1950	3	217	51	3.75
Scenario 7	75%	1950	2	325	76	2.5
Scenario 8	90%	2340	2	130	31	2.5

Table 3-3: Definition of the scenarios

From the first scenario to the last one the penetration of renewable energy resources has been increased. In fact, at the beginning the conventional generation is still preponderant in the grid while in the latest scenario the majority of the synchronous generators are disabled in favor of wind generation. This consideration respects the reality, as renewable energy resources (RES) will have a dominant role in new capacity addition over the upcoming years. While RES-HPP(Hydro Power Plants) net generation capacity is expected to remain stable until 2025, the installed wind and solar net generation capacity are forecast to increase by 80% and 60% respectively [19].

The first scenario (Scenario 1) considers only conventional generation with all the renewable resources and the HVDC grid disabled. The other scenarios (Scenario from 2 to 7) consider an increasing penetration of unconventional generation units until the last one (Scenario 8) that considers a renewable penetration of 90% with only two conventional synchronous generator enabled. The last case can also be representative of the reality over the upcoming years. By 2025, 22 countries in the EU are expected to have a RES capacity penetration level higher than 50%. [19] Eight countries, such as Denmark, Germany, Great Britain, Greece, Ireland, Northern Ireland, Netherlands and Portugal, will reach full hourly load penetration level (100%). However, it should be noted that this result does not mean 100% penetration occurs simultaneously for these eight countries on the same hour.

In Table 3-3 $\%P_{gen}$ is defined as $\%\ P_{gen} = \frac{P_{gen}}{P_{nom}} * 100$ and identifies the percentage of the rated power each conventional unit is providing to the grid. For each scenario the total inertia, 2H, of the system has also been calculated. This is calculated as:

$$2H = \frac{\sum_{i=1}^{n} 2Hi * Si}{\sum_{i=1}^{n} Si} \tag{3-1}$$

In equation (3-1) Hi and Si are respectively the inertia constant and the nominal apparent power of the i^{th} generator, with n the number of total generators in the grid. The inertia constant Hi of all the synchronous generators in the grid has been considered equal to 5 s.

As could be seen in Table 3-3 with decreasing conventional generation the total inertia of the grid decreases. In fact in the grid only the conventional rotating generation is providing inertia to the system.

In each scenario the active power generation provided by unconventional generation is split in two parts. Half (50%) of this power is provided equally by the three wind parks with

DFIG, the remaining 50% is given by the type 4 wind generator unit and then managed by the full converters in the HVDC grid.

It has to be noted that the number of DFIG wind turbines in each of the three wind parks has remained constant in all the scenarios and is equal to 65. With the increase in RES generation, from Scenario 2 to Scenario 8, it is the set point of the wind turbines power production that changes.

3.1.1. Scenario 1

The first scenario could be seen as a reference for all the further analysis, in fact this case presents only conventional generation. Only the eight synchronous based generation units are feeding the grid and the HVDC grid is disabled. The load power request is given equally by the synchronous units and the system inertia is maximum.

3.1.2. Scenario 2 and Scenario 3 (25% of RES)

In Scenario 2 and 3 there is a 25% of renewable penetration in the grid, notably all the 3 DFIG wind turbines are feeding the system and also the wind park in the HVDC is enabled. Half of the RES power generation is given equally by the DFIG turbines and half is given by the full converter part of the grid. The difference between the two cases is given by the number of conventional generating units that are working. In Scenario 2 all the eight synchronous machines in the grid are enabled while in Scenario 3 only six of them are working. In particular in Cell 1 only one generator unit in bus 1.9 and in bus 1.10 is enabled.

3.1.3. Scenario 4 and Scenario 5 (50% of RES)

In these two cases the RES penetration of 50% has been considered. In Scenario 4 there are only six conventional generating units as in Scenario 3 while in Scenario 5 only four conventional synchronous machines are feeding the grid. In Cell 1 all the conventional generators in bus 1.9 are disabled and in bus 1.10 only one synchronous machine is working. In Cell 3, bus 3.12, only one of the hydraulic power units is enabled.

3.1.4. Scenario 6 and Scenario 7 (75% of RES)

The RES penetration in the Pan-European grid is increased and the overall renewable production covers 1950 MW of the 2600 MW requested by the grid. In Scenario 6 only three conventional units are feeding the grid while the rest is given by wind DFIG turbines and the

full-scale converters wind generation in the HVDC grid. Only one generator in bus 1.10 in Cell 1 and the two generators in Cell 2 are enabled.

In Scenario 7 only the two conventional units are feeding the grid, one slack generator in Cell 2 and SG 1.10 (1) in Cell 1. The remaining 1950 MW are given by the RES wind generations.

3.1.5. Scenario 8 (90% of RES)

The last Scenario foresees a renewable penetration of 90%, where nearly all of the power request is given by the wind power generation units and the rest is fed by the only two conventional units enabled one in bus 2.11 in Cell 2 and SG 1.10 (1) in Cell 1.

3.2. Testing scenarios

In the conducted analysis only the most significant comparisons between scenarios have been reported case by case. It has been chosen to investigate principally scenario 1, 3, 5 and 7 with 0%, 25%, 50% and 75% of renewable wind production respectively. These cases have been considered as more significant for doing the comparison because the set-point of synchronous generators is remaining the same while more and more conventional generators are disabling to make room at the increasing wind production. Moreover a comparison between cases with the same number of synchronous generators enabled but lower set-point to make room at the increasing wind has been studied to analyze the contribution of the increasing wind while the inertia of the system is constant. In one analysis the difference between scenarios with the same renewable penetration but different number of conventional generating units enabled has also been considered.

3.3. Voltage and frequency ranges

As explained in Chapter 1.5, there are variation ranges in generation buses that should be respected by regulation otherwise the power units could be disconnected from the grid leading to aggravation of the system behavior and cascading outages.

With reference to the first scenario, where there is only conventional generation, the hydraulic and gas turbine generating units work with a set point of generating power of 325 MW. The connection generating point is 20 kV so the type required by the regulation to be considered for FRTC (fault-ride-through-capability) is type D. Since the capacity of all the

synchronous units is above 75 MW and the connection point is at 20 kV in all the further scenarios the type to be considered is also type D. The FRT capability as well as the OVRT capability is reported in the plot in Figure 3-1.

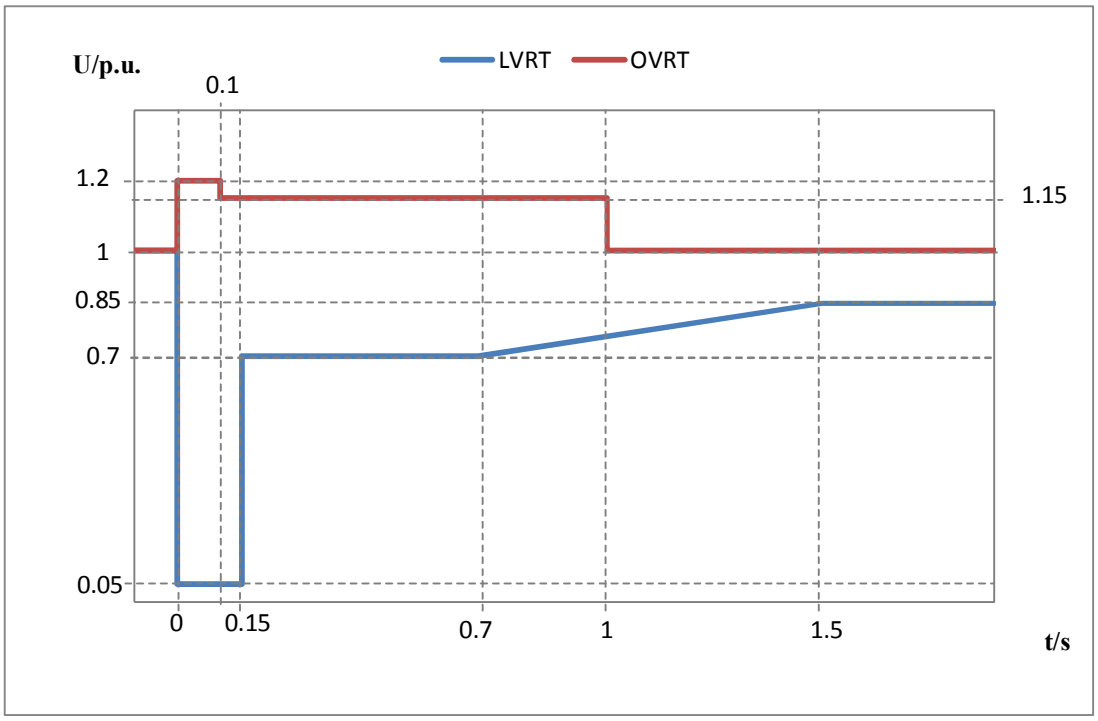

Figure 3-1: LVRT and OVRT of synchronous power plants of type

Concerning the three renewable wind parks generators, i.e. DFIG, since they are composed of 65 wind turbines units in parallel and the rated power of each unit is 6 MW, the type required by regulation to be considered for FRTC is type D. The FRT capability in case of low voltage and over voltages of the DFIG units of type D is reported in Figure 3-2.

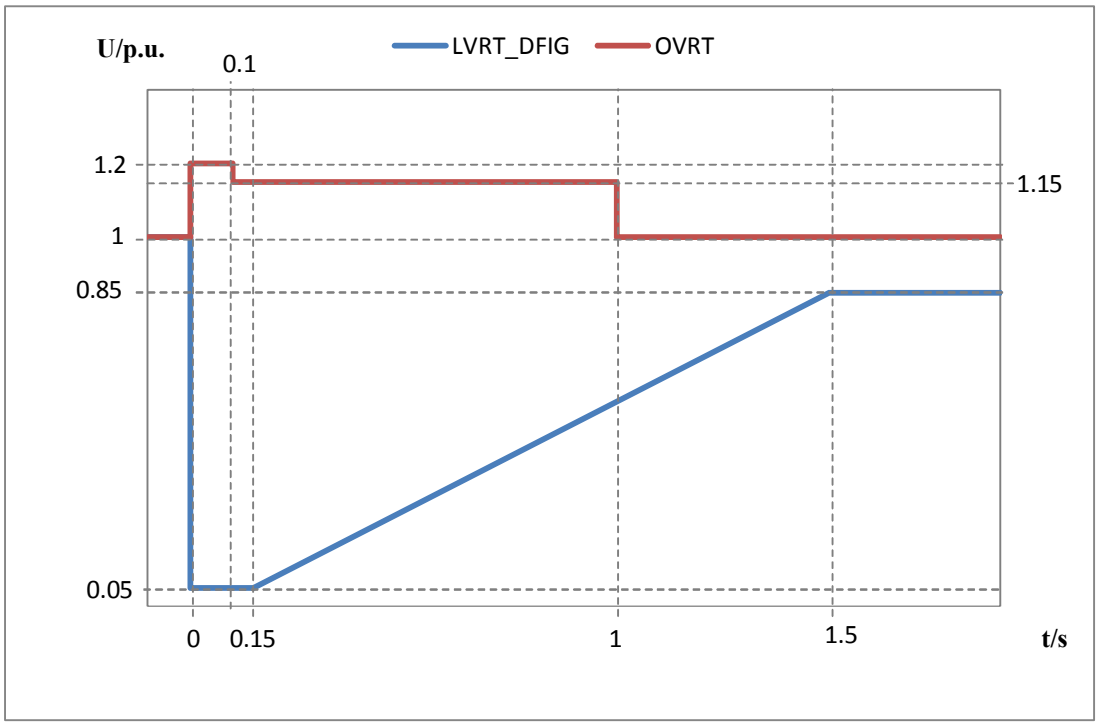

Figure 3-2: LVRT and OVRT of power park modules of type D

For all the generating buses the frequency ranges should stay between 47.5 and 51.5 Hz, or 0.95-1.03 p.u. with a base of 50 Hz. Regarding all the other buses the variations ranges, stated by the regulation EN 50160, can be used as limits even if suited for voltages up to 150 kV. It is in favor of security that those variation ranges are also used for higher voltage levels, i.e. 220 kV and 400 kV as in the analyzed grid. Pointed out this, in the analyzed network, under normal operating condition, the mean value of the fundamental frequency measured over 10 s shall be within a range of:

- 50 Hz ± 1% (i.e. 49.5 - 50.5 Hz) for 99.5% of a year;
- 50 Hz - 6%/+4% (i.e. 47.0 – 52.0 Hz) for 100% of a year.

Chapter 4

Simulation Results: Three-phase fault

In this chapter the simulation's results of a three phase fault analysis are discussed. The first part reports a brief explanation about damping capability of DFIG control system while the following paragraphs report rotor angle, voltage and frequency transient stability issues after the defined event. The conducted analysis has shown that the stability in general is getting worse with increasing wind power penetration in place of conventional generators due to the decrease of system inertia. Despite this in some cases the behavior after the fault is improved with more inverter connected generation as the post-fault oscillations are no longer present.

4.1. Introduction

The most severe disturbance allowing for transients stability assessment is a three-phase fault applied to a network element (i.e. lines or buses). It has thus been decided to perform a three-phase fault in a tie line to study in the worst circumstances the transient behavior of the Pan-European Grid. For every conducted analysis the fault event is intended as a three phase fault in the tie line 3.7-4.3b with fault resistance and reactance respective R_{fault}=0.001 Ω and X_{fault}=0.001 Ω. The fault occurs in the middle of the line and it is intended to be cleared at 150 ms. This value has been chosen because the most common fault clearing time in Europe is currently 150 milliseconds. The analyzed scenarios, with different RES penetration and number of synchronous generator active, are explained in detail in Chapter 3.1.

In the following sections, after a first paragraph with considerations regarding the damping capability of DFIG, attention will be focused on rotor angle, voltage and frequency transient stability issue caused by the three-phase fault.

4.2. Damping capability of DFIG

As explained in Subparagraph 2.4.2 the PI block in the Speed-Ctrl controller, part of the DFIG model, has the task of damping the oscillation excited at a grid fault in the drive train system. The influence of this controller has been analyzed observing the speed trend of the DFIG with the damping controller enabled or not. This analysis has been conducted, as could be seen in Figure 4-1, for the DFIG 1.9 in Scenario 7. The plot also shows the speed trend with different values of the proportional gain Kp of the PI controller, i.e. for one case the standard value assigned in the DIgSILENT model ($Kp = 1$) as well as $Kp = 10$ and $Kp = 50$.

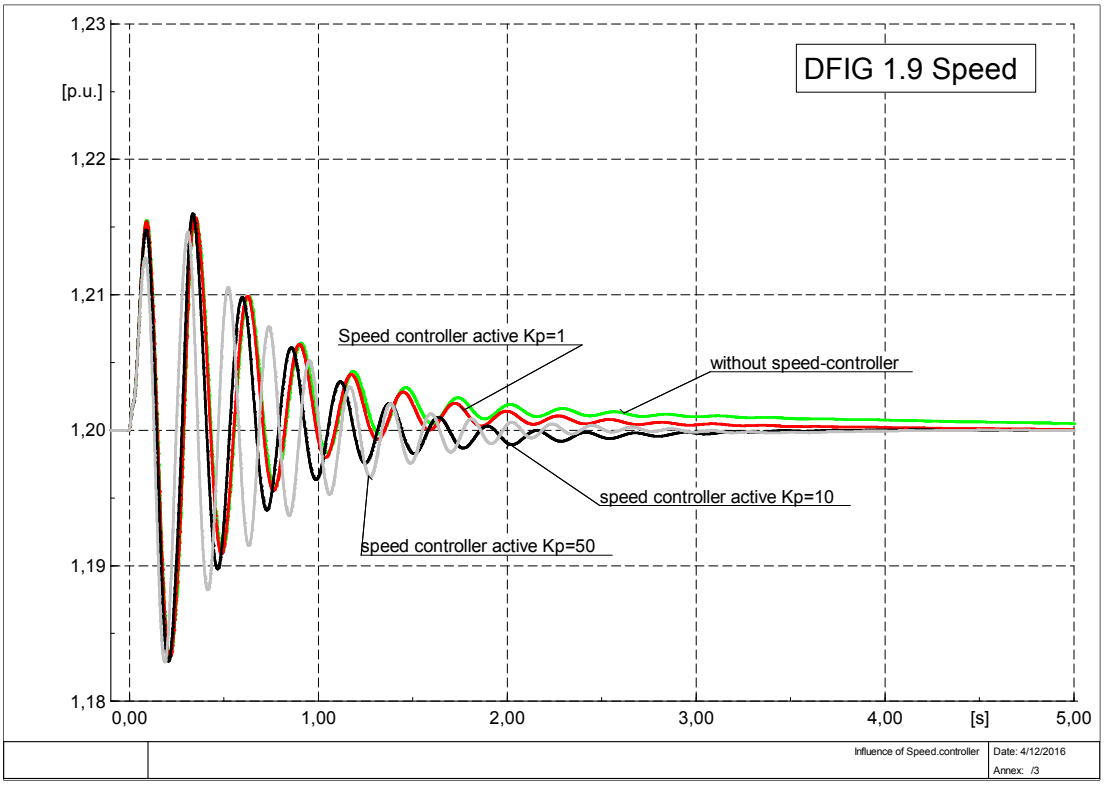

Figure 4-1: Speed of DFIG 1.9 with different setting of the Speed-Controller

As could be seen with the presence of the damping controller the speed reaches the steady-state values faster while with increasing proportional gain the speed is more damped. On the contrary, as could be seen in Figure 4-2, higher value of the proportional gain Kp leads to

more stress in the machine. Notably the power output is pushed to change much more to follow the reference given by the speed controller in order to damp the oscillation in the drive train system.

The system analyzed is a strong grid so it should also be said that different values of the gain do not influence the overall stability as could be the case in a smaller and weaker grid.

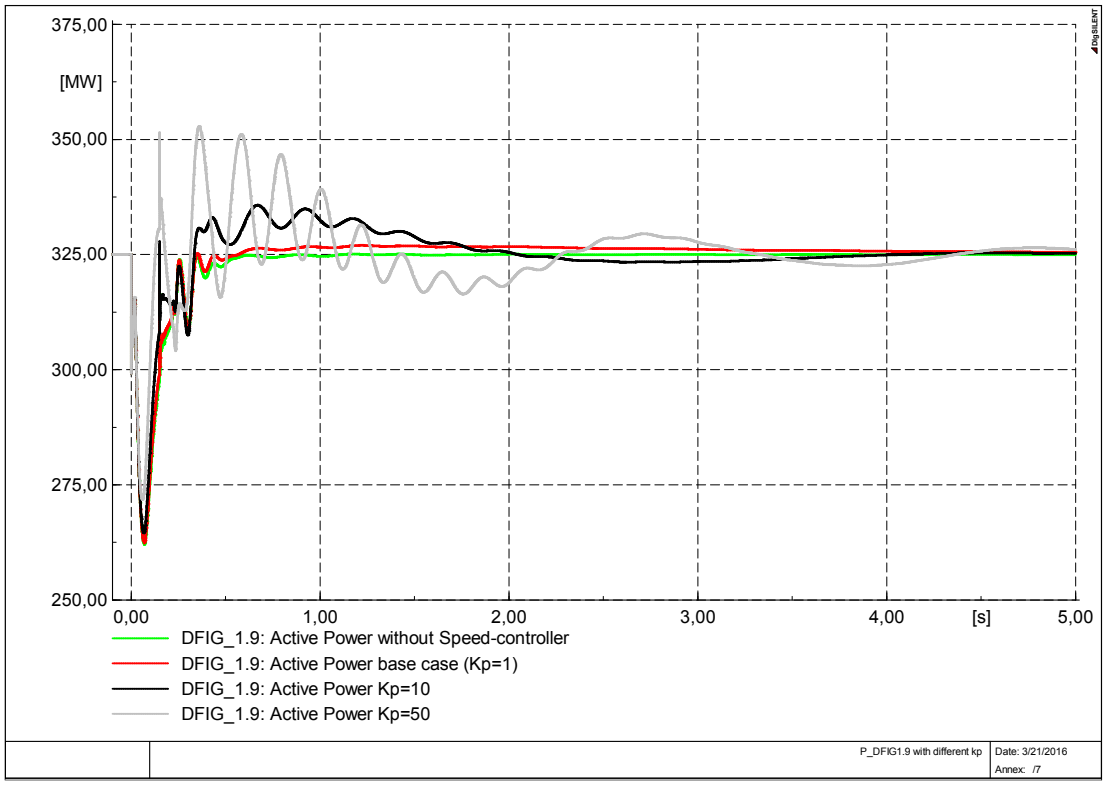

Figure 4-2: DFIG 1.9 active power with different setting of the Speed-Controller.

4.3. Rotor angle stability

Transient stability is defined as the ability of synchronous generator rotor angle to regain their operating equilibrium following a transient fault in the network. As seen in Subparagraph 1.3.4 an indicator that can be used for rotor transient stability consideration is the TRASI index. In its definition the rotor angle is defined with the reference to the reference machine angle. Therefore, as could be seen in Figure 4-3, rotor angle can also be specified based on the following reference frames. To clarify, the respective name in the software environmental is reported in brackets.

- Rotor angle with reference to (w.r.t.) reference machine voltage ($firot$);

- Rotor angle w.r.t. a reference machine rotor angle ($firel$);
- Rotor angle w.r.t. local bus voltage ($fipol$).

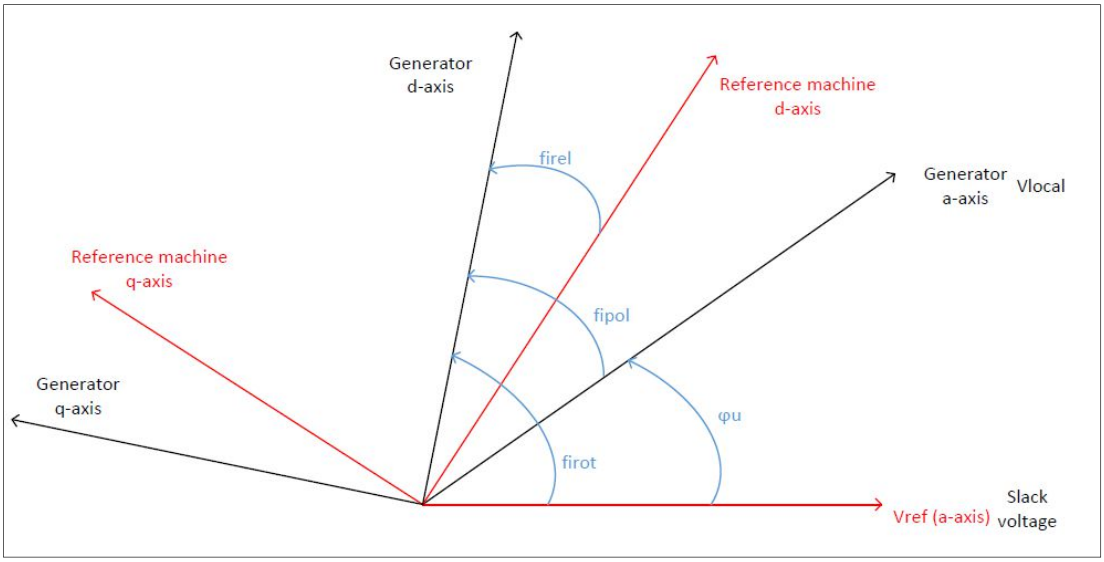

Figure 4-3: Rotor angle definition

In the following analysis the rotor angle is specified w.r.t. the rotor angle of the reference machine, so with the $firel$ angle in the software environment.

In a first analysis the TRASI index has been used to compare different scenarios with the same amount of active synchronous machines but with different wind power penetration. Two different cases have been analyzed: Scenario 1 as the reference with only conventional generation and Scenario 2, with the same number of synchronous machines active but with 25% of wind power penetration. Other two cases are then compared: Scenario 3, with 25% of wind penetration, and Scenario 4 with 50% wind power penetration and both with six synchronous generators enabled. Finally a comparison has been drawn between the four scenarios, respectively Scenario 1, 3, 5 and 7 with the same power set-point of the synchronous machines active but with increasing wind power penetration. To complete the analysis the maximum rotor angle deviation from the steady state value after the fault has been calculated for all scenarios.

4.3.1. TRASI Scenario 1-Scenario 2

For each of the analyzed case the maximum rotor angle difference $\delta_{\max\_d}$ has been calculated within the software as reported in Figure 4-4 and Figure 4-5.

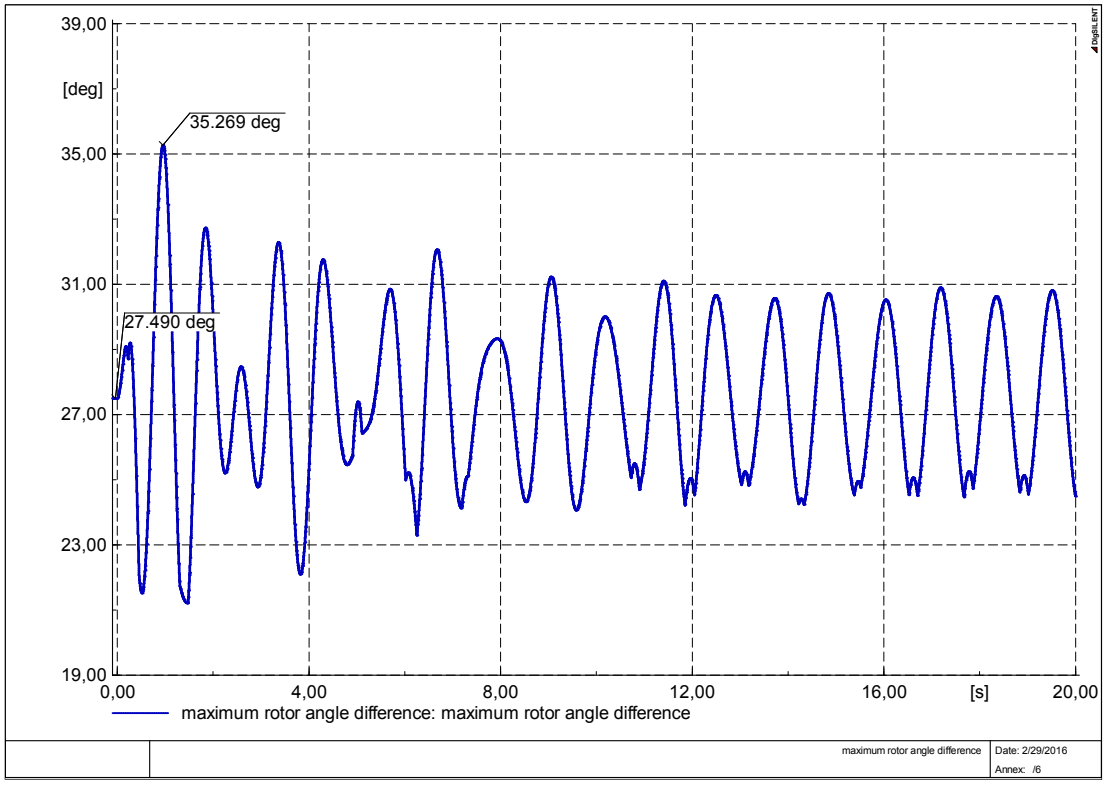

Figure 4-4: Maximum rotor angle difference $\delta_{max\ \_d}(t)$ SCENARIO 1

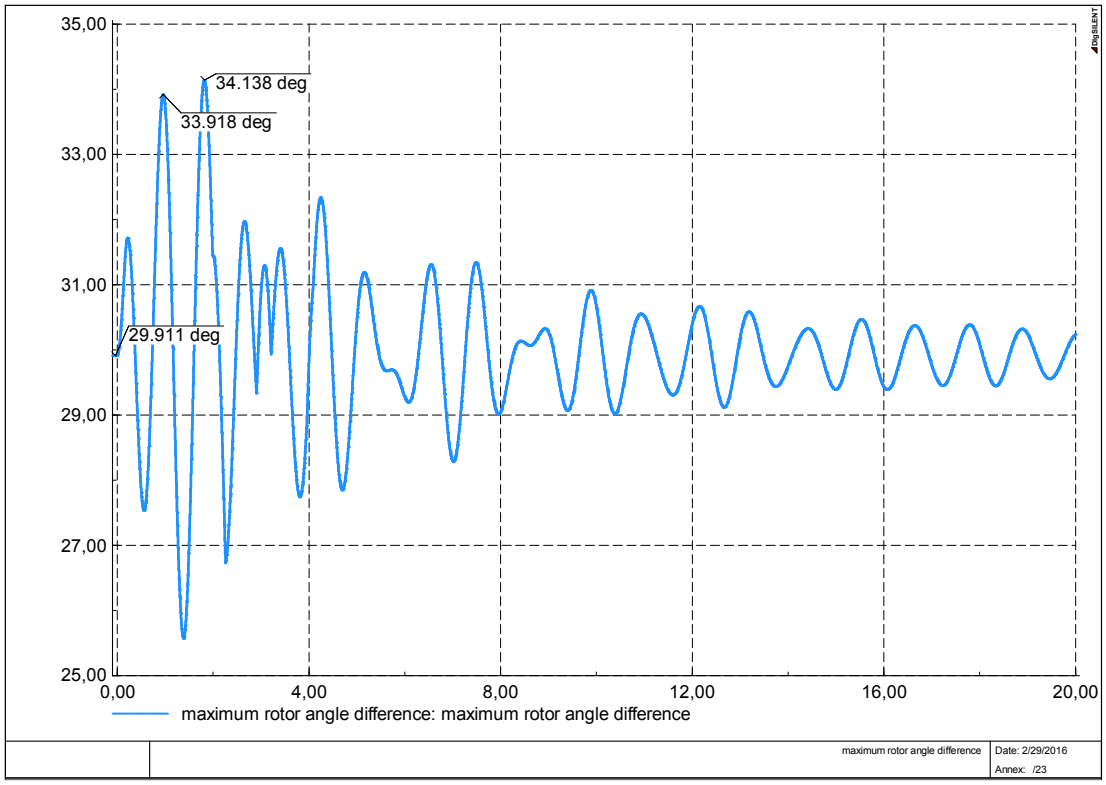

Figure 4-5: Maximum rotor angle difference $\delta_{max\ \_d}(t)$ SCENARIO 2

The resulting index TRASI, transient rotor angle severity index, defined in Subparagraph 1.3.4 in Equation (1-1), is reported in Figure 4-6.

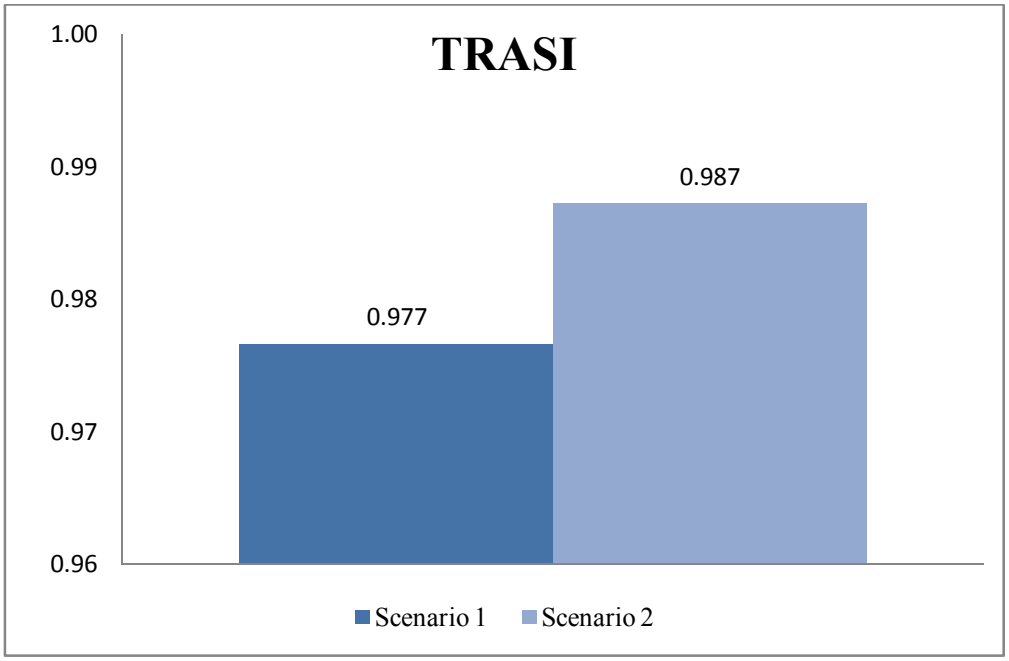

Figure 4-6: Comparison of TRASI index in the two scenarios with different wind penetration

It can be seen from the comparison that there is an improvement in rotor angle stability from Scenario 1 to Scenario 2. That is due to the power rush flow contribution of the DFIGs in the moment of the fault so the fault power contribution of synchronous generator is reduced, which in turn reduces the impact in the electromagnetic forces of the synchronous generators. As seen in Figure 4-7, the power injected by the DFIGs, immediately after the fault, is increasing except the case of DFIG 3.12 due to the proximity of the faulted line.

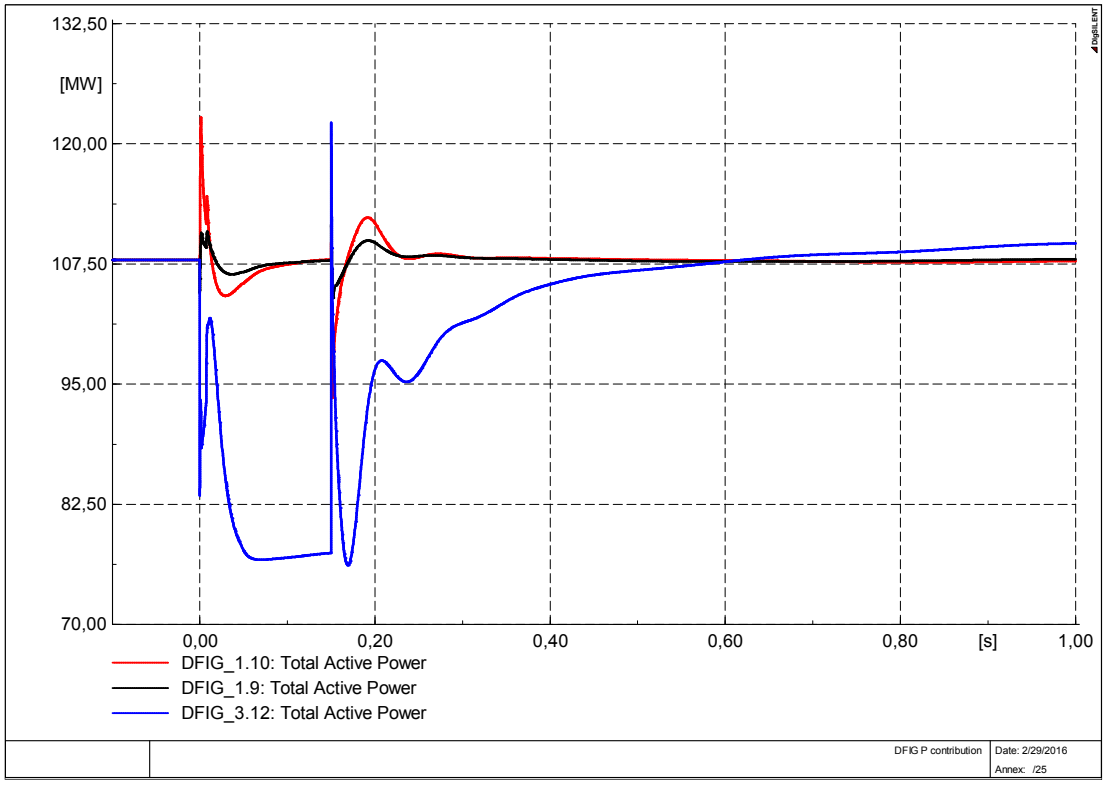

Figure 4-7: Power contribution of DFIG during fault in Scenario 2

4.3.2. TRASI Scenario 3-Scenario 4

The two scenarios analyzed, Scenario 3 and Scenario 4, are characterized by wind power penetration of 25% and 50% and six synchronous generators on-line. The maximum rotor angle difference for the two cases is displayed in Figure 4-8 and Figure 4-9.

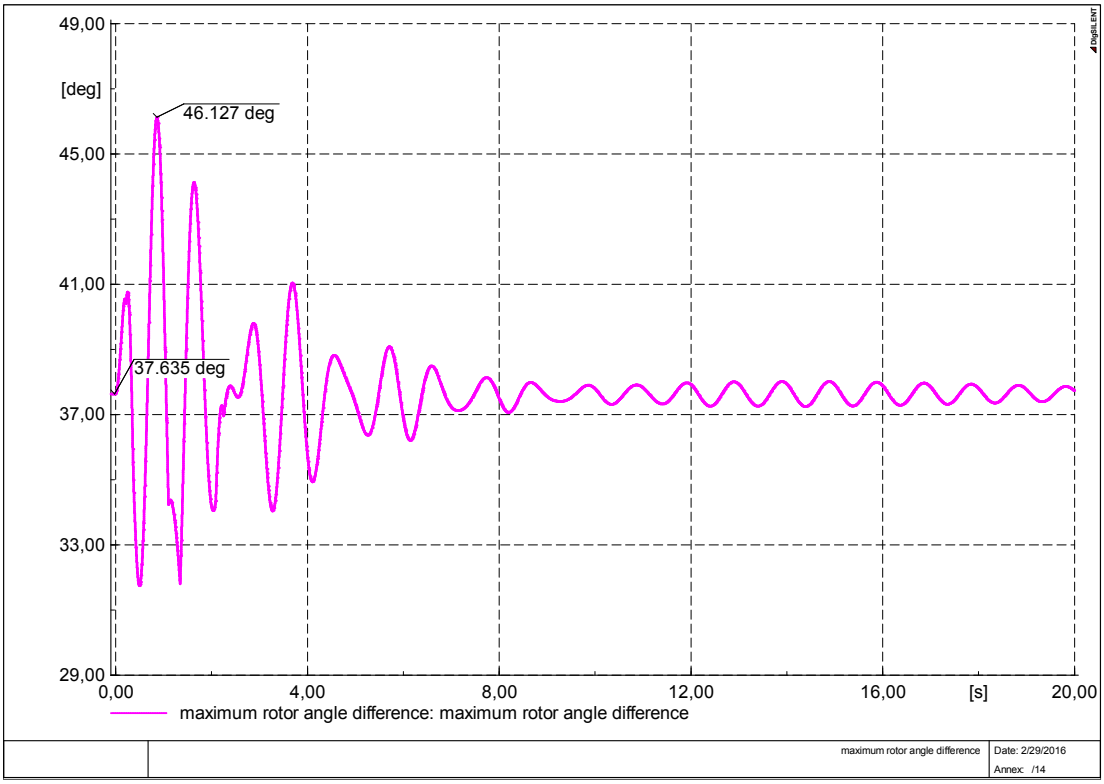

Figure 4-8: Maximum rotor angle difference $\delta_{max\ \_d}(t)$ SCENARIO 3

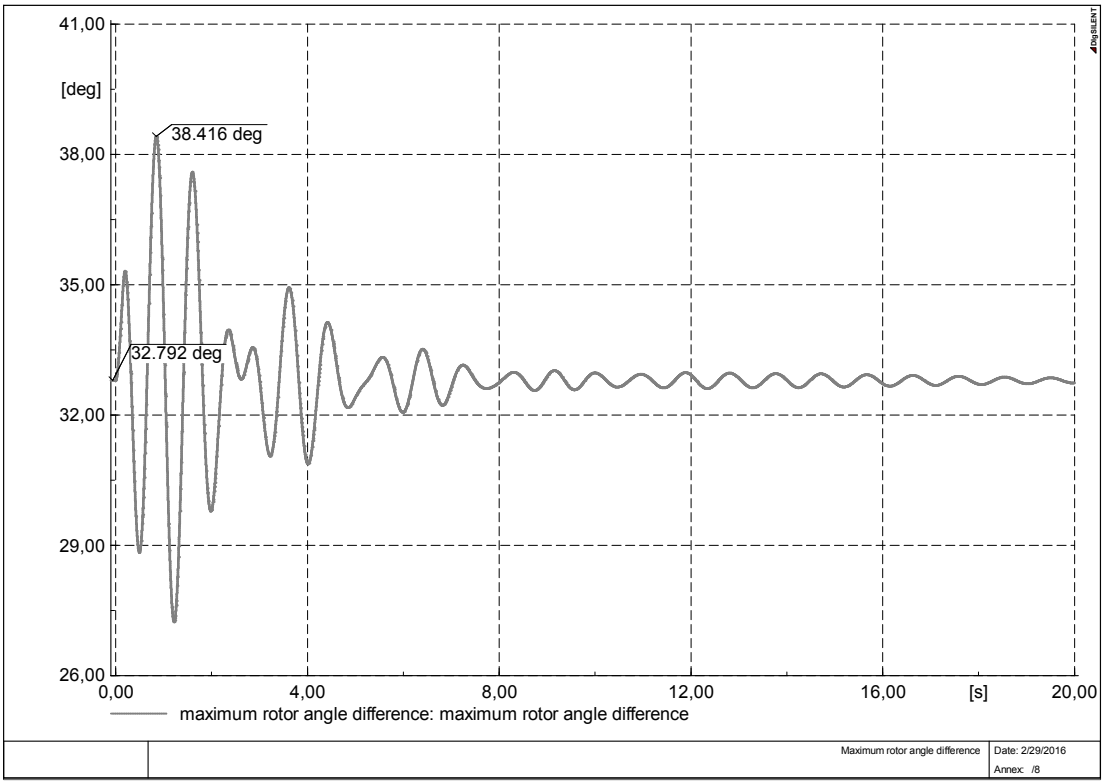

Figure 4-9: Maximum rotor angle difference $\delta_{max\ \_d}(t)$ SCENARIO 4

As seen in Figure 4-10 the TRASI index is improving in Scenario 4 when compared to the one with 25% of wind penetration (Scenario 3).

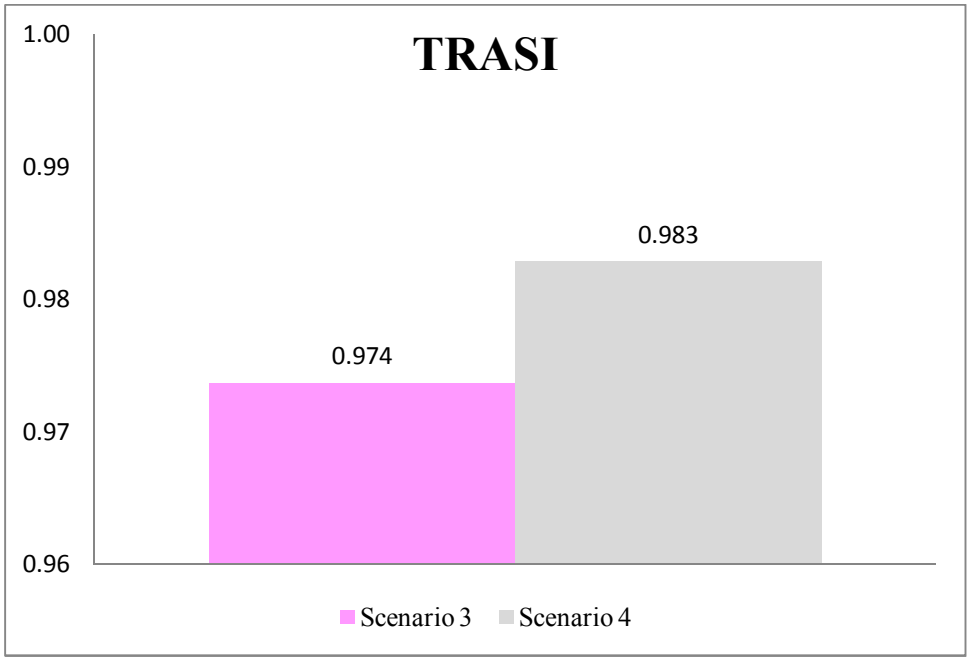

Figure 4-10: Comparison of TRASI index in the two scenarios with different wind penetration

The improvement could be due to the difference power set-point of the synchronous generators. In Scenario 3 the six synchronous machines in the grid are working with a steady state power of 325 MW while in Scenario 4 they are working at 217 MW. In fact if the generators work at less power than the nominal one, they have more power to support the restoring after the fault. In Figure 4-11 the power injected, after the clearance, by the generators nearer to the fault (SG 3.12) has been compared in the two scenarios. It can be seen that the power has a bigger variation in Scenario 4, in the case with lower set-point of the synchronous generator. The machine in Scenario 4 is accelerating less in the moment of the fault due to the lower difference between the mechanical torque, constant, and the decreased electrical torque, as could be clearly seen in Figure 4-12. Equally after the clearance the machine in Scenario 4 is decelerating more due to the bigger difference between the constant mechanical torque and the increased electrical torque. This behavior brings to lower speed oscillations that lead to a more stable behavior. However the improvement could be also due to the increasing penetration of RES.

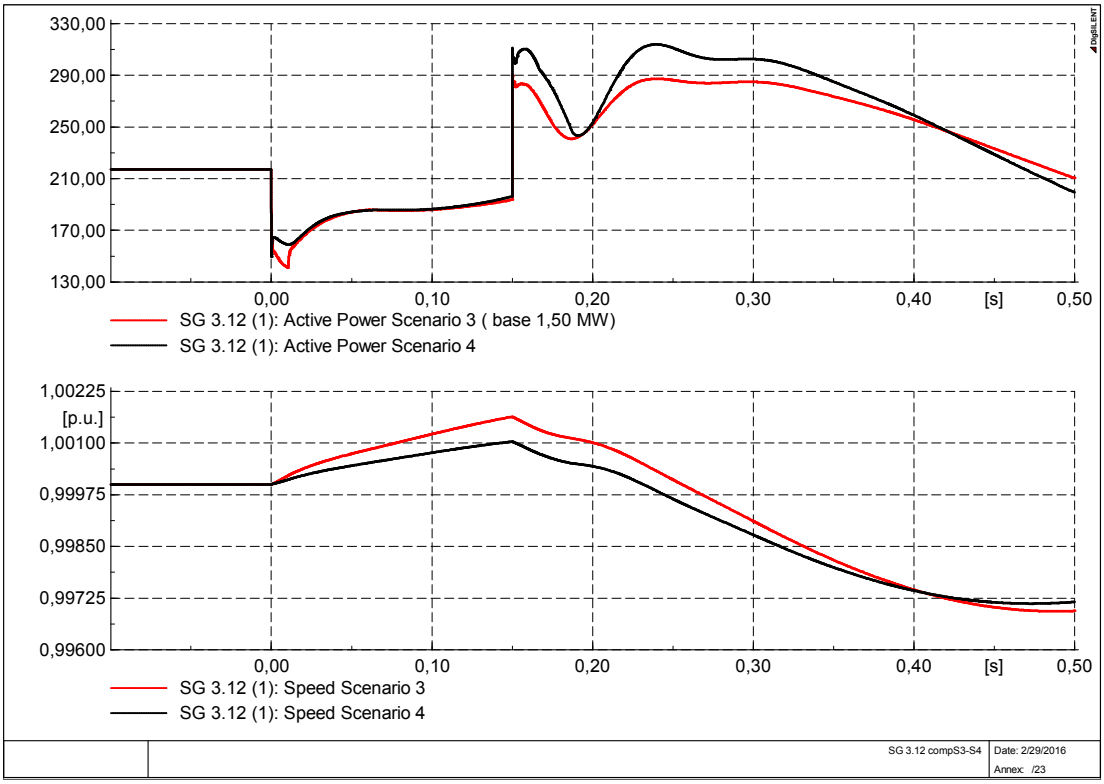

Figure 4-11: Comparison between active power injected and Speed by the SG3.12(1) following the fault in Scenario 3 and 4

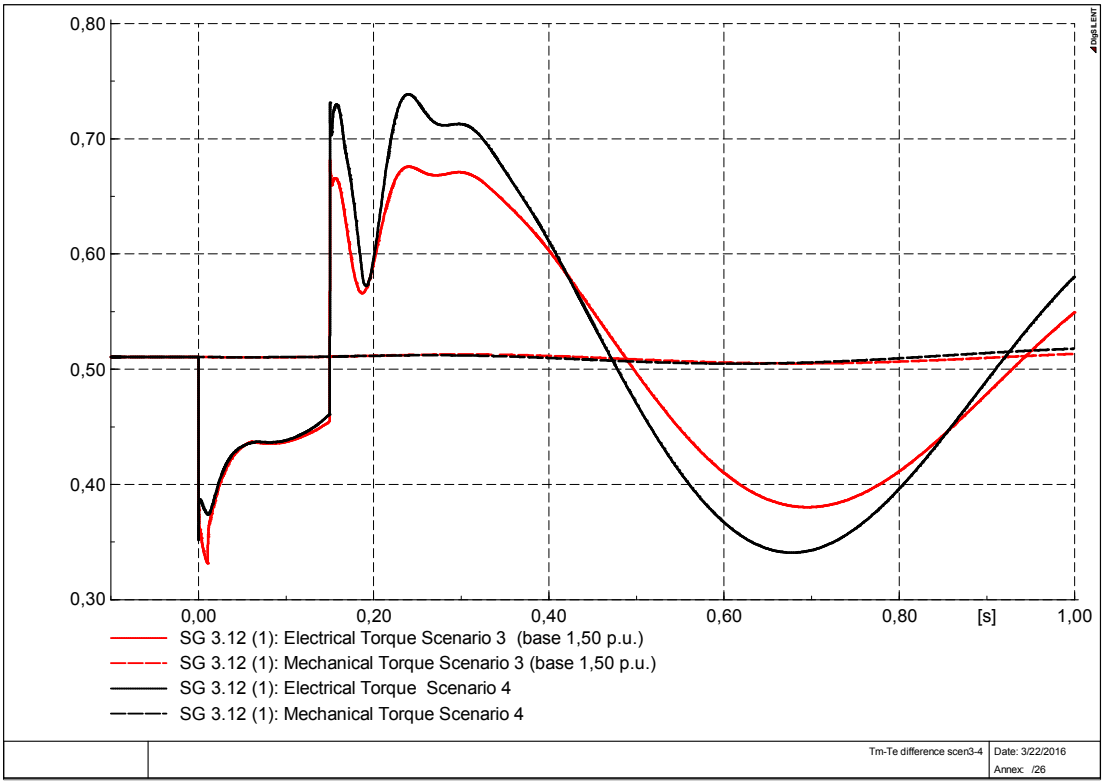

Figure 4-12: Comparison between electrical and mechanical torque in scenario 3 and 4

Deeper analysis, briefly presented below, has shown that the better behavior in term of rotor angle stability in the analyzed case is due to the lower set-point of the generators instead of the increasing wind penetration. To clarify, a comparison has been drawn between Scenario 4 and Scenario 5 with the same wind power penetration (50%) but with a different power's generator set-point, of 217 MW and 315 MW respectively. As seen in Figure 4-13 the TRASI index is better in the case with more synchronous generating units and lower generator's set point, i.e. Scenario 4.

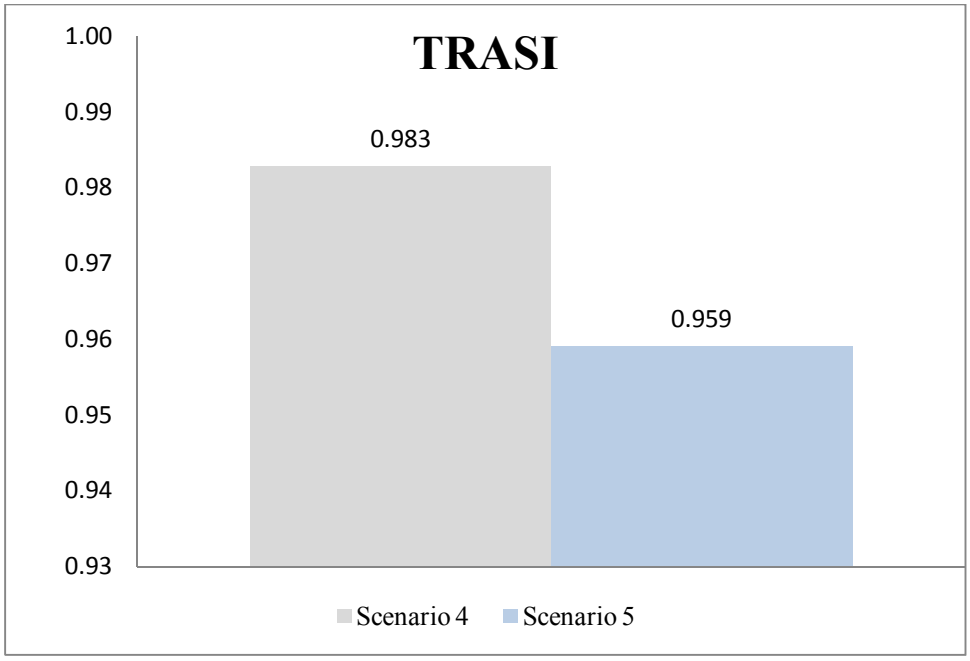

Figure 4-13: Comparison of TRASI index in the two scenarios with different generators set-point but same amount of RES penetration.

4.3.3. TRASI between scenarios with the same set-point of power

It is interesting to investigate the TRASI index in the case of same set-point of power of the synchronous generators while the amount of wind power production is increasing. Scenario 1, Scenario 3, Scenario 5 and Scenario 7 have been compared: the power set-point is 325 MW in all the four cases while the amount of conventional generator is becoming lower to make room to the increasing wind power generation of respectively 0%, 25%, 50% and 75% respectively.

The comparison between the TRASI index in these four scenarios is shown in Figure 4-14.

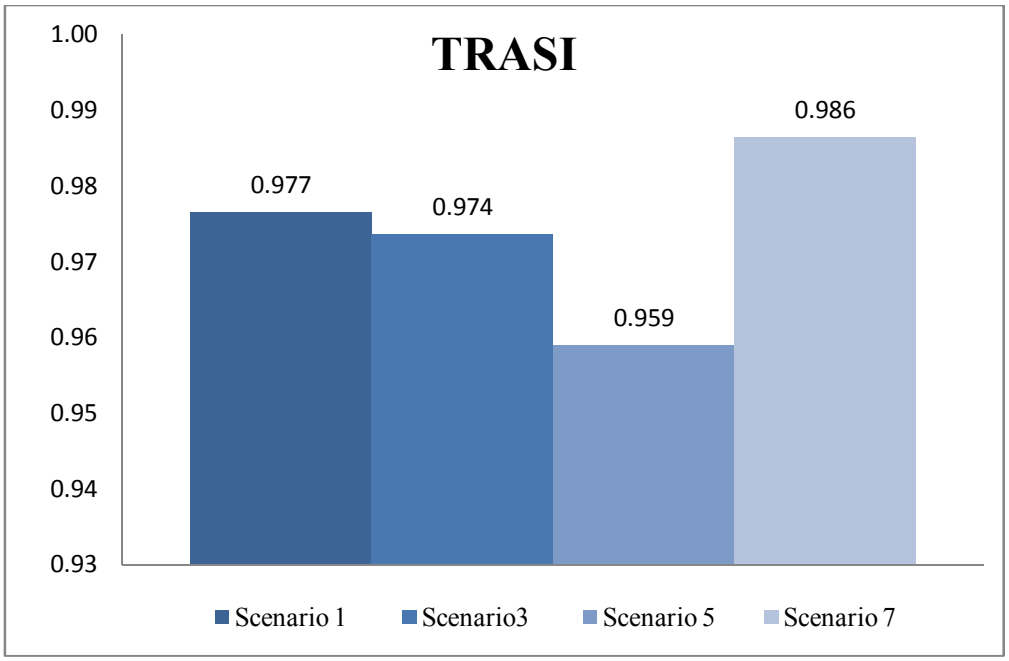

Figure 4-14: Comparison of TRASI index in the four scenarios with different RES penetration

As shown by Figure 4-14 the TRASI is becoming lower in the first three cases with the increase of wind power penetration, in fact the inertia of the system is decreasing and thus the angular separation of the synchronous generator is increasing. On the contrary in Scenario 7 the TRASI index seems to be better in comparison with all the three previous cases, even though the inertia of the system is lower and the wind power generation is increased to 75%. In this scenario only two conventional units are enabled, the slack generator SG 2.11(2) and the generator in bus 1.10, SG1.10 (1). The stability behavior is better in Scenario 7 due to the fact that both of the synchronous generators in the bus nearer to the fault, bus 3.12, are disabled. On the other hand, in the other scenarios, Scenario 1, 3 and 5, at least one or both are feeding the grid. These machines are more subjected to oscillations due to the vicinity of the fault, and this lead to a worst transient behavior.

In general comparing the speed, the frequency, the electrical torque and the active power injected into the grid by one synchronous generator it can be seen that there is more variation in the frequency, torque and in the electrical power after the fault with more penetration of wind. This is shown for the generator SG 1.10(1), enabled in all the four analyzed cases, in Figure 4-15 and Figure 4-16.

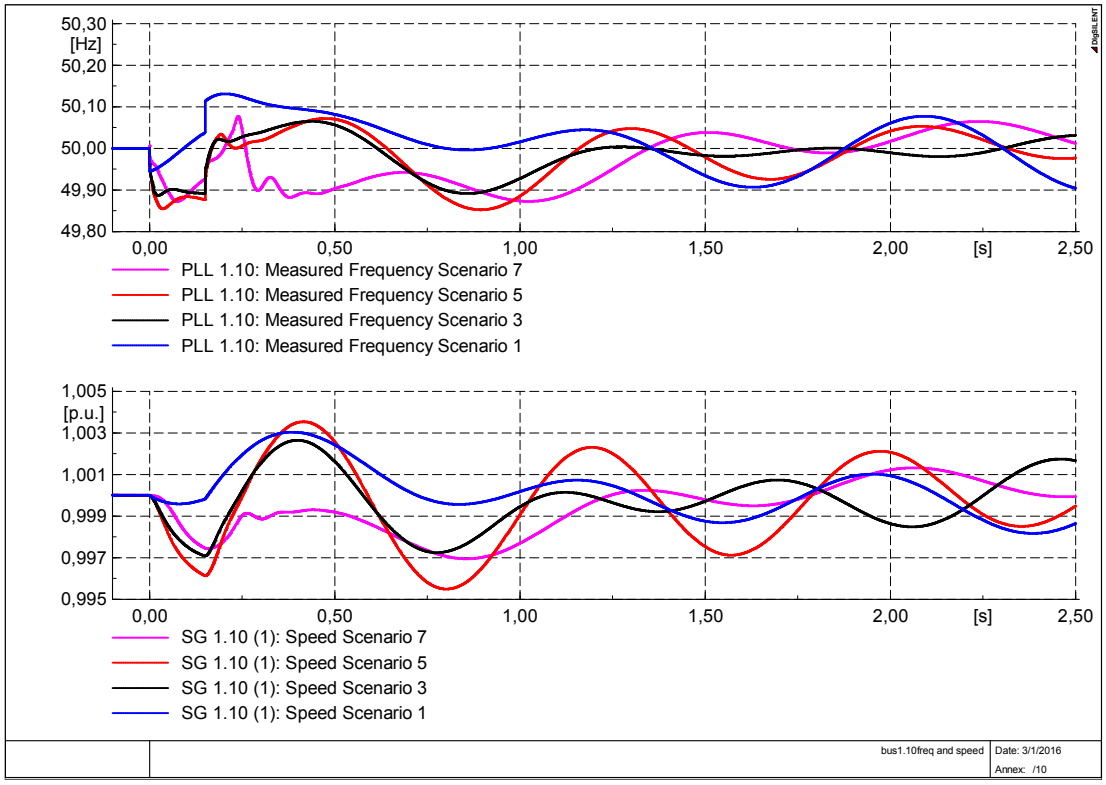

Figure 4-15: Comparison between frequency and rotor speed in bus 1.10 in Scenario1,3,5 and 7

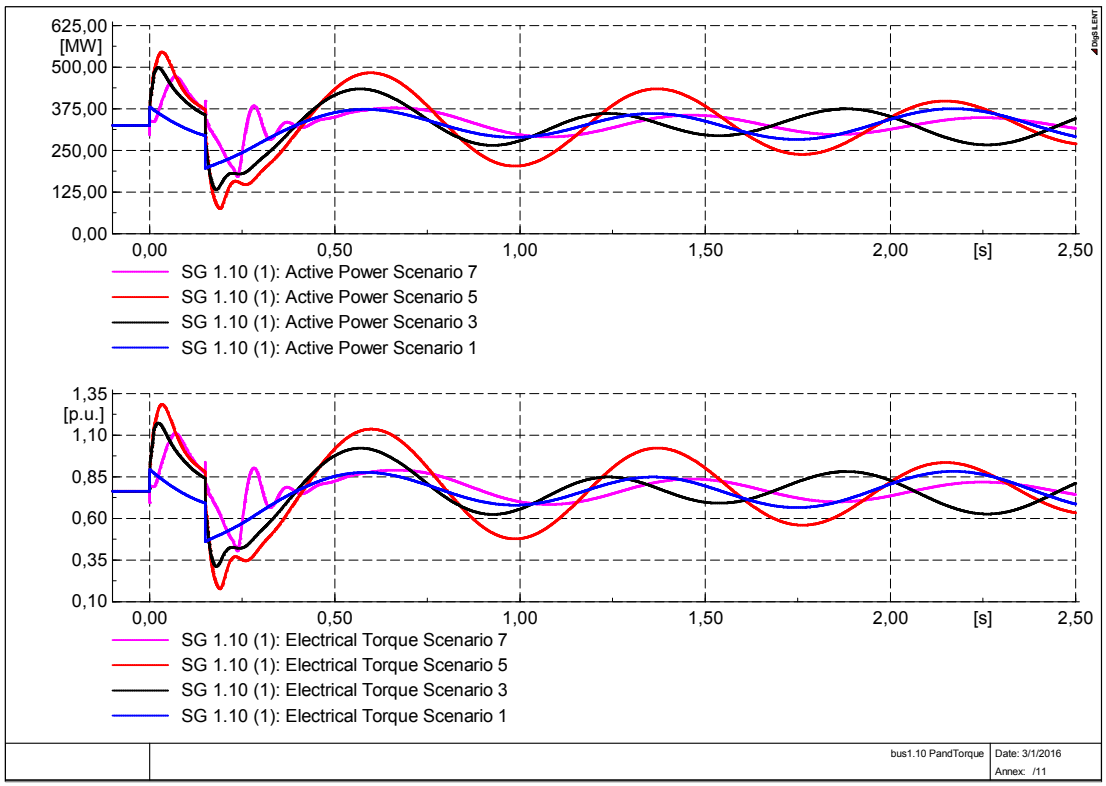

Figure 4-16: Comparison between active power and electrical torque in bus 1.10 in Scenario 1,3,5 and 7

4.3.4. Maximum rotor angle deviation

The estimation of maximum generator's rotor angle deviation from the steady-state value after the fault is also interesting for a complete stability evaluation. In fact the TRASI index is a comprehensive approach and it refers to the overall system while the maximum rotor angle deviation is a local issue. In that sense a generator could have a lower maximum angular deviation than another case but the TRASI of the system where it is connected could be worse.

For every different scenario analyzed the maximum rotor angle deviation $|\Delta\varphi max|$ that occurs after the fault from the steady state values has been calculated. The rotor angle deviation $|\Delta\varphi|$ can be defined as in Equation (4-1) with φ the rotor angle of each synchronous generator w.r.t. the reference machine's rotor angle, i.e. the $firel$ angle in PowerFactory environment.

$$|\Delta\varphi| = \max\left(\left|\varphi_{max} - \varphi_{steady-state}\right|; \left|\varphi_{min} - \varphi_{steady-state}\right| \right) \quad (4\text{-}1)$$

The maximum rotor angle deviation $|\Delta\varphi max|$ in each scenario can finally be calculated considering the maximum between the rotor angles deviation of each generator. In fact considering the maximum deviation of the $firel$ angle it has been considered the maximum angular deviation of the generator's rotor that occurs with respect to the SL generator's rotor.

The maximum rotor angle deviation and the respective synchronous generator where it occurs in each scenario are reported in Figure 4-17.

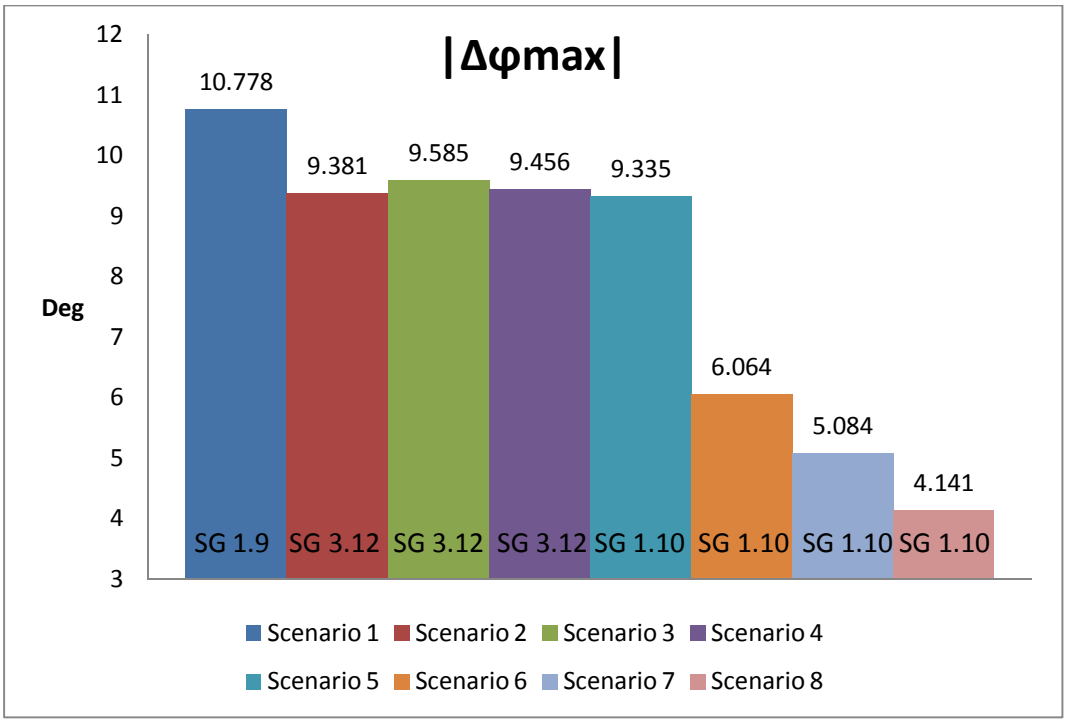

Figure 4-17: Maximum rotor angle deviation respect to the rotor of the SL generator. The considered angle is the one w.r.t. the reference machine rotor angle.

The maximum rotor angle deviation in the first scenario is bigger than in the other scenarios because in this scenario there are only conventional generation units and thus there is no contribution by the DFIG and the converter connected generation that mitigate the synchronous contribution during the fault.

Scenario 2 and 3 have the same amount of RES penetration, 25%, but in Scenario 3 there are less synchronous generators enabled and consequently the system presents less inertia, the stability behavior is worse and the maximum angular difference is bigger.

Scenario 5 has a lightly lower maximum angular deviation comparing with Scenario 4 even if two of the synchronous generators are switched off. On the contrary the previous analysis with the TRASI index has shown that it is Scenario 4 which behaves better in term of overall stability. Figure 4-18 reports the rotor angle w.r.t the rotor angle of the reference machines of all the generators enabled in Scenario 4 and 5. As can be seen in the plot of Scenario 4 there are lower oscillations in the rotor angular position apart in the generator near to the faulted lines (SG 3.12). In Scenario 5 bigger oscillations are present also in the generator 1.10. It can be concluded that Scenario 5 overall behaves worst in terms of rotor angular stability as seen with the TRASI index analysis.

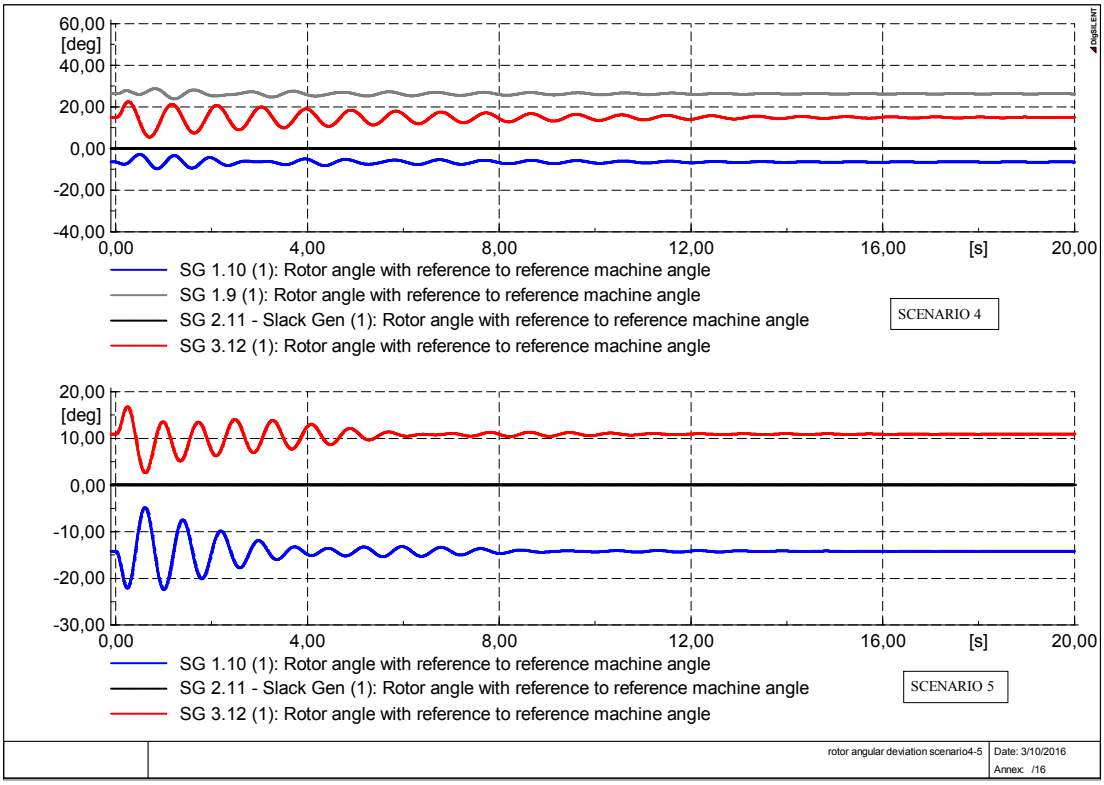

Figure 4-18: Rotor angles w.r.t reference machines angle of the enabled generator in scenario 4 and 5.

The maximum rotor angle in the last three cases is really small comparing to the previous analyzed cases. That is due to the shut off of both of the generators SG 3.12 that are nearer to the faulted line. The synchronous generators behavior is not so severe because the machines enabled are far from the faulted line and there is also the DFIG contribution.

4.4. Frequency stability

Frequency stability is defined as the ability of a power system to maintain a steady-state frequency following an imbalance caused by fault. To evaluate the frequency behavior after the defined event the initial frequency nadir has been used, which is the largest drop following a fault event in the network. The evaluation of the frequency peak after the clearance of the fault is also interesting. The analysis was done considering a simulation time of 1 s following the fault. A first comparison between four scenarios has been done; Scenario 1, 3, 5 and 7 were compared considering increasing wind power penetration, respectively 0%, 25%, 50% and 75%. The analysis was performed comparing the measured frequency by PLL (phase measurement device) in the generators buses and in the main ac grid buses. It is also interesting to evaluate for each cells which is the more critical bus in term of frequency stability, i.e. determine the buses with the bigger frequency nadir and peak in each cell.

In Scenario 1, the base case scenario, without any renewable resources, the bigger variation in frequency following the fault occurs in bus 2.5 as seen in Figure 4-19.

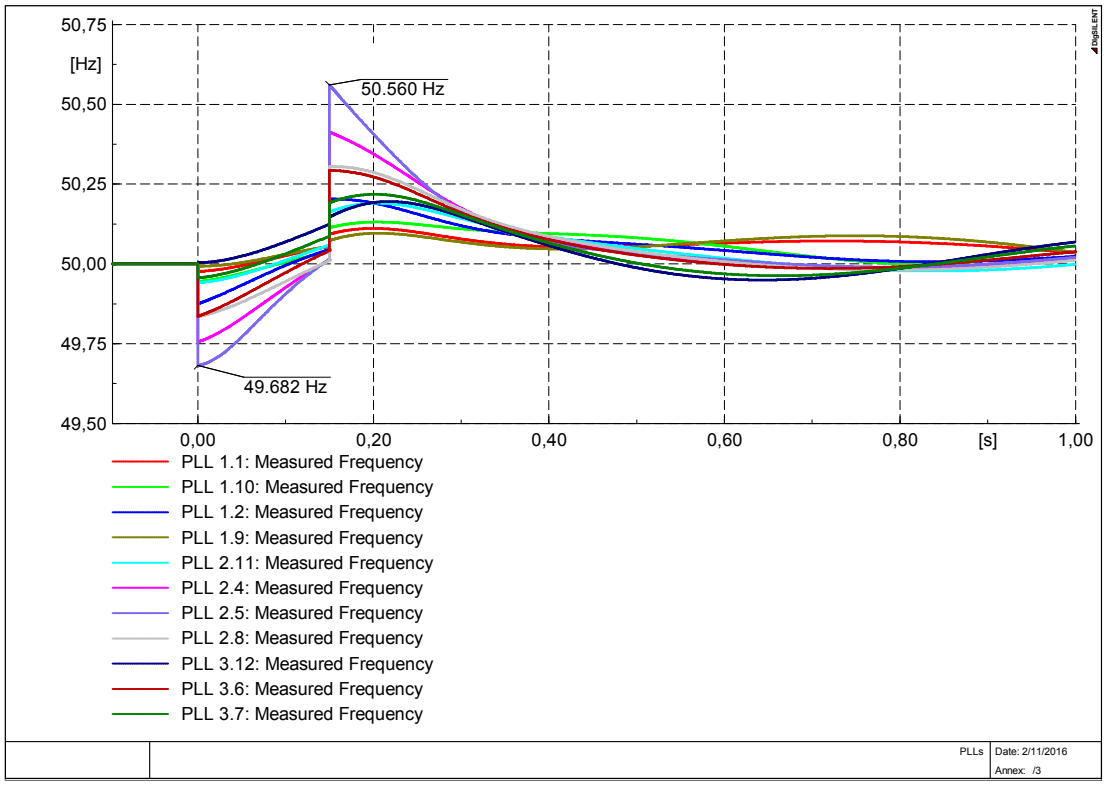

Figure 4-19: Frequency trend in the main buses after a three-phase fault in Scenario 1 (no RES)

The frequency drops to the value of 49.682 Hz and rises up to the value of 50.560 Hz. Also the near bus 2.4 is subjected to a big excursion. A comparison analysis between each frequency trend in each of the three AC cells has shown that the critical buses are: bus 1.2 for Cell 1, bus 2.5 for Cell 2 and bus 3.6 for Cell 3. It should be noted that critical frequency buses are placed in buses where loads and principal transmission lines are connected.

In Scenario 3 two generation conventional units, SG 1.9(2) and SG 1.10(2), are switched off to make room for 25% of renewable wind generation. As seen in Figure 4-20 also in this case the deeper frequency occurs in bus 2.5, with a dip of 49.7 Hz and a peak after the clearance of 50.249 Hz. Also the frequency in bus 2.4 and 2.8 is changing more than the frequency in other parts. As the base case, critical buses are bus 1.2 in Cell 1, bus 2.5 in Cell 2 and bus 3.6 in Cell 3.

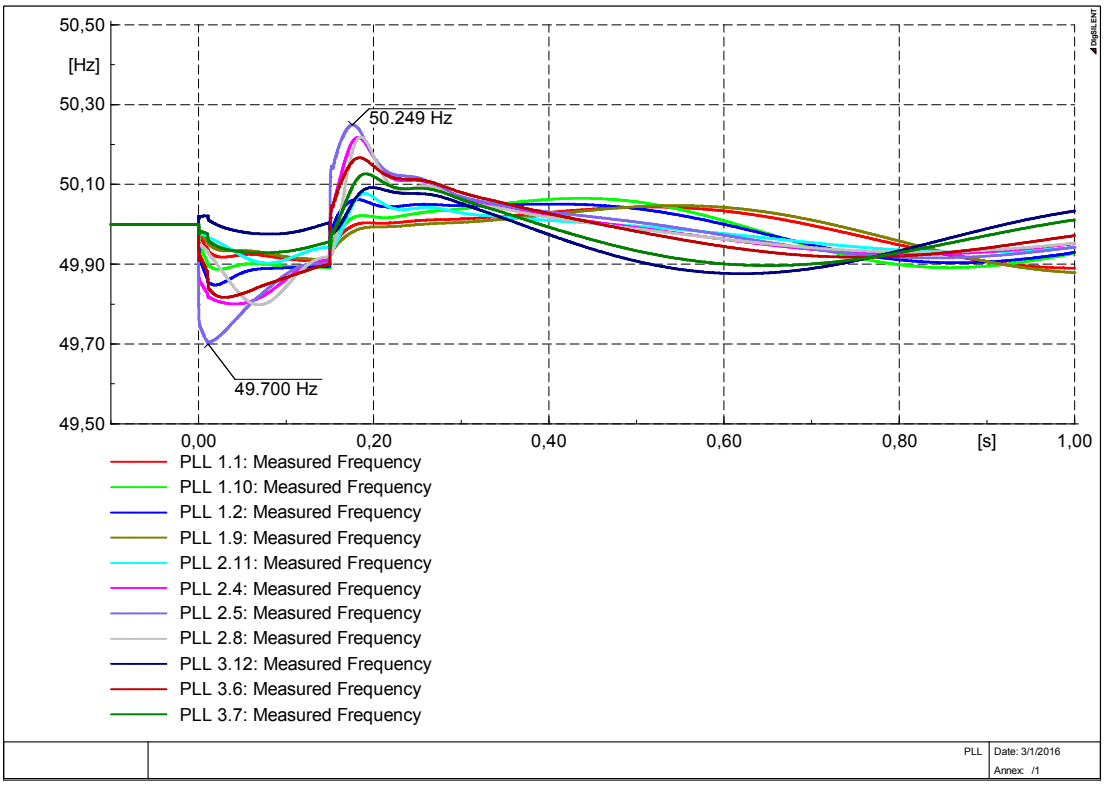

Figure 4-20: Frequency trend in the main buses after a three-phase fault in Scenario 3 (25% of RES)

In Scenario 5 the wind power generation is increased to 50% and four synchronous generation units, SG 1.9(1)&(2), SG 1.10 (2) and SG 3.12 (2), are disabled. As shown in Figure 4-21 the bigger excursion occurs in the bus 2.5 and the frequency drops till 49.703 Hz and reaches the value of 50.265 Hz after the clearance of the fault. Bus 3.6 and 2.4 also show deep variation. The critical buses in term of frequency stability in Cell 1 are bus 1.9 and 1.1 as well as bus 1.2. In this scenario the dip in frequency is bigger in generation bus like 1.9 as well because both of the synchronous machines in this bus are disabled to make room for the increasing wind. In Cell 2 the critical bus is bus 2.5 while in the third cell the critical one is bus 3.6.

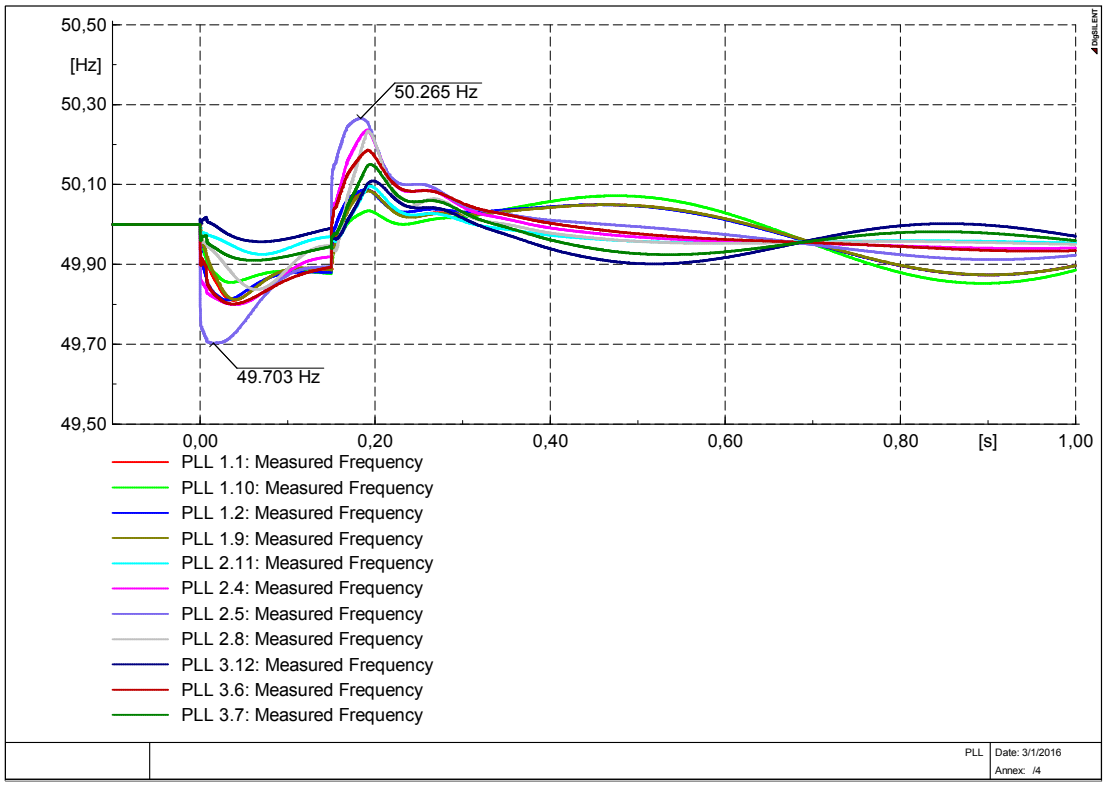

Figure 4-21: Frequency trend in the main buses after a three-phase fault in Scenario 5 (50% of RES)

In Scenario 7 the wind power penetration is increased to 75% and only two synchronous generators are working, one of the slack machines SG 2.11(2) and synchronous generator SG 1.10(1). The frequency trend in the main buses is shown in Figure 4-22.

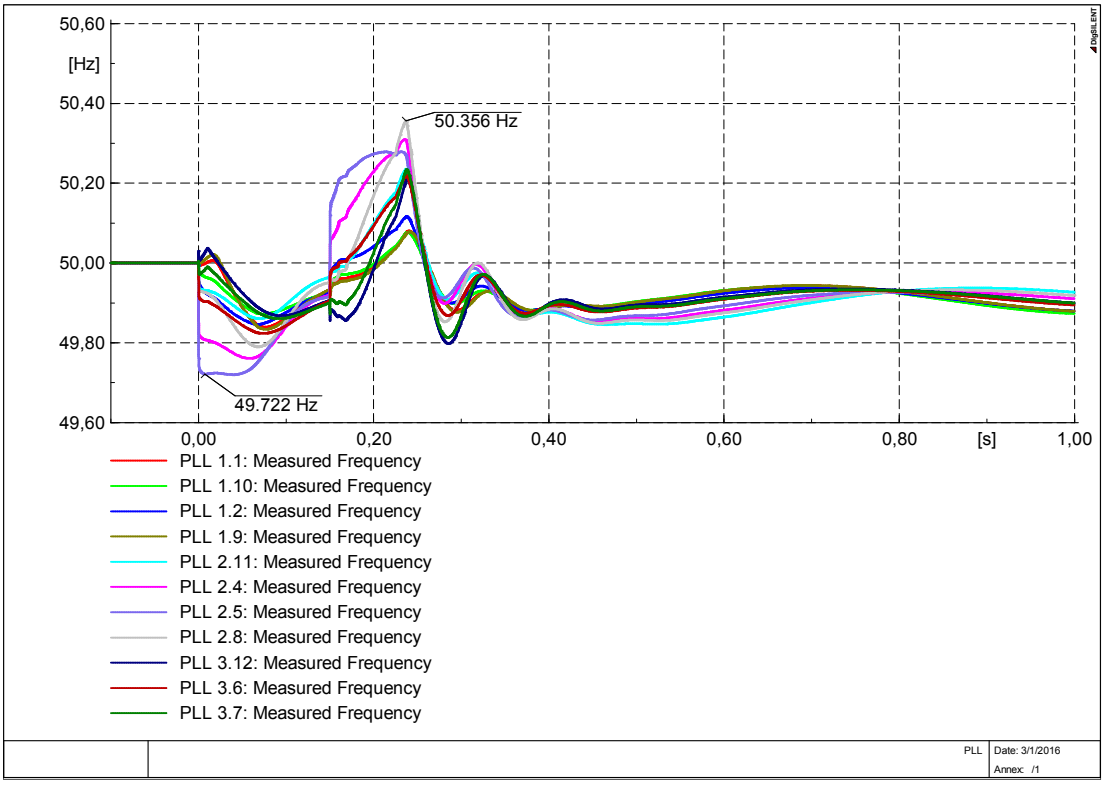

Figure 4-22: Frequency trend in the main buses after a three-phase fault in Scenario 7 (75% of RES)

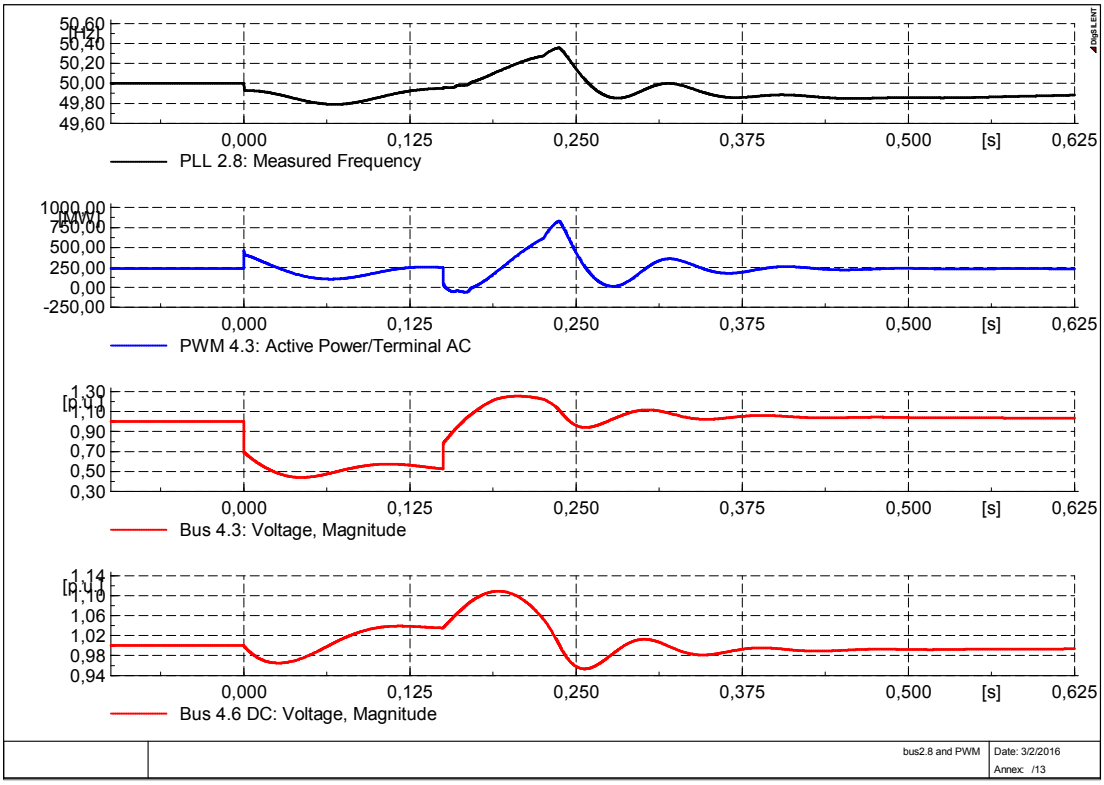

Figure 4-23: Over-frequency in bus 2.8 and the behavior of the near PWM 4.3 master converter

The bigger drop occurs in bus 2.5 till the value of 49.722 Hz. The max over-frequency occurs instead in bus 2.8, in which the frequency reaches the value of 50.356 Hz. The over-frequency peak in this bus is due to the after fault behavior of the near PWM converter, PWM 4.3. As shown in Figure 4-23, the converter is pushing power in the AC side after the clearance of the fault to bring the voltage in the respective bus to a constant value. In fact this PWM converter has to work as the master controller and therefore has the task to maintain constant voltage in the AC and DC bus. The critical buses in each cell are bus 1.9 and 1.1 for Cell 1. In fact all the synchronous generators in that bus are turned off so the frequency presents more variations. For Cell 2 and Cell 3 the critical buses are bus 2.5 and 3.6 respectively.

Regarding the previous plot one fact should be clarified: the frequency at the moment of the fault and after the clearance has a step variation. This frequency trend is not realistic in a power grid where there is synchronous generator active with inertia capability; the frequency cannot have such an instantaneous variation. In fact the step that can be seen in the plot is due to the measurement; the measured frequency is coming from a Phase Measurement Device (PLL) connected in the relative bus. PLL gives as output the frequency deriving it from a voltage angle measurement in the relative bus. Observing the speed, see Figure 4-24, of the synchronous active generators, it can be seen that there is no step variation as expected.

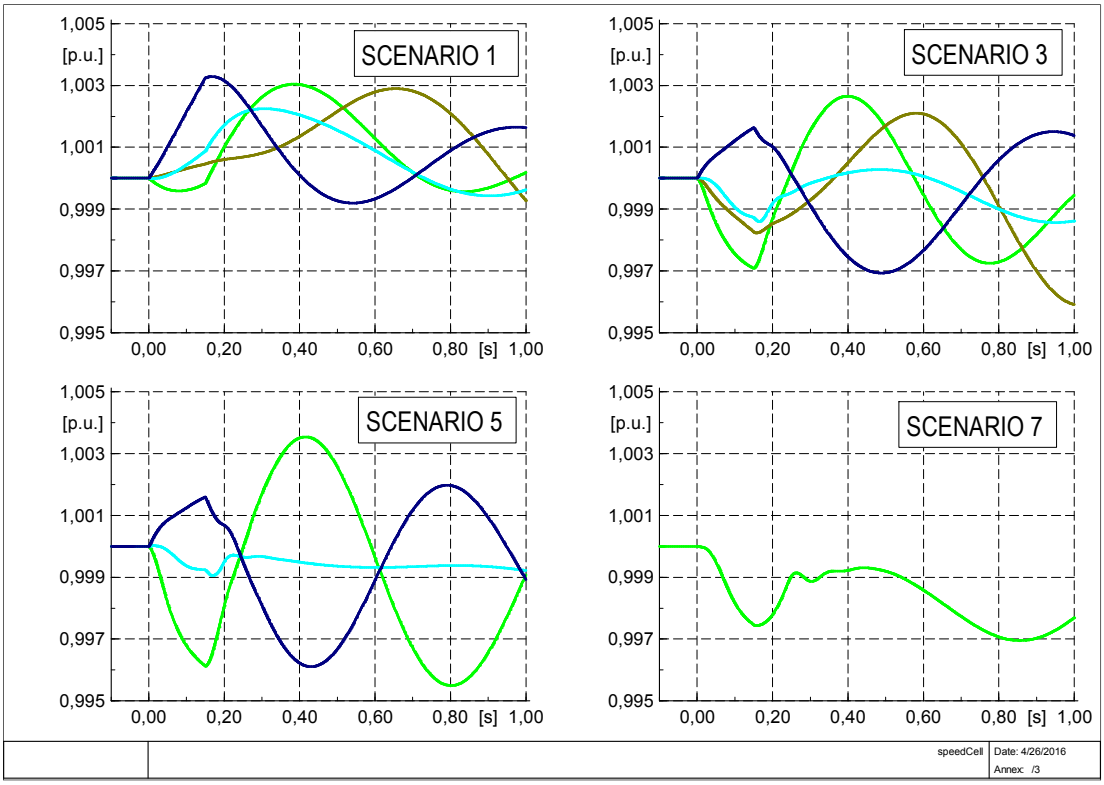

Figure 4-24: Synchronous generator speed in Scenario 1, 3, 5 and 7. The legend is reported below:

SG 1.10 *SG 1.9* *SG 2.11 (SL)* *SG 3.12*

The frequency analysis has shown that the more critical bus in terms of larger drops and peaks is bus 2.5 in all the scenarios apart from Scenario 7 in which the biggest peak occurs in bus 2.8 as explained before. In Figure 4-25 the comparison between the frequencies in bus 2.5 for all the four analyzed scenarios is reported. The biggest peak occurs in the case of no RES penetration. In fact the grid has only synchronous generators without converter connected generation that contributed to shape the after fault characteristics.

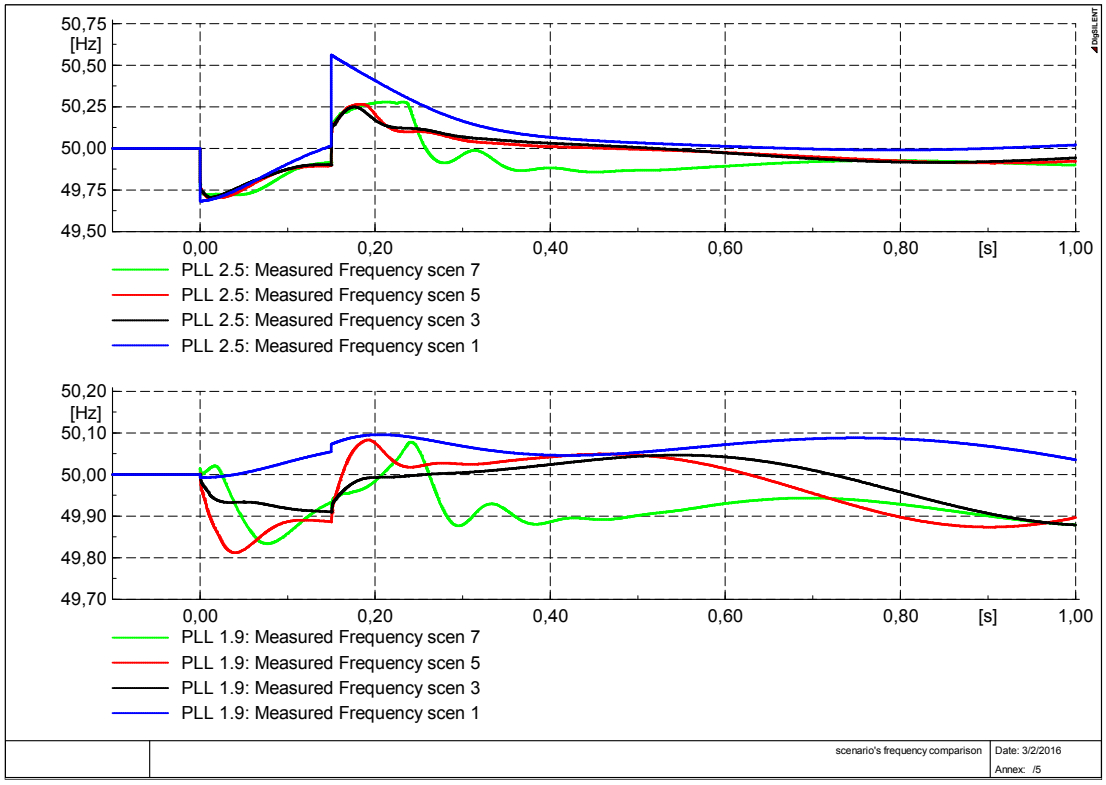

Figure 4-25: Frequency trend comparison in bus 2.5 and 1.9 in the 4 analyzed scenarios

A comparison between the frequencies in bus 1.9 is also reported in Figure 4-25 to visualize the difference between the presence or not of active synchronous generator in that bus. In bus 1.9 there are synchronous generators enabled till Scenario 3. In Scenario 5 and 7, where only DFIG are feeding the bus, the frequency reaches its lowest value. In fact without synchronous generator to give the frequency a reference, the frequency follows the DFIG speed changing due to the variation of the electrical torque. The behavior is shown in Figure 4-26 for the DFIG 1.9 in Scenario 5, for comparison the trend with also a conventional unit connected in the bus, e.g. Scenario 3, is as well reported in the plot. This plot shows that the electrical torque in the moment of the fault is increasing (in absolute values) and so the DFIG is decelerating and the frequency has a dip too. Then the torque starts to decrease and consequently the machines accelerate and the frequency follows. This behavior is emphasized in the case with only DFIG in the bus.

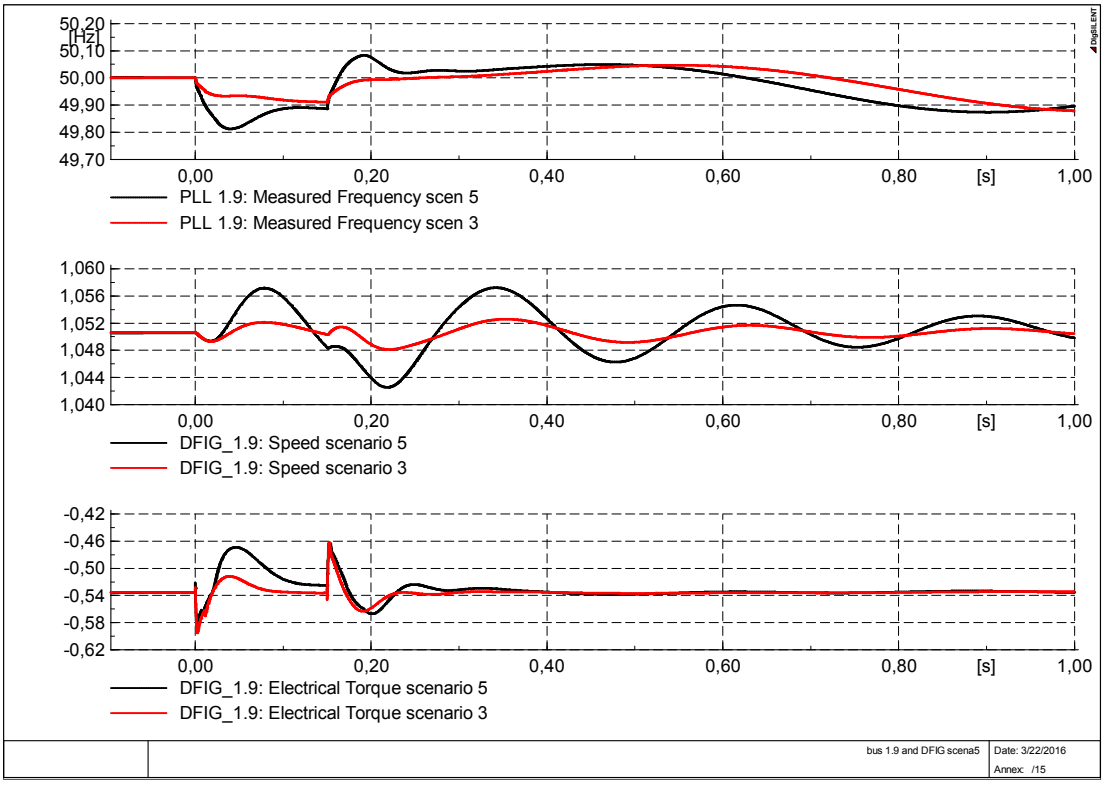

Figure 4-26: DFIG 1.9 behavior in Scenario 5 and for comparison in Scenario 3

The frequency ranges, defined by the EU normative, in distribution systems in case of grid fault are 50 Hz -6%/+4% (47.0 – 52.0 Hz). Furthermore in generation buses, to ensure the connection of the generation units, the frequency ranges should stay between 47.5 and 51.5 Hz, i.e. 0.95-1.03 p.u. with a base of 50 Hz. As can be appreciated in the above plots in all of the main buses in the Pan-European grid the frequency stays within the limits in all the scenarios. The system security is ensured as it should be possible for all the generators to remain connected to the grid.

4.4.1. Fast Fourier Transform-FFT

A longer time simulation, following the fault for 20 s, has shown that there are different behaviors in term of reaching a steady-state condition without oscillation after the clearance of the fault with different penetration of RES and disabling of conventional generators. An interesting analysis is the FFT (Fast-Fourier-Transform) of the magnitude of the frequency following the fault. In fact, the frequency oscillates from the steady state value (50 Hz) after the clearance of the fault. Using the predefined analysis function in PowerFactory it is possible to evaluate the magnitude of the preponderant harmonics in the frequency.

A comparison between the behavior in different scenarios was done comparing the frequency in two main generation buses to observe the difference in the case of gradual turn off of conventional units to make room at higher penetration of wind generation. The comparison was done between the base case, Scenario 1 and Scenario 3, Scenario 5 and Scenario 7 observing the frequency in bus 1.9 and bus 3.12. The plots are reported in Figure 4-27 reported below, for bus 1.9, and Figure 4-31 for bus 3.12.

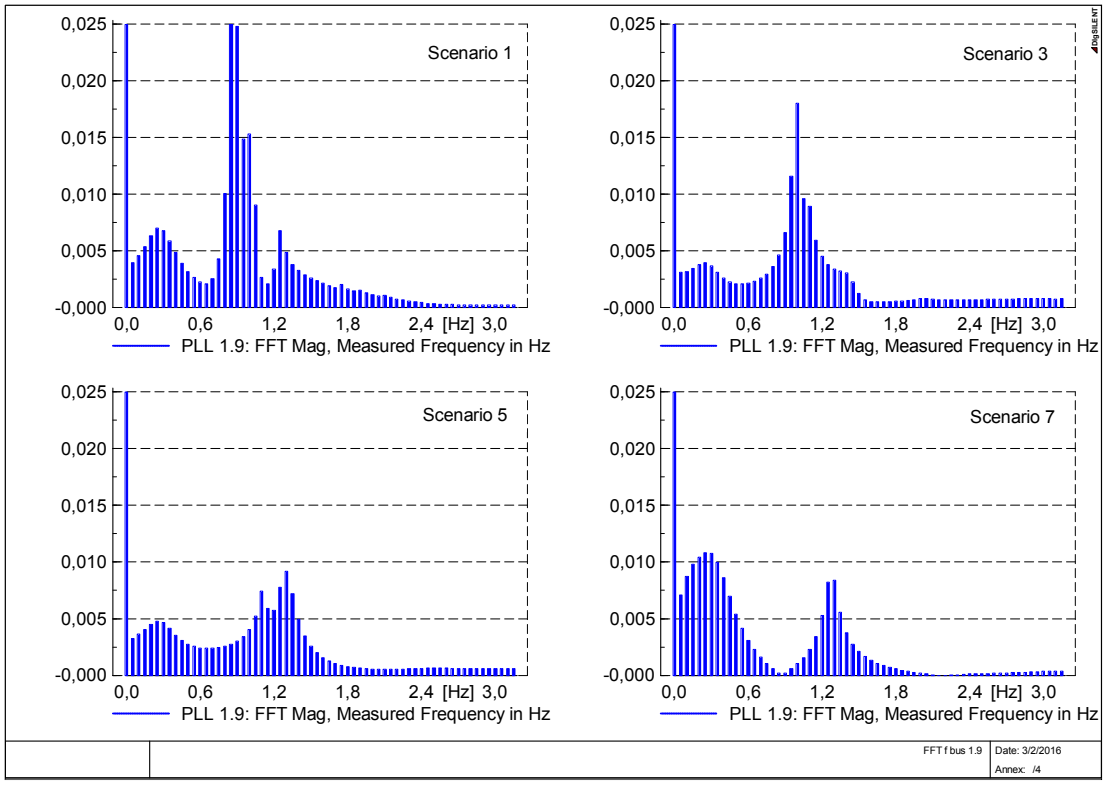

Figure 4-27: FFT in bus 1.9 in four different scenarios

In Scenario 3 in bus 1.9 there is only one synchronous generator enabled while in the Scenario 5 and 7 there is only wind power production feeding that bus. In the base case the preponderant harmonics are around 0.8-0.9 Hz so there are main oscillations with a period of 1.11-1.25 s. In particular, as could be seen in Figure 4-28, the principal oscillations are around 0.86 Hz (oscillating period of T=1.162 s), i.e. these oscillations are inter-area oscillations. Inter-area oscillations are associated with the swinging of units of generation in one area against a group of generators in another area. This concept can be translated into an inter-cell grid by considering a group of generators in one cell swinging against a group of generators in another cell. Usually inter-area oscillations are in the range of 0.1 to 1.0 Hz while local oscillations, i.e. swinging of units in a small part of the system with respect to the

rest of the power system, are from 1.0 to 2.0 Hz. When observing the rotor speed and the supplied active power of synchronous generators in Figure 4-29 it can be noticed that generator SG 1.9 in Cell 1 is oscillating against the slack generator SG 2.11 in Cell 2 with a phase shift of almost 180º.

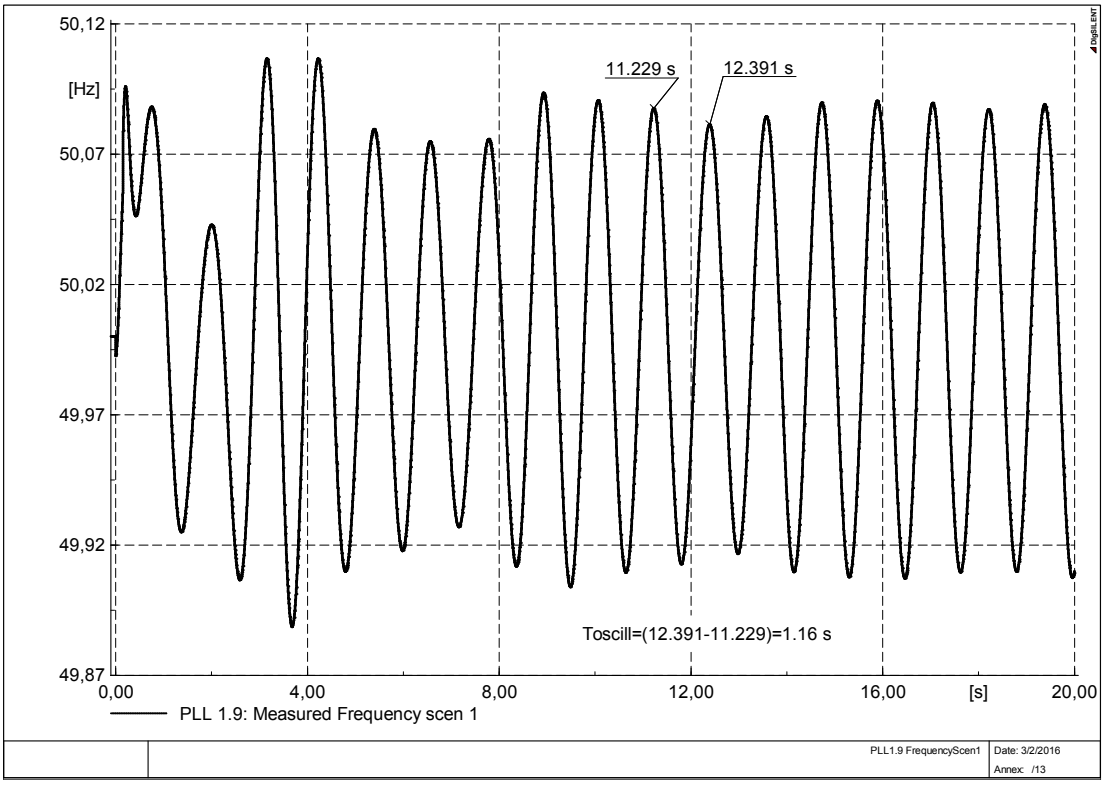

Figure 4-28: Frequency in bus 1.9 in Scenario 1

With the disabling of conventional generation, Figure 4-27, the preponderant frequency harmonics, principally due to the inter-area oscillations contribution, are damped while the frequency oscillations are moved to smaller values, meaning to higher values of period of oscillation. In the last case, Scenario 7, the harmonics around 0.8-0.9 Hz have completely disappeared and the main harmonics are around 0.25 Hz and therefore have a bigger period of oscillation, i.e. around 4 s, and around 1.3 Hz, so with a period of 0.77 s. The presence of harmonics with bigger period of oscillation in the last analyzed scenario, i.e. the increasing of lower frequency harmonics, is due to bigger variation in the initial frequency immediately after the fault and its clearing. It can be concluded that with increasing converter controlled generation, even if the behavior immediately after the fault is worse, the frequency oscillations are eliminated, as can be appreciated in Figure 4-30.

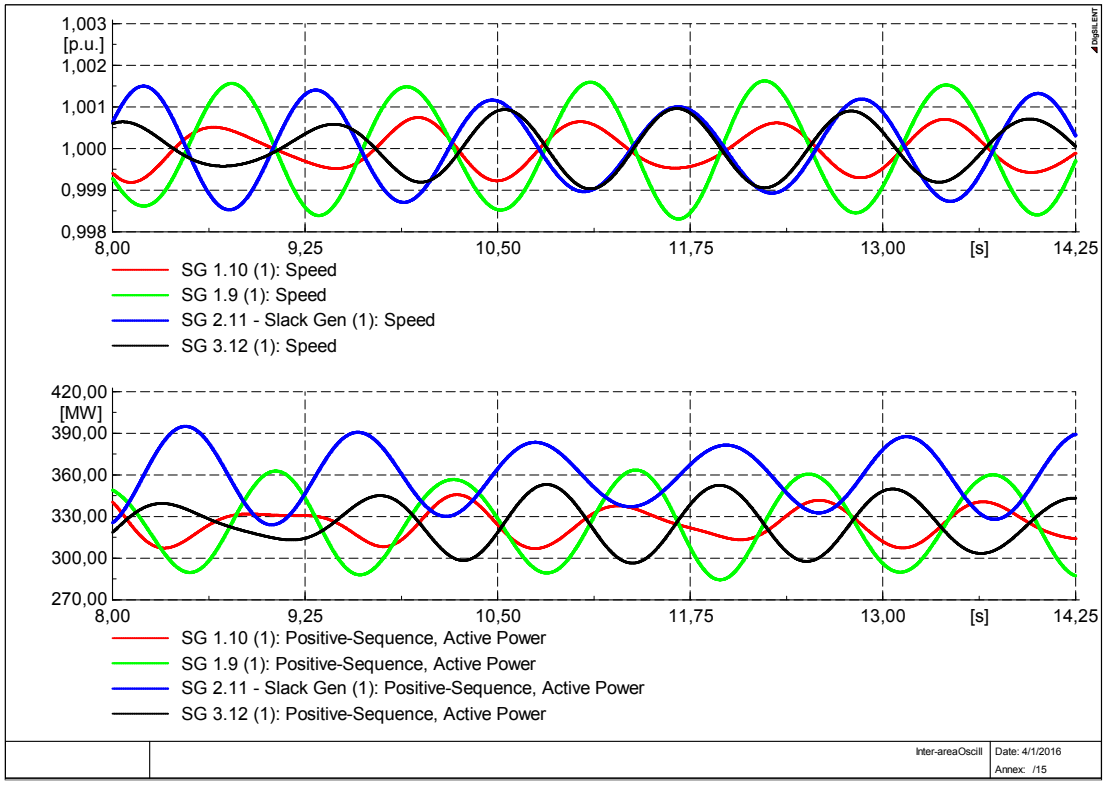

Figure 4-29: Inter-Area oscillations; SG 1.9 is oscillating against SG 2.11

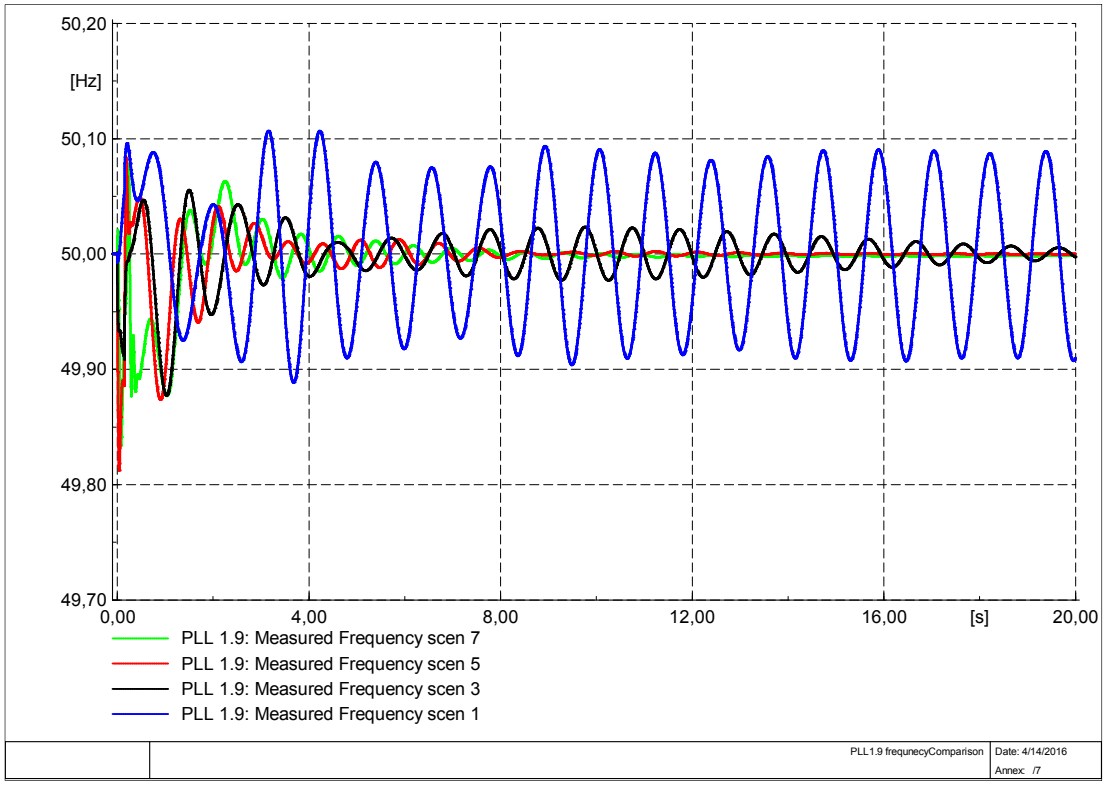

Figure 4-30: Frequency in bus 1.9 in Scenario 1, 3, 5 and Scenario 7

The behavior in the generator bus 3.12 regarding the frequency magnitude oscillations is similar to the previous analyzed bus. The FFT of the magnitude of the frequency in bus 3.12 is reported in Figure 4-31 for the four analyzed scenarios.

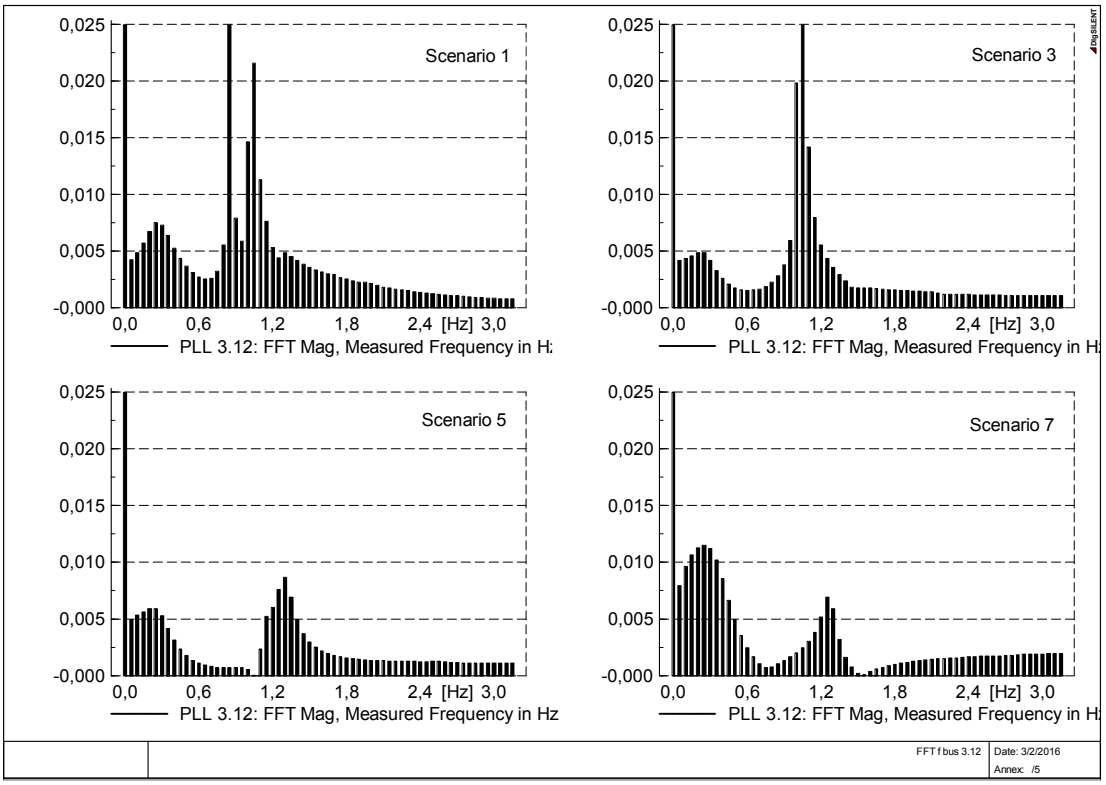

Figure 4-31: FFT in bus 3.12 in four different scenarios

In Scenario 1 and 3 both of the synchronous generators are feeding the bus while in Scenario 5 one of the synchronous machines is disabled and in Scenario 7 there is only DFIG production. Also in this case it can be concluded that with increasing wind power penetration the main harmonics observed in the base case are no longer present and without synchronous generation in the bus there are frequency magnitude components with bigger period of oscillation.

4.5. Voltage stability

Voltage stability is the ability of a power system to regain a stable behavior after being subjected to severe events like faults. As summarized in Chapter 3.3 the EU normative establishes predefined ranges of variation of the voltages in generation buses. Within these ranges it should be possible for the generators to remain connected to the system and ensure system security. To observe if the voltage is staying within the defined ranges the voltages variation in all the generator buses such as bus 1.10, bus 1.9, bus 2.11 and bus 3.12 in all the scenarios are plotted below from Figure 4-32 to Figure 4-39.

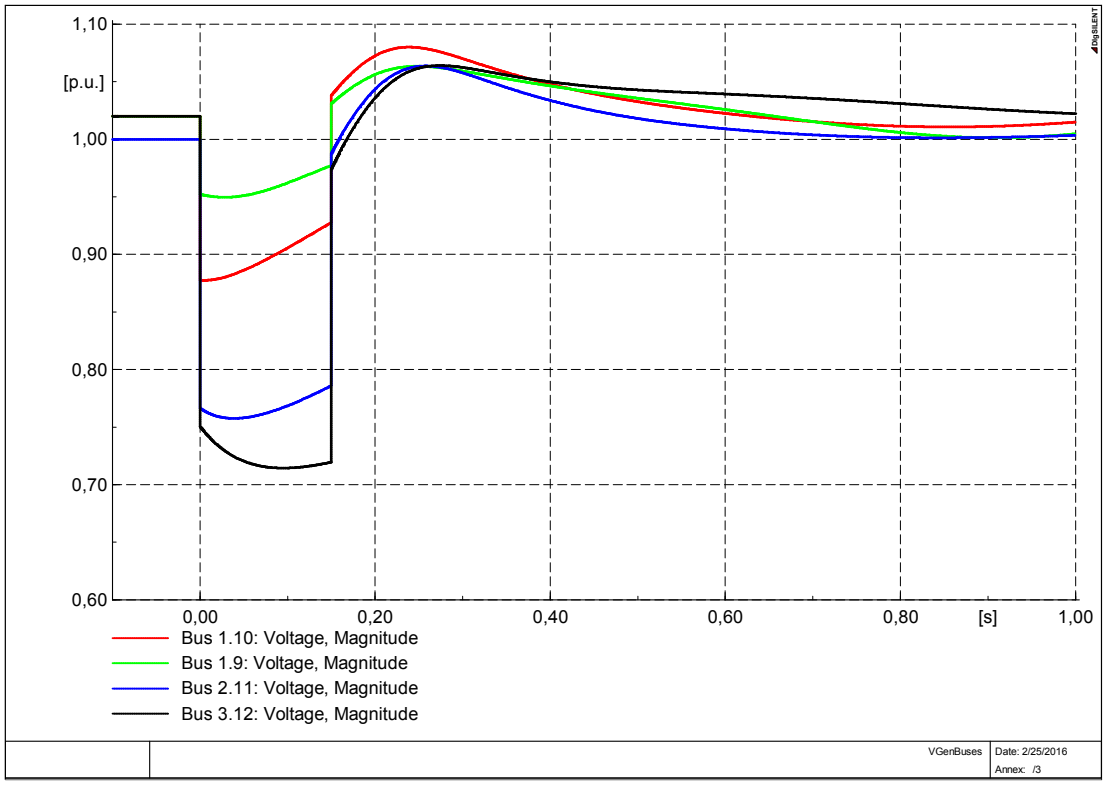

Figure 4-32: Voltages in the generators buses in SCENARIO 1

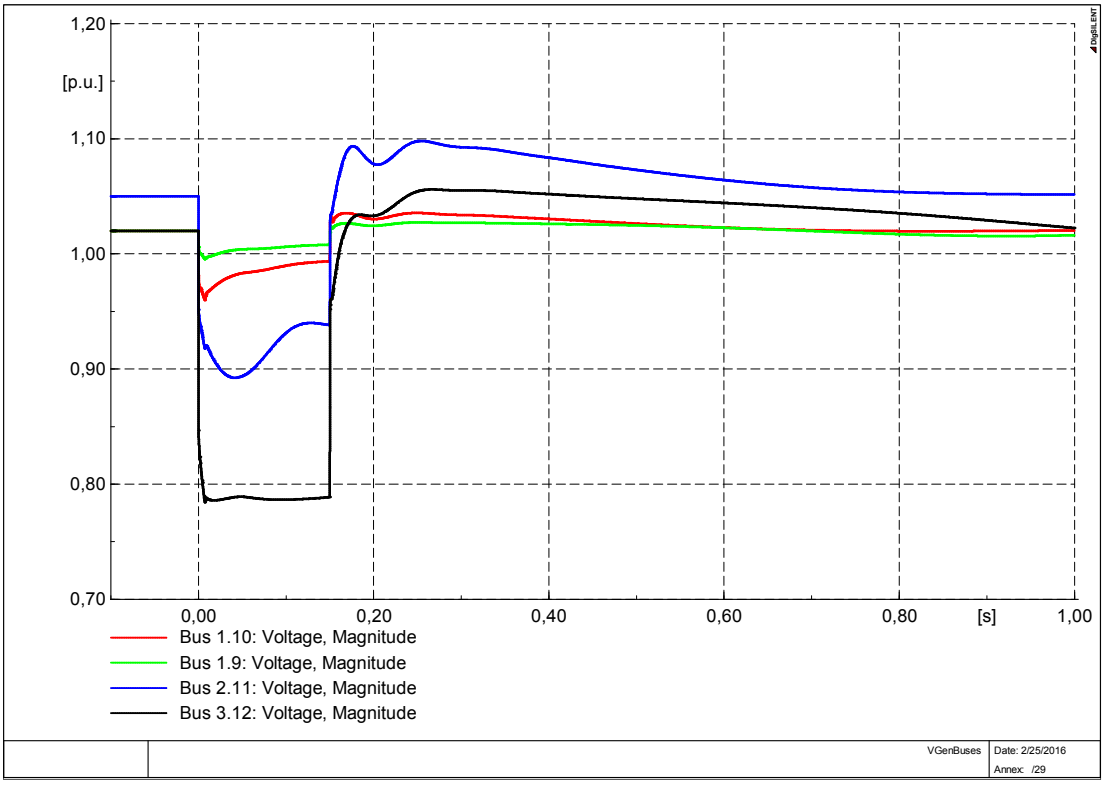

Figure 4-33: Voltages in the generators buses in SCENARIO 2

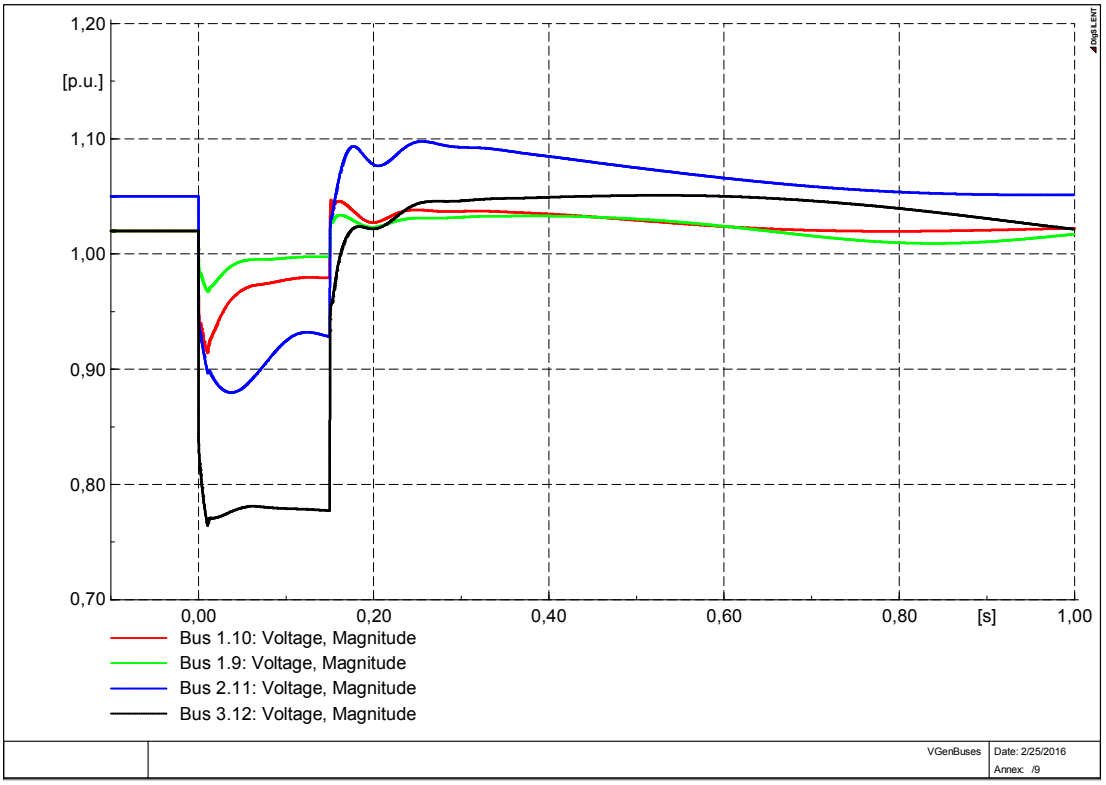

Figure 4-34: Voltages in the generators buses in SCENARIO 3

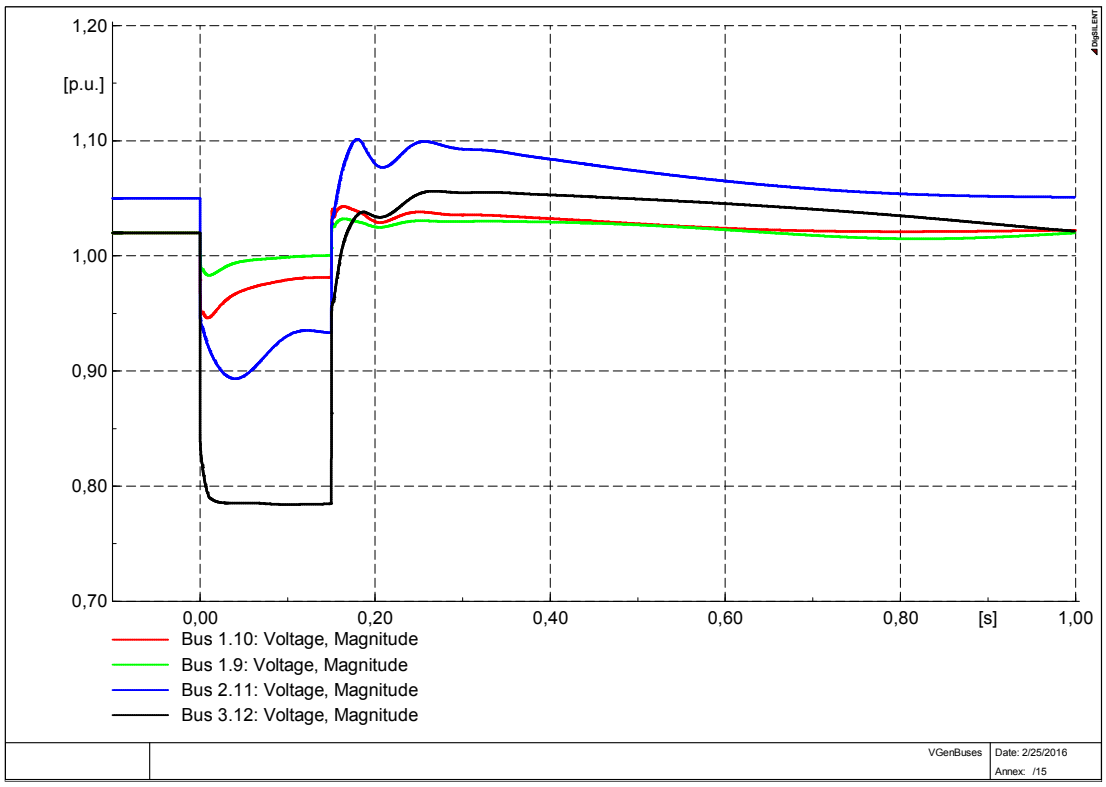

Figure 4-35: Voltages in the generators buses in SCENARIO 4

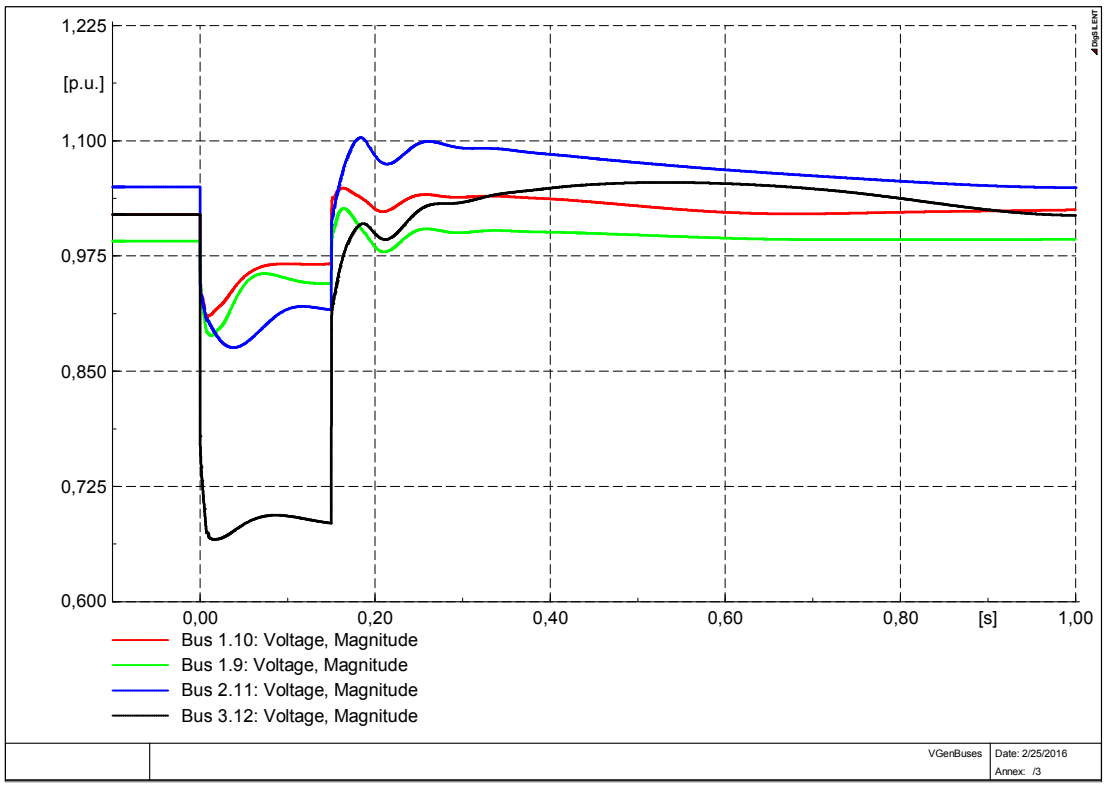

Figure 4-36: Voltages in the generators buses in SCENARIO 5

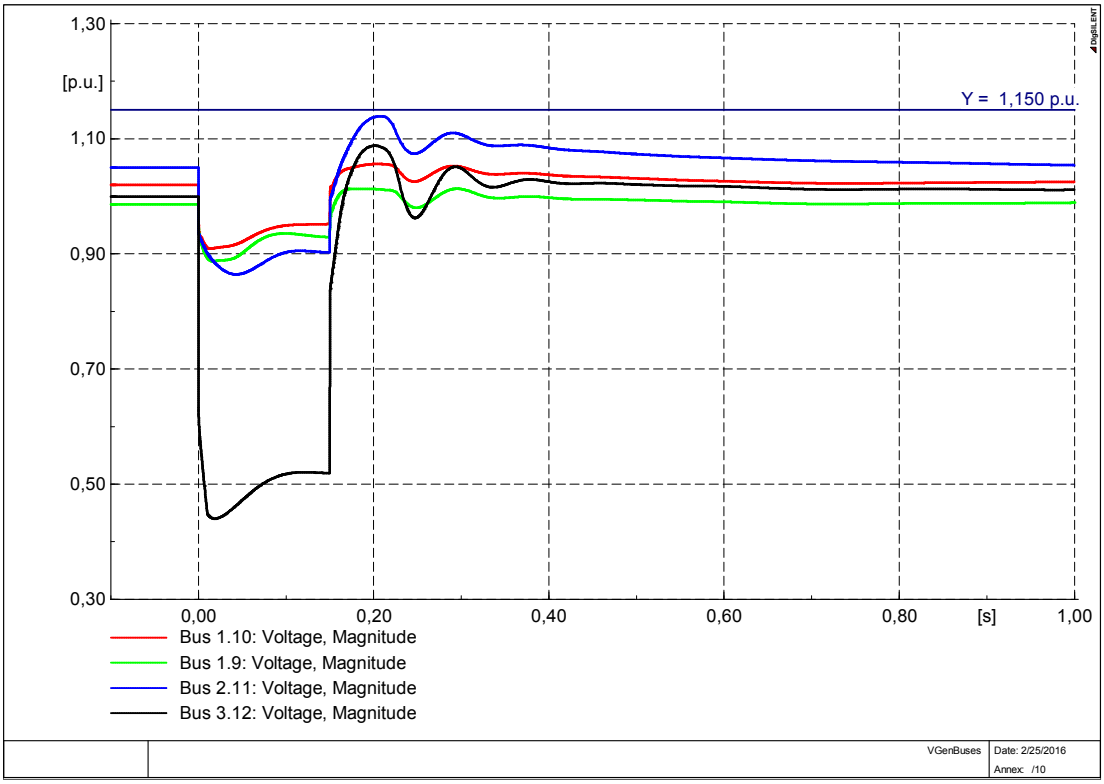

Figure 4-37: Voltages in the generators buses in SCENARIO 6

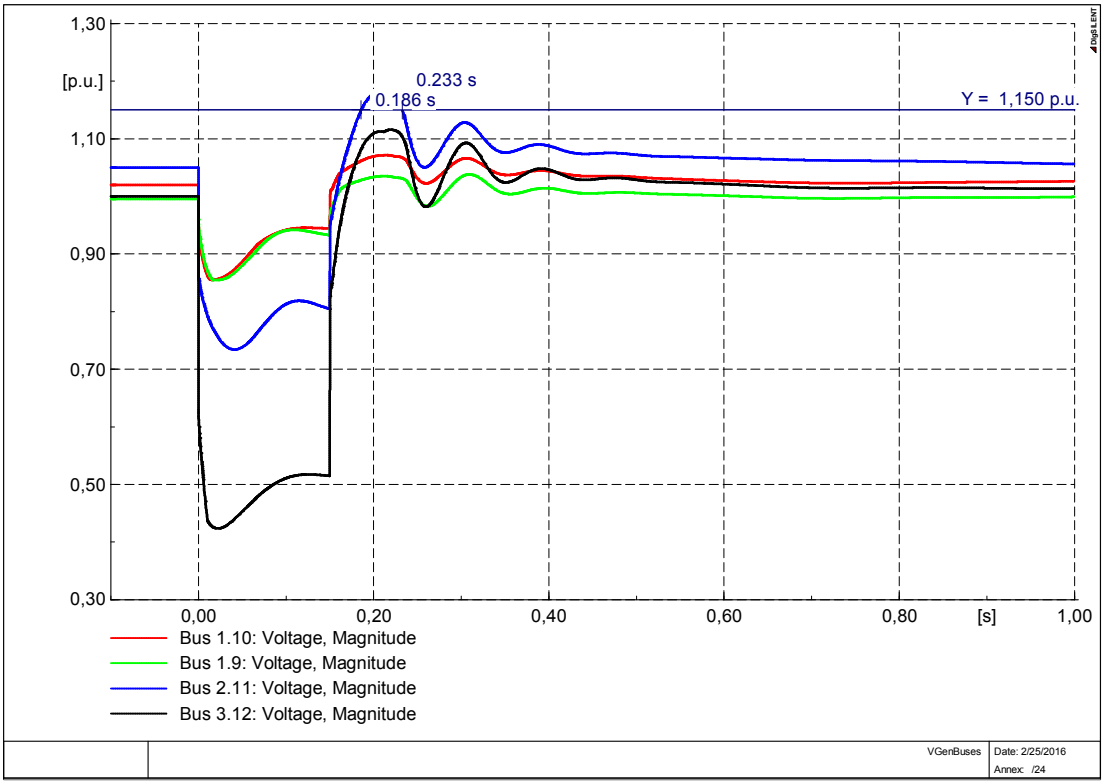

Figure 4-38: Voltages in the generators buses in SCENARIO 7

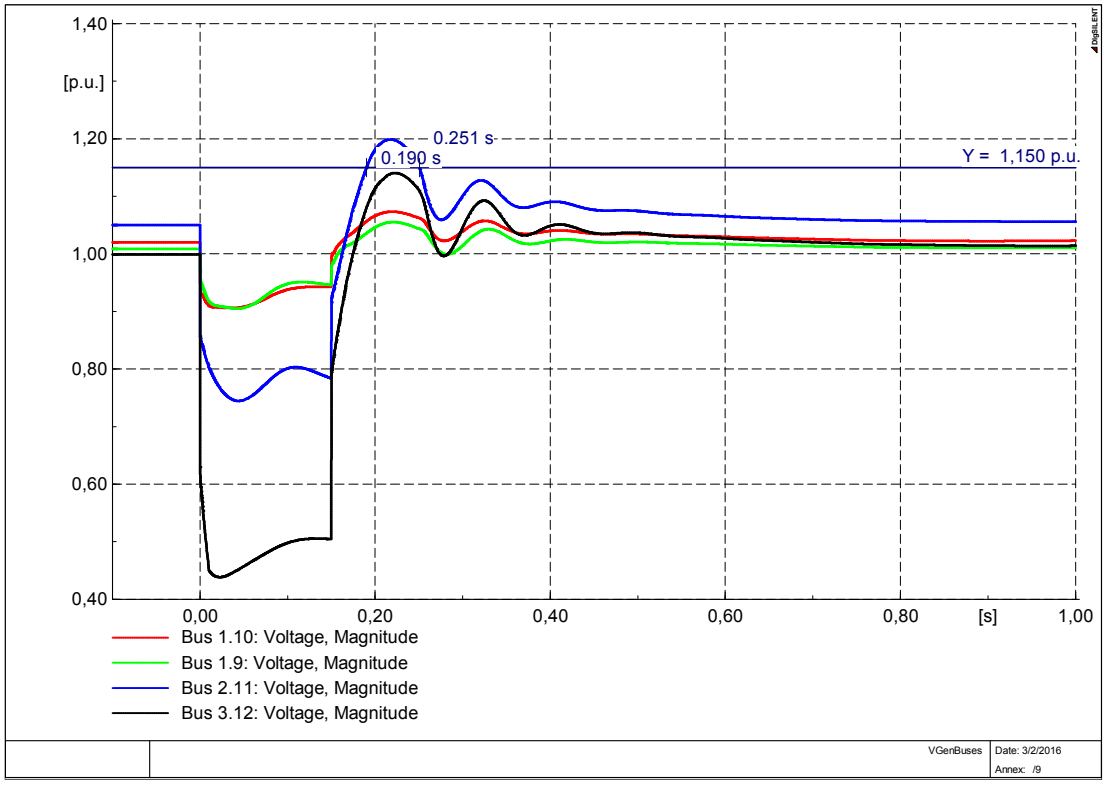

Figure 4-39: Voltages in the generators buses in SCENARIO 8

In all the analyzed scenarios the voltages are staying within the LVRT and the OVRT variation limits. Only in the last two scenarios, Scenario 7 and Scenario 8, the voltages in generation bus 2.11 are going over the limits of 115% (1.15 p.u.) respectively for 47 ms and 61 ms. In any case safety is guaranteed as the period of over-voltage is lower than 1 s.

Observing two scenarios with the same amount of conventional generator active but increasing wind power production is interesting to detect any differences in behavior in terms of voltage response after the fault. A comparison between Scenario 3, 25% of RES, and Scenario 4, 50% of RES, both with six synchronous generators active, is carried out as an example. Analyzing the voltage trend of both scenarios it can be seen which bus in each cell has the larger drop and overvoltage. The critical buses in term of larger overshoot and sag are reported in Table 4-1.

	Scenario 3		Scenario 4	
	larger sag	larger overshoot	larger sag	larger overshoot
Cell 1	1.2	1.3	1.2	1.3
Cell 2	2.5	2.5	2.8	2.5
Cell 3	3.7	3.12	3.7	3.12
Cell 4	4.3_b	4.3	4.3_b	4.3

Table 4-1: Critical buses in each cell for Scenario 3 and 4

The comparison between the voltages in the critical buses in each cell in the two analyzed scenario is reported in the plot in Figure 4-40.

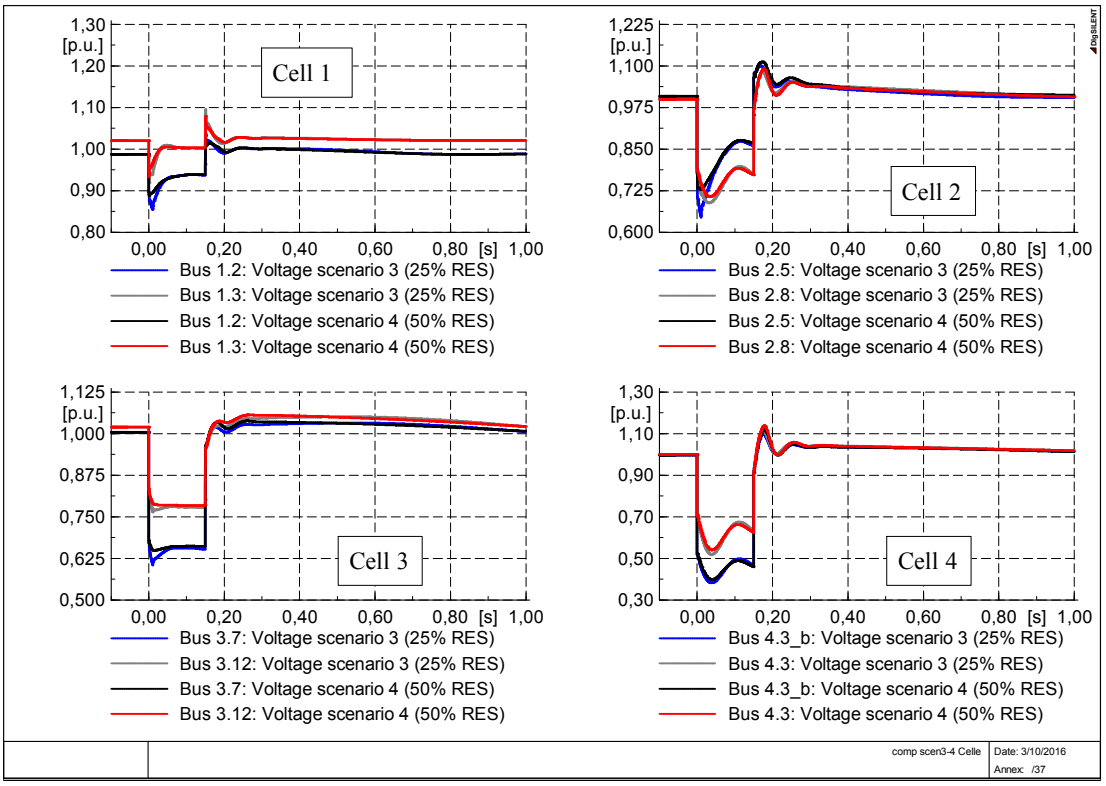

Figure 4-40: Comparison between voltages in more critical buses of each Cell in Scenario 3 (25% RES) and Scenario 4 (50% RES)

As could be seen, the voltage dip is not changing significantly from one scenario to another. Moreover it could also be said that there is a little improvement with more renewable penetration as the voltage, in comparison, has a larger drop in Scenario 3. The main reason for the similar behavior is the fact that the DFIG, in the two cases, has the same reactive power capability. In fact from Scenario 3 to Scenario 4 the set-point of each wind generators has been increased but the number of wind power plants is remaining the same, i.e. 65 units. It's clearly that due to the presence of power converters in the DFIG the active and reactive

power control are decupled and the capability of reactive power supplying is defined by the capability curve, which fixes the limits of reactive power operating limits. The number of DFIG is kept unchanged so the reactive power capability in the two scenarios does not change. As shown in the plots in Figure 4-41 the DFIG reactive power contribution of the three machines is not changing from one scenario to the other.

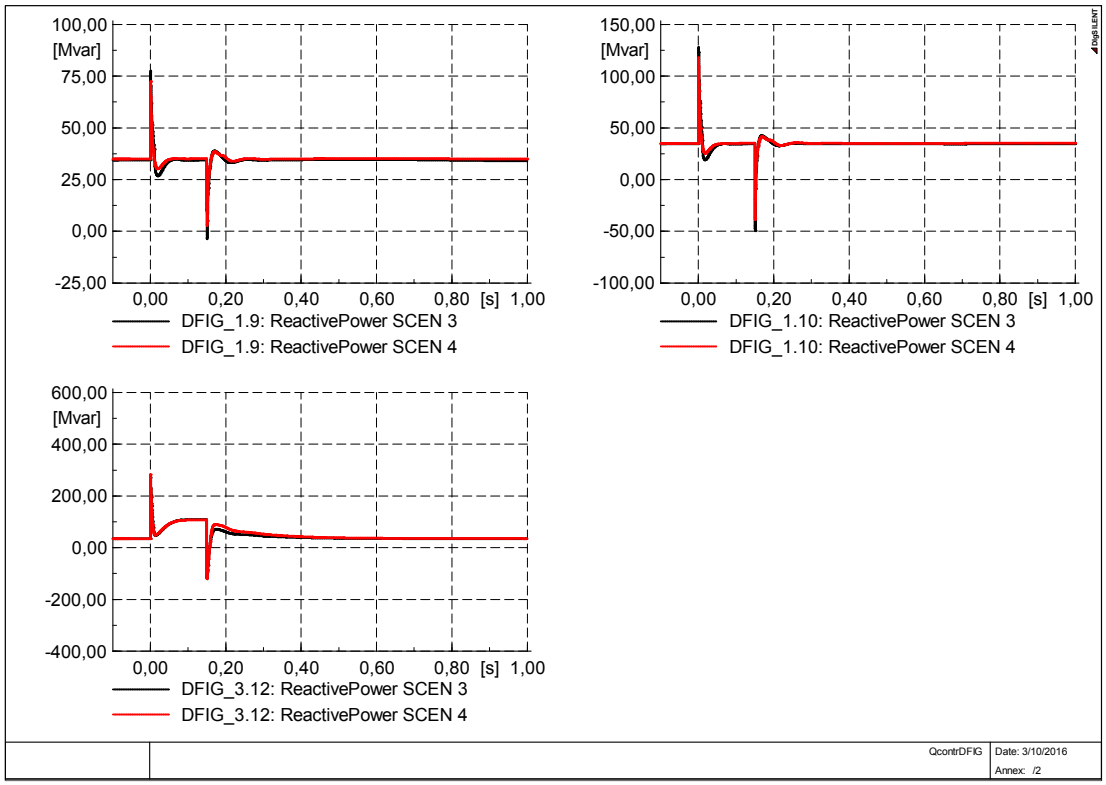

Figure 4-41: DFIG Q contribution in Scenario 3 and 4

The little voltage improvement in Scenario 4, with more RES penetration, is clarified observing synchronous generator behavior. Synchronous generators in Scenario 4 are working with a lower active power set-point to make room at the increasing wind generation. For that reason the conventional generation has a larger possible range of variation of active as well as reactive power supply. Notably they can provide reactive power to the grid with a bigger range of variations to sustain the voltages. In Figure 4-42 and Figure 4-43 the reactive and active power contribution of the synchronous generators in Scenario 3 and 4 are plotted in comparison. As seen from the plots the reactive power contribution in the two scenarios has a small difference; for example for the generator SG 1.9 the reactive power contribution from the pre-fault value has a lower variation during the fault in Scenario 4, i.e. the Q contribution is decreasing less, and consequently the voltage has a lower variation.

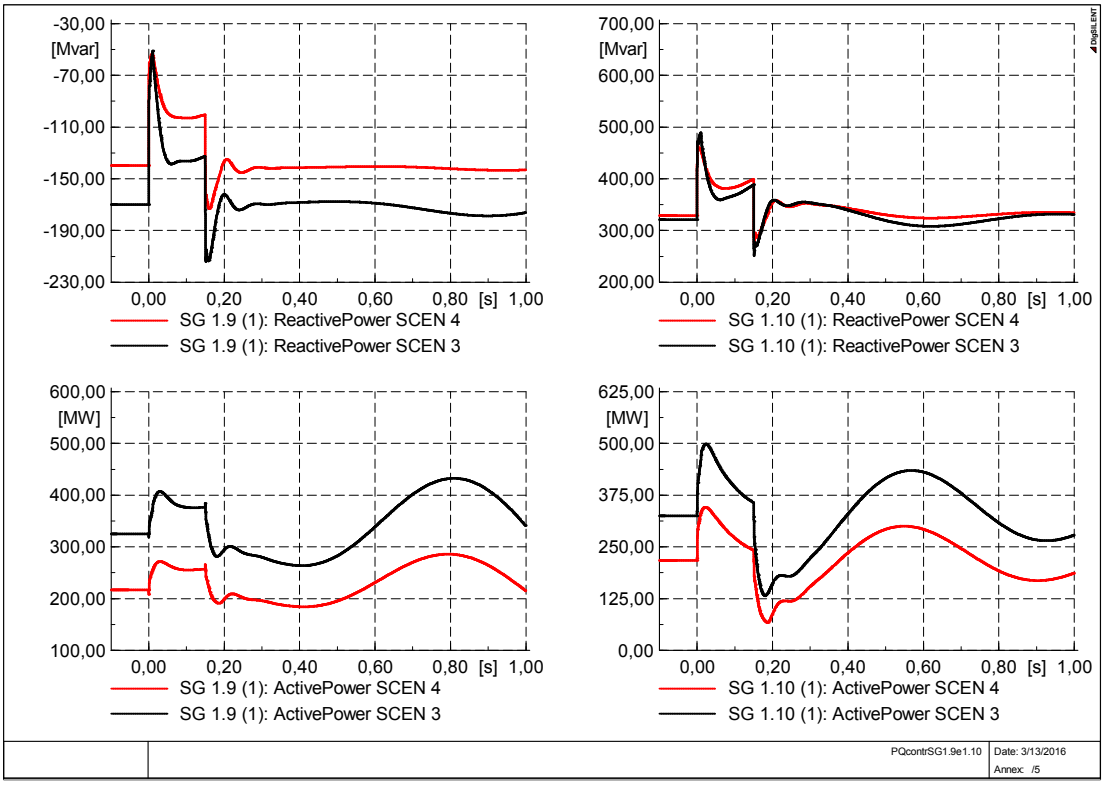

Figure 4-42: Reactive and active power contribution of the synchronous generators SG 1.9 and SG 1.10 in Scenario 3 and 4

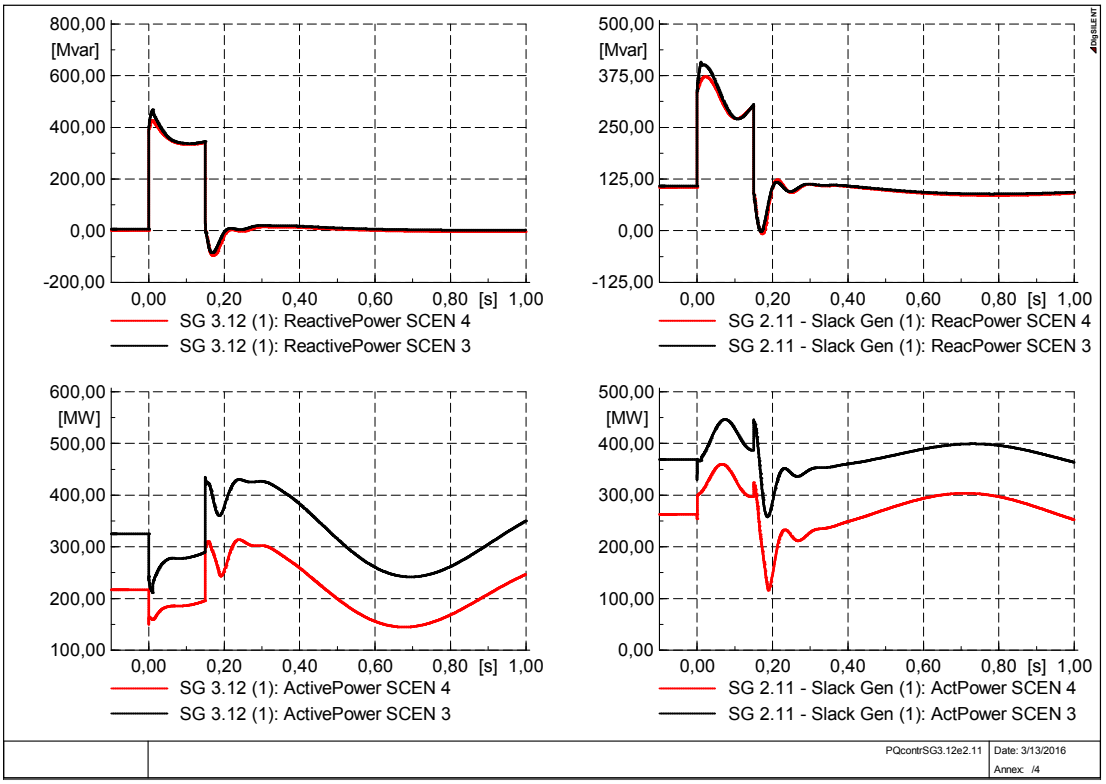

Figure 4-43: Reactive and active power contribution of the synchronous generators SG 3.12 and SG 2.11 in Scenario 3 and 4

Figure 4-44 shows a plot of the generator buses' voltage in the two scenarios. The voltage behavior, as explained before, is not changing significantly from one scenario to another apart from a little improvement in Scenario 4.

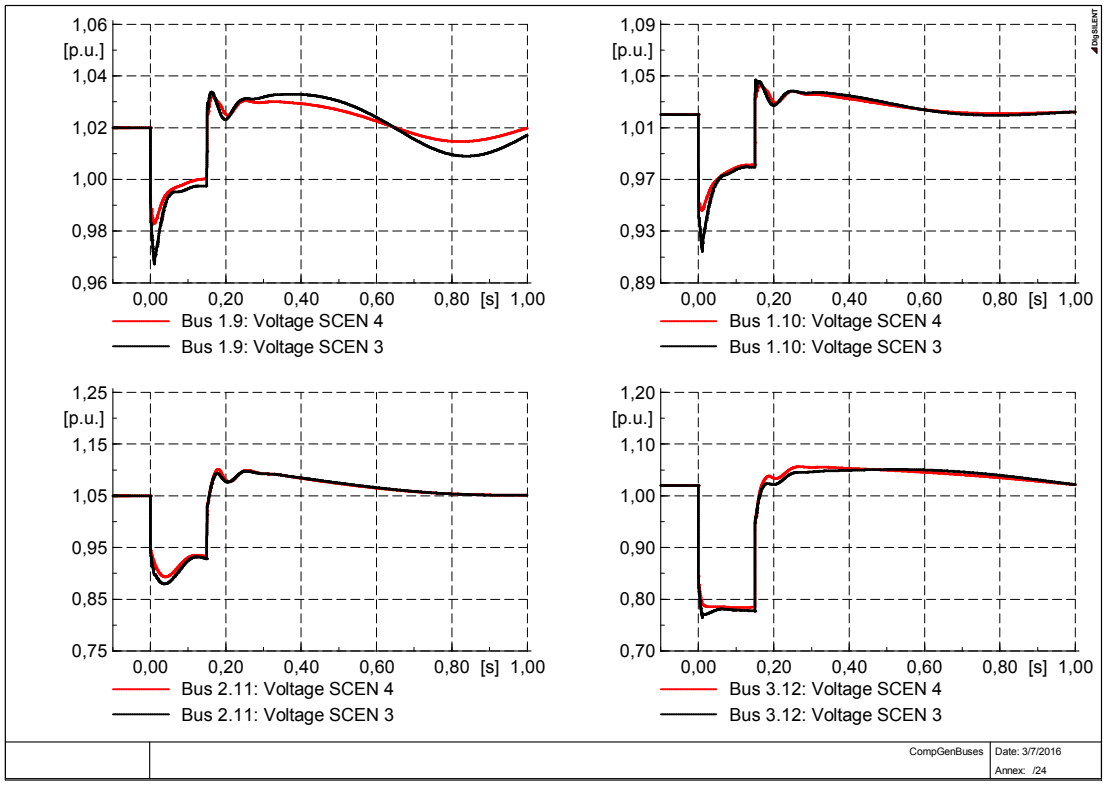

Figure 4-44: Voltage behavior in generator buses in Scenario 3 (25%RES) and 4 (50% RES)

Chapter 5

Simulation result with load step

In this chapter the simulation's results of a load step analysis are presented and discussed. After an imbalance between generation and consumption the frequency has variations that are influenced by the inertia of the system. For that reason the analysis has been focused on frequency stability issues after the disturbance with increasing inverter connected generation, which generally does not provide inertia response. In particular the rate of change of frequency ROCOF in the moment of the imbalance has been calculated.
The conducted analysis has shown that the frequency has faster variation with increasing wind power production. However regarding the capacity of reach steady state stability after the disturbance there is an improvement with increasing RES.

5.1. Introduction

In a power system in normal operating conditions an imbalance between power generated by generation units and the power requested by loads could occur due to a sudden increase of load or turning off of a generation unit. Thus it is interesting to analyze how the Pan-European grid behaves after a more common disturbance like a load step. The analyzed situation considers an increase of 2% of power demand by loads in the entire grid, represented by a load step of 10% in load 1.3 in Cell 1.

In the following section attention will be focused on frequency stability after this type of disturbance. The analysis has been done between four Scenarios: 1, 3, 5 and 7 with increasing wind power penetration of 0%, 25%, 50% and 75% respectively.

5.2. Frequency stability

The frequency, with reference to EU normative, should stay in the range of 50 Hz ± 1% (49.5-50.5 Hz) under normal operating condition, and also in the case of increasing/decreasing load demand. After a load step, the increasing request of power by the load causes a frequency drop due to the imbalance between the generation and load power. The entity of the frequency drop after the disturbance is correlated to the amount of rotational inertia present in the grid. As in the analyzed scenarios there is an increasing of wind power penetration, with a consequently decreasing of inertia, a worse frequency behavior should be expected. It is therefore of interest, in this view, to evaluate the ROCOF, i.e. rate of change of frequency, in the analyzed scenarios. The rate of change ROCOF [Hz/s] may be either the time derivative of the frequency, namely df/dt, typically evaluated in the time of perturbation, or the incremental ratio $\Delta f/\Delta t$ of frequency across a suitable time interval Δt ; from 200-300 ms to 500 ms. In the conducted analysis this parameter has been calculated with the plot function in PowerFactory as incremental ratio taking a time interval Δt ≈0.371s.

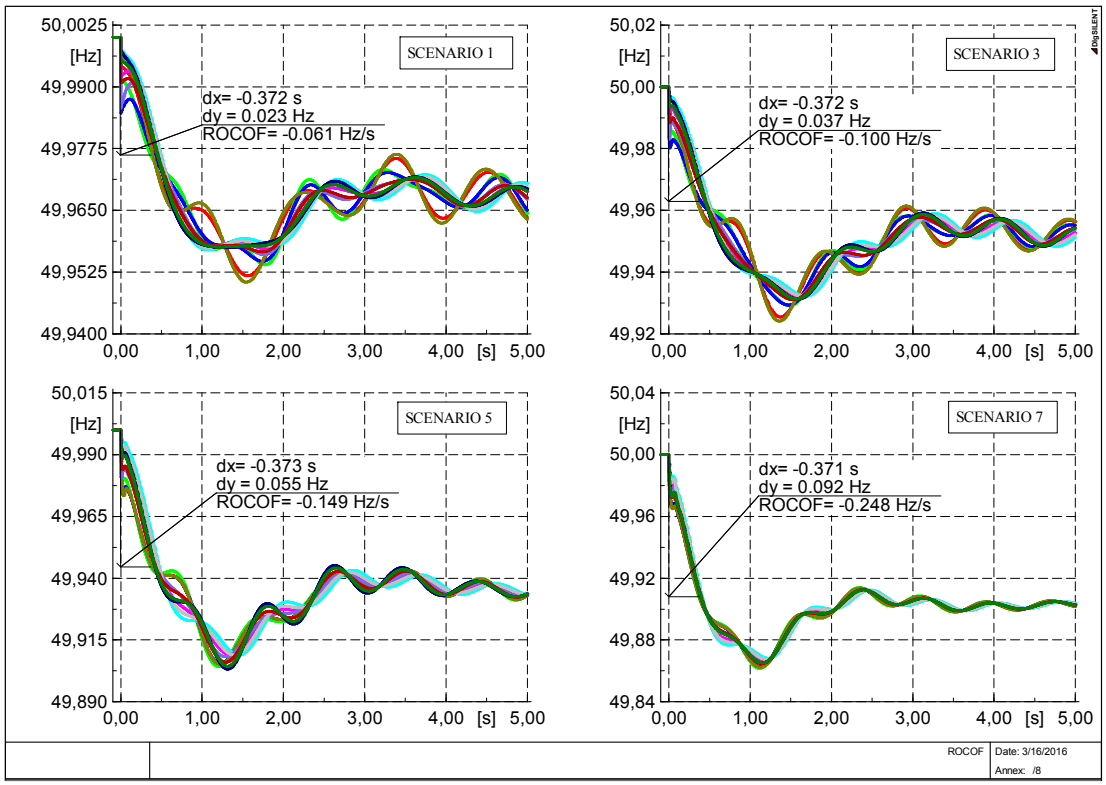

Figure 5-1: ROCOF in Scenario 1 (0% RES), 3 (25% RES), 5 (50% RES) and Scenario 7 (75% RES)

Figure 5-1 shows that the ROCOF is increasing, as expected, from Scenario 1 to Scenario 7. Clearly the inertia of the system is decreasing due to the reduction of synchronous machines active to make room to increasing penetration of wind power. Lower rotational inertia means faster frequency dynamics, so in the case of the analyzed loads step, larger frequency variations after the disturbance. As shown in Figure 5-2 the minimum value reached by the frequency in the analyzed cases gradually decreases from Scenario 1 to 7 and the minimum value is reached faster with more RES penetration.

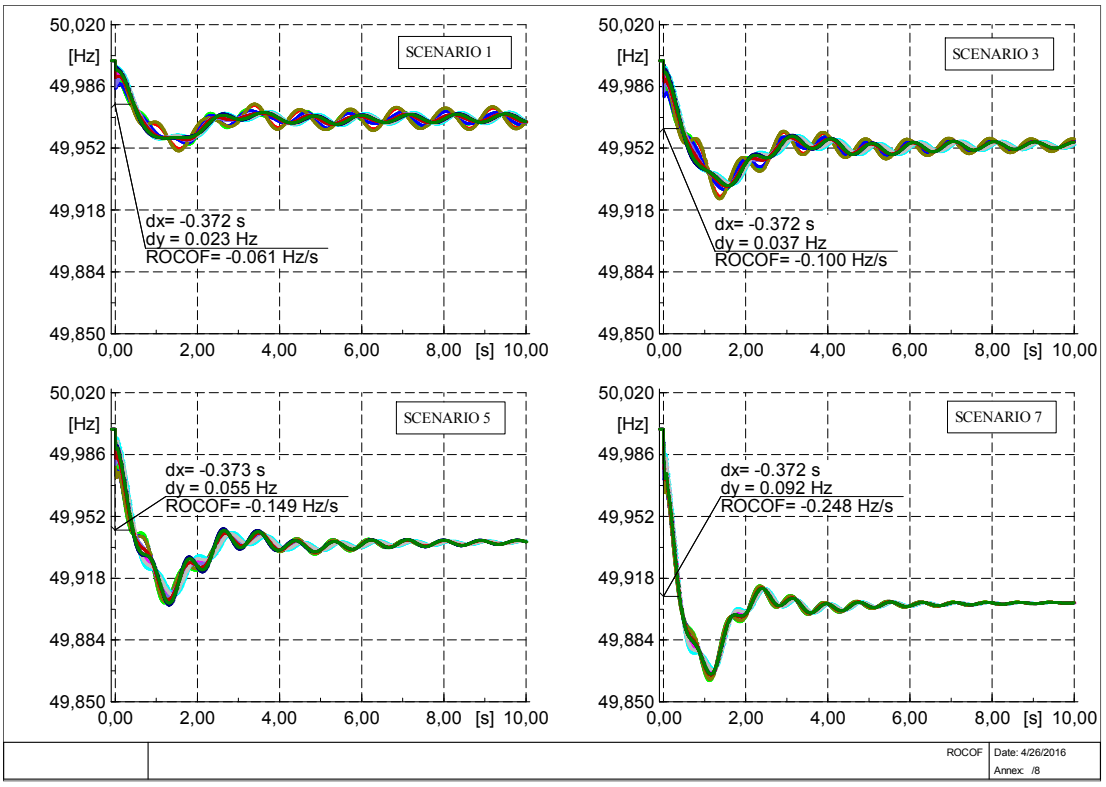

Figure 5-2: Minimum frequency reached value in Scenario 1 (0% RES), 3 (25%RES), 5 (50% RES) and Scenario7 (75% RES)

Even though there is an increasing of wind penetration and less inertia response from Scenario 1 to 7 the normative fixed frequency limits (±1%) are not reached in any of the scenarios.

In Scenario 1 and 3 the minimum frequency value is reached by the frequency in bus 1.9 while in Scenario 5 the minimum is in bus 3.12 and in Scenario 7 in bus 1.10. All of these buses are generation buses and in all the cases there is at least one synchronous generator enabled. In fact the frequency reaches a lower value due to the inertial response (IR) of the

synchronous machines and the initial imbalance between electrical and mechanical power; at a few seconds from the event the generator is decelerating, and the frequency follows.

To better understand the previous consideration a clarifying explanation is shown below. The synchronous machine SG 1.10 behavior in Scenario 7 is reported in Figure 5-3.

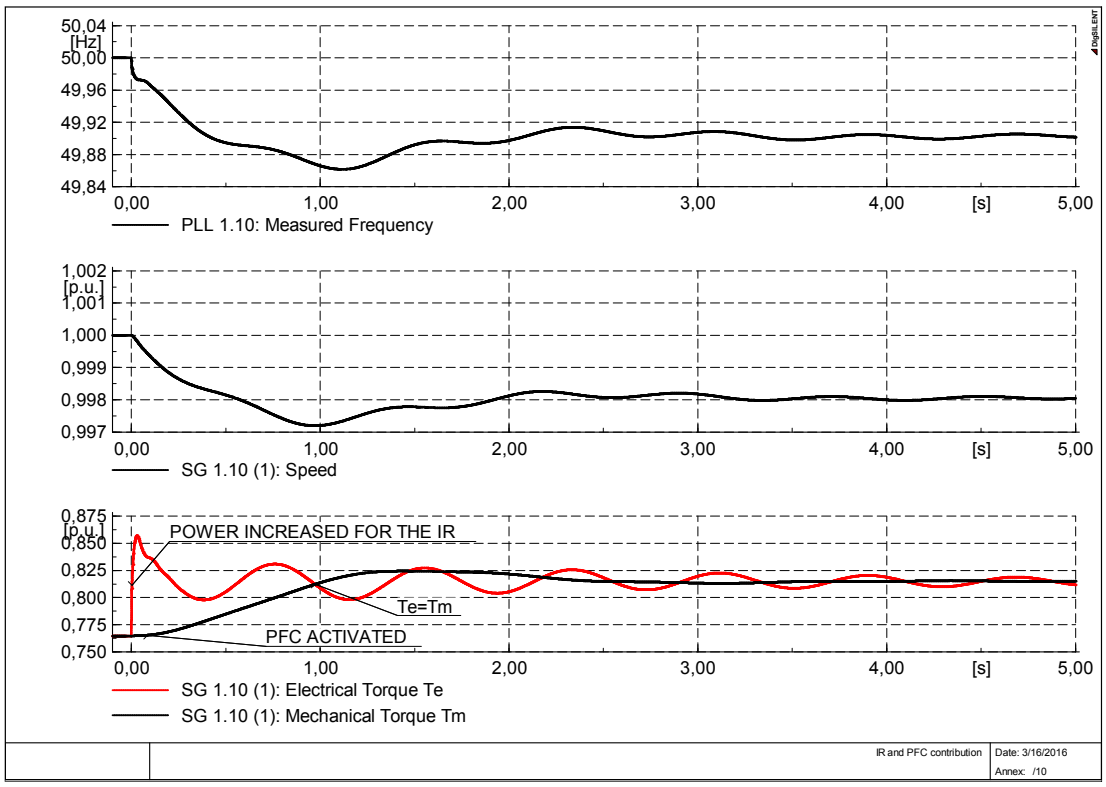

Figure 5-3: IR (inertial response) and PFC (primary frequency control) contribution in Scenario 7 in SG 1.10

After the disturbance, the IR takes effect, for a few seconds at most; the IR of synchronous machines is the inherent release of kinetic energy stored in rotors rotating generators, the electrical power increases as well as the electrical torque. Within a few seconds from the event, the primary frequency response is activated by the governor. The governor activates PFC (primary frequency control) when frequency deviation exceeds certain limits and changes the power output set-point to the prime movers. Mechanical torque as well as mechanical power is increased and thus also the electrical power increases to balance the difference between requested and generated power. When the mechanical torque is becoming greater than the electrical torque the synchronous generator starts to accelerate and the frequency recovers. Usually the primary frequency control, which should be completely deployed by 30 s from the events, stabilizes the frequency to a steady state value which is

different from the nominal frequency one. The secondary control reserve then has the task of bringing the frequency back to its nominal value and free up the primary frequency reserve.

Observing the frequency trend in a bigger time interval, e.g. 50 s in Figure 5-4, it can be seen that the frequency recovers to a stable value that is lower than the nominal frequency of 50 Hz as said before. Bringing back the frequency to the pre-event steady state value is the task of the secondary frequency control (SFC); this should be done within 15 minutes. In our model the SFC is not implemented as only the transient behavior (i.e. within 10 s) is of interest to the analysis.

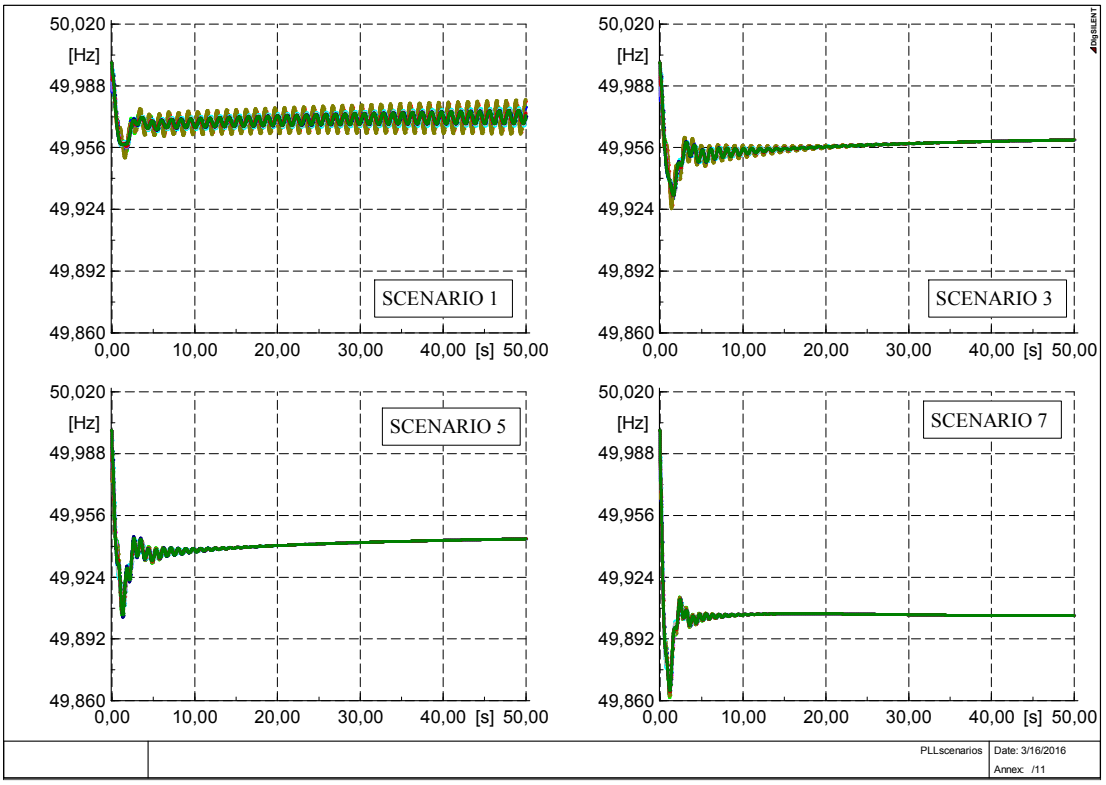

Figure 5-4: Frequency trend in principal grid buses in Scenario 1(0% RES), 3(25% RES),5(50% RES) and Scenario7(75% RES)

The frequency in all the scenarios recovers to a stable value. However in Scenario 1 the frequency after the primary control intervention recovers to a "stable value" but with low frequency oscillation. In fact by zooming in on the plot in Figure 5-5, it can be seen that the principal oscillation are around 0.859 Hz (oscillating period of T=1.164 s), i.e. this oscillation are inter-area oscillation. Inter-area oscillations are due to the swinging between generators in different cells. As shown clearly in Figure 5-5 in plot C the generator units in

Cell 1, SG 1.9, is swinging with a phase shift of 180° against the generators SG 2.11, i.e. the slack units in Cell 2.

This trend could also be noted observing the injected power by the two generators: where the power has a peak in generator SG 2.11 there is a minimum in the power of synchronous generator SG1.9 in Cell 1.

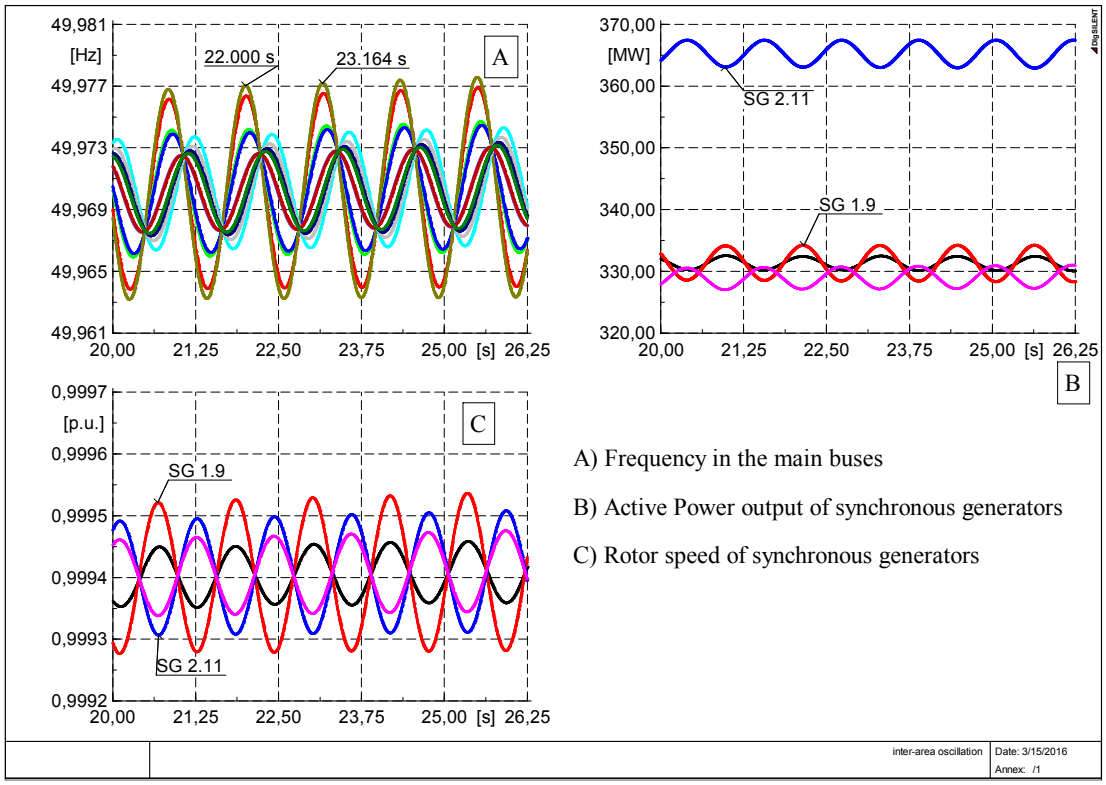

Figure 5-5: Inter-area oscillation observation. In plot B) and C) the legend is reported below:

SG 1.10 *SG 1.9* *SG 2.11 (SL)* *SG 3.12*

The inter-area oscillations, except in the base case, are no longer present in the other scenarios with increasing RES, notably wind power generation. The wind penetration has a worse effect on the frequency's initial variation due to the consequent decrease in IR but has a positive contribution to the achievement of steady-state equilibrium after disturbances. In fact inter-area oscillations are more probable in big interconnected system connected with long tie lines of limited capacity. In the analyzed cases, from Scenario 1 without RES generation to the following scenarios, the power flow changes due to the HVDC contribution in Cell 4 and thus the power comes also from Cell 4 bringing all the system to a better behavior.

Chapter 6

Conclusion

This work presented simulation studies, carried out in the Pan-European grid with the software DigSilent PowerFactory, with the aim to study the stability of interconnected power grids with increasing RES penetration. A three-phase fault and a load step have been investigated.

The Pan-European reference grid, developed within the framework of the ELECTRA project, served as a basis for the analysis. The studies involved the definition of eight scenarios with different wind power penetration levels. Not all scenarios have been considered in the simulation, but relevant scenarios were chosen on case-by-case basis.

The first analysis, a three-phase fault on a tie line, included the analysis of rotor angle, frequency and voltage stability.

The rotor angle has been analyzed utilizing the TRASI index as a comparative indicator. It has been found that the transient stability in general gets worse with increasing inverter connected generation (wind power plants) due to the decreasing of the system's inertia. But the stability can improve with increasing wind power penetration if the fault is far from the synchronous machines. Notably, if the system presents massive distributed RES penetration and conventional rotating generations are located in areas with low probability of severe fault, system security is ensured. Moreover, transient stability showed to be improved in the case of mixed generation of SGs and wind power compared to the case of pure synchronous generation. In fact, the improvement of transient stability is expected, because SGs are working at a lower active power set point therefore increasing the stability margin.

Regarding the frequency behavior after the disturbance, it has been observed that the frequency variation ranges are not exceeded and the security of the system is ensured even with high wind penetration. The analysis showed that the frequency reaches a higher peak value without RES penetration, but with increasing wind generation there are more

oscillations immediately after the fault. Even if the behavior immediately after the fault is worse with increasing inverter connected generation the frequency oscillations after the clearance are no longer present. In fact, without wind power production, the system is subjected to inter-area oscillations after the clearance of the fault, while oscillations are better damped with increased RES. To prevent inter-area oscillations, power system stabilizers (PSS) can be used. PSS can be added to generators' automatic voltage regulator (AVR) to improve stability but an appropriate parameter design is very important to operate in an effective way. Notably, power system stabilizers have to be tuned to obtain efficient damping of inter-area oscillations. In the conducted analysis, PSS were not added to the model, because the scope of the project was to analyze the Pan-European grid with increasing wind production, and inter-area oscillation were registered only in the base case without wind production.

With regards to voltage stability, the simulations have shown that the voltage stays within the predefined admissible variation ranges and the system security is guaranteed. A comparison between two scenarios with increasing wind has shown that the voltage dips are not changing significantly under different wind power penetrations.

The second sets of simulations involved a study of the behavior of the grid after a power imbalance caused by a load step in one cell. Frequency stability has been analyzed with particular focus on the rate of change of frequency (ROCOF). It could be concluded that the frequency behavior, i.e. the ROCOF value, is worse with increased wind power penetration. With more wind production, i.e. lower presence of rotating generations, system inertia decreases and frequency dynamics are faster so initial variations in frequency are larger. The conducted analysis has however shown that there is a faster achievement of a stable frequency value with increased RES penetration connected with converters.

Finally it can be concluded that the increasing power generation share of renewable resources does not necessarily lead to worse stability behavior. In fact, as seen, the presence of renewable generation can positively contribute to achieve steady state equilibrium after a disturbance and reduce oscillations. But it is also true that future regulations will require RES units to deliver frequency stabilizing services, e.g. frequency sensitive mode (FSM) capability and energy storages with synthetic inertia capability (see Annex) to support the power system.

Chapter 7

Bibliography

[1] European Commission document, "A European strategic energy technology plan, towards a low carbon future", 2014.

[2] ELECTRA, "Project deliverable D3.1: Specification of smart grid high level functional architecture for frequency and voltage control", 2015.

[3] P. Kundur, J. Paserba, V. Ajjarapu, G. Andersson, "Definition and classification of power system stability", *IEE Transactions on power systems*, vol.19, no. 2, pp. 1387-1401, May 2004.

[4] L. Meegahapola, D.Flynn, "Impact on transient and frequency stability for a power system at very high wind penetration", IEE Power and Energy Society General Meeting, Minneapolis, USA, 2010.

[5] C. Liu, Z. Chen, "Transient stability assessment of power system with large amount of wind power penetration: the Danish case study", IEE Conference on Power and Energy, 2012.

[6] P. Kundur, *Power system stability and control*. McGraw Hill, 1994, pp.128-135.

[7] "DIgSILENT GmbH - PowerFactory 15." User Manual, Gomaringen, Germany.

[8] European Commission document, "Final draft Network Code on Requirements for grid connection of Generators", 2015.

[9] CENELEC Technical specification, "CLC/TS 50549-2:2014: Requirements for the connection of a generating plant to a distribution system - Part 2: Connection to a MV distribution system", 2014.

[10] Technical Standard EN 50160, "Voltage characteristic of electricity supplied by public distribution networks", 2011.

[11] CIGRÉ Report "Benchmark Systems for Network Integration of Renewable and Distributed Energy Resources", CIGRÉ Task Force C6.04.02, July 2009.

[12] M. Marinelli, M. Pertl et al. “Functional description of the monitoring and observability detailed concepts for the Pan European Control Schemes” ELECTRA Deliverable D5.4: WP 5: Increased Observability, 2016.

[13] M. Marinelli, M. Pertl, M. Rezkalla, M. Kosmecki, S. Canavese, A. Obushevs, and A. Morch, “The Pan-European Reference Grid Developed in the ELECTRA Project for Deriving Innovative Observability Concepts in the Web-of-Cells Framework,” in 51th International Universities Power Engineering Conference (UPEC), 2016, pp. 1–6, submitted

[14] E.H. Camm, M. R. Behnke, O. Bolado, “Characteristics of Wind Turbine Generators for Wind Power Plants”, IEEE PES Wind Plant Collector System Design Working Group, 2009

[15] Hansen, A. D., Iov, F., Sørensen, P. E., Cutululis, N. A., Jauch, C., & Blaabjerg, F. “Dynamic wind turbine models in power system simulation tool DIgSILENT” Danmarks Tekniske Universitet, Risø Nationallaboratoriet for Bæredygtig Energi. (Denmark. Forskningscenter Risoe. Risoe-R; No. 1440(ed.2)(EN)), 2007

[16] K. Sun, “Slide-Load Modeling”, university of Tennesse, 2015.

[17] Dragan Jovcic, Khaled Ahmed, *High voltage direct current transmission: Converters, Systems and DC grids*, September 2015

[18] T. M. Haileselassie, “Control, Dynamics and Operation of Multi-terminal VSC-HVDC Transmission Systems” , Thesis, Norwegian University of Science and Technology Faculty of Information Technology, cap.3 pp. 51-52, 2011

[19] ENTSOE, “Scenario outlook & Adequacy forecast”, 2015.

[20] Italian technical standard CEI 0-16;V1, “Reference technical rules for the connection of active and passive consumers to the HV and MV electrical networks of distribution Company”, 2014

Annex

Frequency stabilizing services

Distributed generating plants, such as wind power plants and solar generation units, are increasing more and more nowadays in power grids, causing new issues in the frequency control of the system. A typical wind plant appears to the grid as a substantially different generation source than a conventional power plant. The most significant difference is that the wind energy source is inherently uncontrollable. That is due to the fact that most rotating machines in modern wind turbines are decoupled from the grid by an inverter so they not provide the "natural" inertia response that other conventional generation provides. The same could be said for PV units. Such uncontrolled power output can have an impact on the grid, including frequency variations. Without special control, a wind plant does not inherently participate in the regulation of the grid frequency while synchronous generator naturally contributes to system inertia. When inverter connected generation displaces conventional synchronous generator the burden of frequency regulation placed upon the remaining synchronous generator is increased. There is thus a need of prompt future generating units to deliver frequency stabilizing services to the grid. This can be attained with frequency sensitive mode FSM or with the provision by the inverter connected generation of a fast frequency response called "synthetic inertia".

The FSM (Frequency sensitive mode) is defined as an operating mode of a power generating modules or a HVDC system in which the active power output changes in response to a change in system frequency. FSM limits the deviation of the current power system frequency from the target frequency of 50 Hz in case of an unbalance between generation and consumption. ENTSO-E new code [8] has defined different FSM with distinctions regarding the type of the generator. The regulation distinguishes between LFSM-O, limited frequency sensitive mode-over frequency, ad LFSM-U, limited frequency sensitive mode-under frequency. The first one, LFSM-O, is an operating mode which will result in active power output reduction in response to an over frequency while LFSM-U will result in active power output increase in response to under frequency. The distinction between generators in the regulation is not reported but has been already explained in Subparagraph 1.5.1.

With regard to the limited frequency sensitive mode-over frequency of type A, B, C and D power generating modules shall be capable of decreasing the active power output ΔP as shown in Figure 0-1. In case of over frequency where Δf is above the threshold Δf_1 the power generating module has to provide a negative active power output change according to the droop s_1 defined between 2% to 12%. The frequency threshold is between 50.2 Hz and 50.5 Hz.

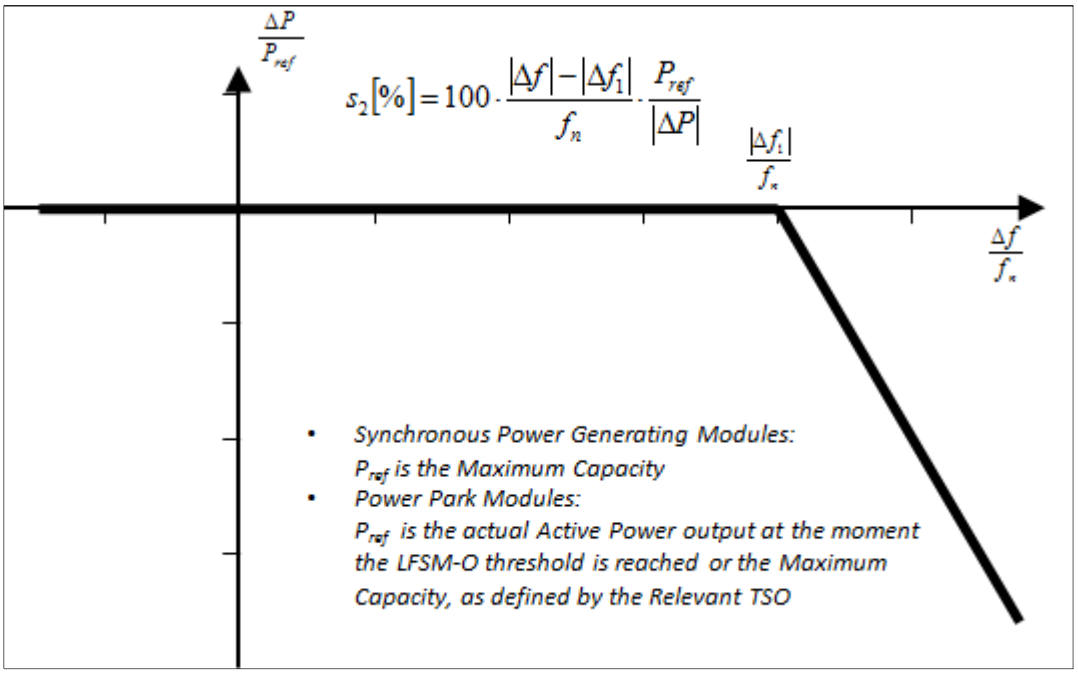

Figure 0-1: Active power response capability of a power generating modules in LFSM-O

In addition, with regard to the LFSM-U of type C and D generators, the power generating module shall be capable of increasing the active power output ΔP as shown in Figure 0-2. In case of under frequency where Δf is below the threshold Δf_1 the power generating module has to provide a positive active power output change according to the droop s_2, in the range of 2-12%. The threshold shall be between 49.8 Hz and 49.5 Hz.

In LFSM-U the power generating module shall be capable of providing a power increase up to its maximum capacity. In case of over frequency the active power frequency response is limited by the minimum regulating level.

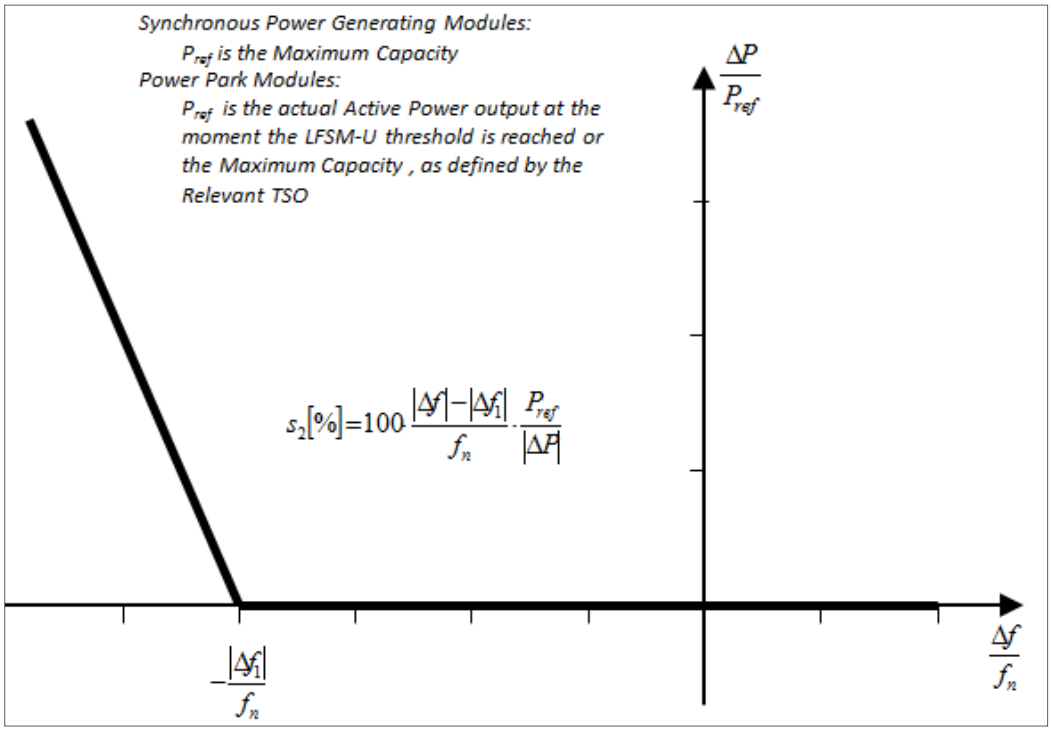

Figure 0-2: Active power response capability of a power generating modules in LFSM-U

Inverter connected based generation units can emulate the inertial response of conventional generator by a special control structure and the availability of energy storage. A disturbance, as an imbalance between generation and load, will result in a rate of frequency change which is inversely proportional to the system inertia. A generating unit delivering inertia will inject extra power to the grid with decelerating frequency and absorb extra power from the grid with accelerating frequency. This behavior can be emulated by inverter connected generation with storage. New regulation will define rules for the active power regulation of storage units; to have an idea of the possible requirements, the Italian standard CEI0-16 V1 [20] is reported as an example.

For the standard [20] storage systems connected in the network have to respect the following requirements. If the power system frequency is exceeding the default under frequency and over frequency threshold there should be a variation of the active power injected or absorbed as in Figure 0-3. The under frequency and over frequency threshold are defined as default respectively 49.7 Hz and 50.3 Hz.

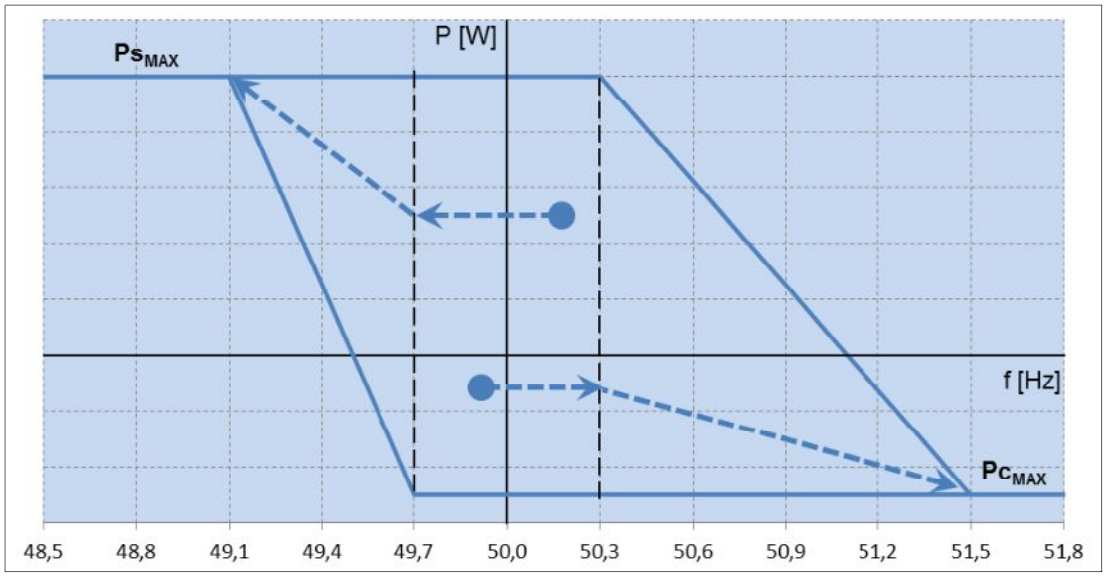

Figure 0-3: Active power regulation in over frequency and under frequency condition

The activation of the regulation is without delay for the default settings but could be changed from 0 to 1 s. In Figure 0-3 P_{SMAX} is the maximum discharge power while P_{CMAX} is the maximum charge capacity of the storage system.